Binuclear Ligand Copper Dioxygen/Nitric Oxide Adducts: Characterization and Reactivity

by

Rui Cao

A dissertation submitted to Johns Hopkins University in conformity with the requirements for the degree of Doctor of Philosophy

Baltimore, Maryland

October, 2016

ABSTRACT

Copper ions are found in a number of enzyme active sites that facilitate many biologically important reactions such as dioxygen activation and bacterial denitrification. These enzyme catalyzed reactions proceed extremely fast in aqueous media and reaction mechanisms are largely unknown. Inspired by these enzymatic reactions and employing coordination chemistry with ligand copper complexes in organic solvents, we can study the formation and reactivity of room temperature unstable copper-O_2/NO adducts that became meta-stable at much lower temperature. For the system we describe here, a phenol-containing binucleating ligand (UN-O^-) is employed, giving rise to a series of phenolate-bridged dicopper complexes of various types. A structurally characterized dicopper localized mixed-valent Cu(II)Cu(I) complex can be oxygenated at -80 °C to form mixture of μ-1,2 and μ-1,1-superoxide complexes. The μ-1,2-superoxide species can be reversibly reduced to form a μ-1,2-peroxide complex (and then reoxidized) using various outer-sphere redox reagents. A stopped-flow kinetic study results reveal an outer-sphere electron transfer process with a small total reorganization energy (λ) of 1.1 eV.

In addition, a new peroxynitrite complex can be generated in two methods. i) The superoxide complex can react with $NO_{(g)}$ to form the peroxynitrite-dicopper(II) species, ii) The mixed-valent Cu(II)Cu(I) complex reacts with $NO_{(g)}$ to form a nitrosyl complex; following oxygenation, it gives rise to the same peroxynitrite complex. The peroxynitrite complex undergoes solvent dependent O-O cleavage pathways with externally added 2,4-di-*tert*-butylphenol (DTBP) added as a substrate. In dichloromethane solvent, the O-O bond cleaves heterolytically to produce nitronium ion leading to *o*-nitration of DTBP.

However, in 2-methyltetrahydrofuran as solvent, the O-O bond undergoes homolysis to generate $\bullet NO_2$ (detected spectrophotometrically) and a putative higher-valent oxyl complex that abstracts a H-atom from DTBP to give a phenoxyl radical; the latter may dimerize to form the bis-phenol product, or couple with the $\bullet NO_2$ present leading to *o*-phenol nitration. Nitric oxide reduction chemistry is also observed in structurally characterized dicopper(I) complex at different temperatures. A hyponitrite intermediate complex is isolated and characterized. The complexes involved are characterized using various spectroscopies such as rRaman, low temp infrared, UV-Vis, EPR and NMR as well as ESI-MS, GC and GC-MS methods.

Advisor: Kenneth D. Karlin, Ph.D.

Committee: David. P. Goldberg, Ph.D., V. Sara Thoi, Ph.D.

ACKNOWLEDGEMENT

It has been a long time since I was a fresh college graduate and applying for higher education in the United States. I was extremely grateful to be accepted to one of the most prestigious school, i.e. The Johns Hopkins University. I owe a lot to all the people who helped me through the Ph.D. program in the chemistry department.

I am very grateful to my advisor Professor Kenneth D. Karlin. Dr. Karlin is an enthusiastic researcher and excellent writer. He spent tremendous amount of time helping students understand the essence of his research and his words often sparked with brilliant ideas. There are always lots of people lining up outside Dr. Karlin's office and waiting to talk to him, yet he managed to squeeze time to provide hands-on coaching on everything I possibly needed, no matter if it were experimental details or literature references. Dr. Karlin also coached me on scientific writings for numerus hours and showed me why it is critical to write down all the details of the experiments. I cannot thank him enough for that. Dr. Karlin is also an exceptional listener and communicator. I always felt very easy to talk to him and he seems to understand every time what I am trying to say and identifies what is important. His ideas always saved me weeks of time if I were to find the answers myself. The only thing I would regret is that I should have talked to Dr. Karlin much more frequently.

I also appreciate Professor David Goldberg very much for all his generous help in the past years. Despite his tight schedule, he managed to attend my Oral exam and Graduate Board Oral exam. Dr. Goldberg is an outstanding researcher and excellent teacher and I learnt a lot from him.

I also very appreciate Professor Sara Thoi for agreeing to be my committee in a very short notice. Dr. Thoi is an extremely energetic professor who really love chemistry.

I want to thank all the members in Dr. Karlin's lab for their help. Especially, I want to thank Jeff Liu and for helping with many things. Jeff is the go to person whenever someone needs help. I also want to thank Max for getting all the X-ray structures and checking my samples even sometimes they are not the ones we hoped.

There are also many other researchers that helped along the road. I would like to thank Dr. Jake Ginsbach and Dr. Ryan Cowley from the laboratory of Professor Edward I. Solomon at Stanford University, for critical collaborations with rRaman spectroscopy and DFT calculations. I learnt a lot of new things from them. I also want to thank Professor Matthew-Kieber Emmons (now at the University of Utah) for helping with DFT calculations.

I also want to thank our collaborators Lee Elrod and Ryan Lehane from the laboratory of Professor Eunsuk Kim at Brown University for helping with low temperature infrared spectroscopy. I want to thank Dr. Kim and Dr. Shunich Fukuzumi (then at Osaka University, Japan) and Dr. Solomon for collaboration and helping with our manuscripts.

Finally, I would like to thank my family for their long lasting support and love. To my wife Lingjie, I felt lucky to meet her at Hopkins. Thank you for always being together with me, for encouraging me when I felt defeated, and for supporting me to pursue my career, even sometimes I am uncertain about where to go. To my parents, who are very supportive and give me unconditional love and everything.

Table of Contents

List of Figures

CHAPTER ONE

Peroxo and Superoxo Moieties Bound to Copper Ion: Electron-Transfer Equilibrium with a Small Reorganization Energy

INTRODUCTION

Molecular oxygen (dioxygen; O_2) is abundant and an important energy source *via* its combustion of fuels (e.g., hydrocarbons, H_2, etc.) most often leading to water as byproduct. Dioxygen is also nature's primary source for energy production *via* cellular respiration. In cytochrome *c* oxidase, the terminal respiratory oxidase, a heme-copper active site mediates four-electron-four-proton reduction of O_2 to water **eq. 1** to generate a proton motive force for downstream ATP synthesis.[1] In the "reverse" process, plants and algae harness sunlight through photosynthesis to replenish the earth with dioxygen, converting and storing 130 terawatt equiv of energy per year **eq. 2**.[2] Less is understood concerning this water oxidation chemistry where manganese cluster bound water molecules facilitate oxidative coupling and O-O bond formation to give dioxygen, possibly *via* as yet undetected peroxide or superoxide Mn-species intermediates except in a report on cobalt cluster chemistry by Frei and coworkers.[3]

$$O_2 + 4H^+ + 4e^- \xrightarrow{respiration} 2H_2O \qquad \textbf{(eq. 1)}$$

$$O_2 + 4H^+ + 4e^- \xleftarrow{photosynthesis,hv} 2H_2O \qquad \textbf{(eq. 2)}$$

In biology, Fe/Cu or Cu and Mn protein active-site complexes mediate dioxygen reduction and water oxidation, respectively. It is useful to consider either process in the context of O_2 reduction in metal-free aqueous solution (Figure 1a). There, the nature of the (ir)reversible steps are understood and reduction potentials and pK_a's are known, see Figure 1a.[4] However, such thermodynamic data are lacking when it comes to O_2 and reduced derivatives when they are bound to metal ions except for Co and Rh.

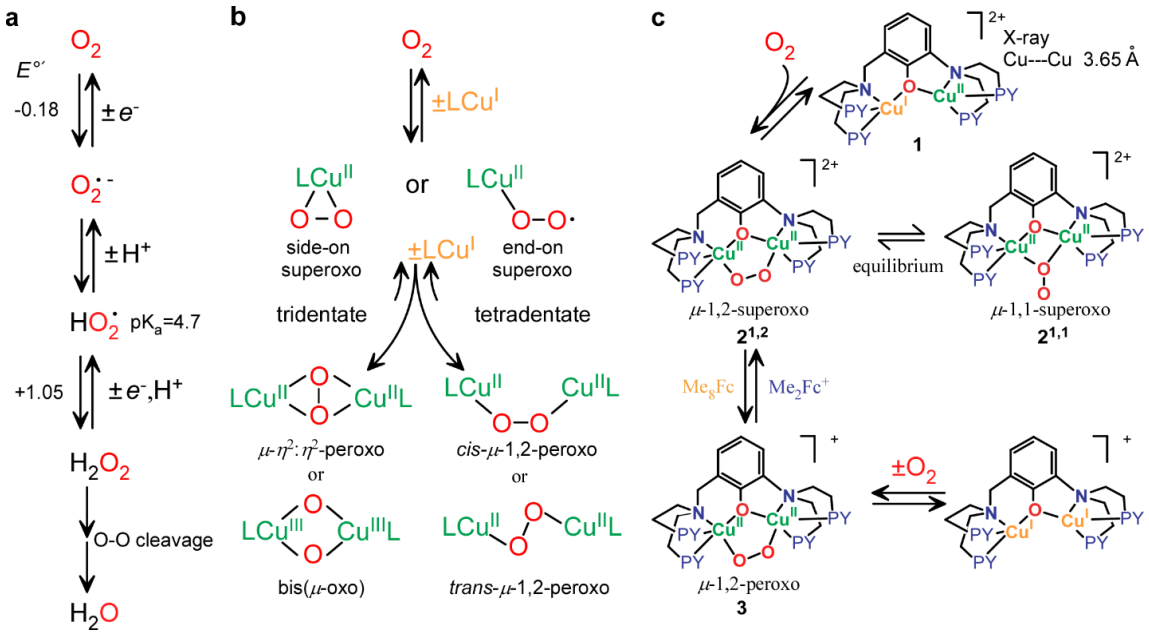

Figure 1. Oxygen reduction and modeling chemistry.

(a) Reduction of molecular oxygen in aqueous media. $E^{o\prime}$ values are the reduction potentials at pH 7 versus NHE[4] (Note: In the text, reduction potential values have been converted to versus SCE, as follows: E_{SCE} (V) = E_{NHE} (V) – 0.242 (V)). (b) Model chemistry of mononuclear LCu^{I} and dinuclear LCu^{I}-$Cu^{I}L$ centers and their reversible reactions with dioxygen. (c) The phenolate-bridged mixed-valent Cu^{I}-Cu^{II} complex $[Cu^{I}Cu^{II}(UN\text{-}O^{-})]^{2+}$ (UN-OH = 2-(bis(2-(pyridin-2-yl)ethyl)amino)-6-((bis(2-(pyridin-2-yl)ethyl)amino)methyl)phenol, UN-O^{-} is the corresponding phenolate) reacts with dioxygen to form a superoxide species, either μ-1,2-$[Cu^{II}_2(UN\text{-}O^{-})(O_2^{\bullet-})]^{2+}$ or μ-1,1-$[Cu^{II}_2(UN\text{-}O^{-})(O_2^{\bullet-})]^{2+}$ isomers, which are in rapid equilibrium (see text). As previously reported, oxygenation of the phenolate dicopper(I) complex $[Cu^{I}_2(UN\text{-}O^{-})]^{+}$ gives the peroxide species $[Cu^{II}_2(UN\text{-}O^{-})(O_2^{2-})]^{+}$. At the center of attention in this report is the

interconversion chemistry of μ-1,2- $[Cu^{II}_2(UN\text{-}O^{-})(O_2^{\bullet-})]^{2+}$ and the peroxide $[Cu^{II}_2(UN\text{-}O^{-})(O_2^{2-})]^{+}$ *via* the use of outer-sphere ferrocenium derived redox agents.

At a fundamental level of knowledge, to uncover how biological transformations occur, such as dioxygen (or derivatives) utilizing reactions in hemes, non-heme iron, copper and manganese enzymes, and/or to build practical and efficient systems for carrying out such reactions as O_2 reduction to water or hydrogen peroxide (i.e., for fuel cells) or water oxidation catalysis, those reactions which are critical to societal energy concerns, the interrelationships of superoxide, (hydro)peroxide and hydroxyl radical must be elucidated wherein entities are bound to metal ions in various environments.

For example, what are the reaction mechanisms for metal-superoxide conversion to metal-peroxide or hydroperoxide species, these in principle being reversible processes involving species with intact O–O bonds? What are the relevant thermodynamics? Surprisingly, even the conversion of a heme-superoxide ("oxy" heme) to heme-(hydro)peroxide (i.e., electron/proton addition), as occurs in the very well studied enzyme P450 monooxygenase enzymes, or their synthetic model compounds, is not thoroughly studied in terms of reaction mechanism or elucidation of applicable thermodynamic parameters.[5]

For an O_2-derived species bound to one or several metal ions, thermodynamic properties relating to redox or protonation will be considerably altered, whether or not in water, in organic solvent, or in a protein active site. For the latter, great variability in local dielectric environment and presence of 2nd-sphere effects (e.g., local amino acid-derived dipoles, or H-bonding groups) may occur, potentially changing the inherent

thermodynamic properties. The complexity of the metal-oxygen species' chemistry is increased by the possibility of having varying superoxide or peroxide coordination modes which likely depends on the nature of the metal ion's surrounding environment, that defined by a ligand or 1st coordination sphere at an enzyme active site. Depending on ligand denticity (e.g., tridentate or tetradentate), a superoxide moiety ligated to copper(II) ion may be bound in an end-on or side-on (η^2) fashion (Figure 1b).[6] Another type of complexity occurs if there are two (or more) metal ions bound to the (su)peroxo entity. Dinuclear Cu_2O_2 species commonly form in LCu^I-O_2 chemistry, deriving from the reversible reaction of a cupric superoxide complex with a second mole equiv of the original LCu^I chelate. Most generally, if the ligand (L) is a tridentate donor, either a $\eta^2:\eta^2$–peroxo or bis-μ-oxo product forms Figure 1b). By contrast, with tetradentate ligands, cupric-superoxide species are led to form *trans*-μ-1,2-peroxo- or *cis*-μ-1,2-peroxo-dicopper(II) complexes (Figure 1b).[6-7]

For the system we describe here, a phenol-containing binucleating ligand ($UN\text{-}O^-$) is employed, giving rise to a series of phenolate-bridged dicopper complexes of various types. We previously showed that a mixed-valent phenolate-bridged Cu(I)Cu(II) complex, $[Cu^{II}Cu^{I}(UN\text{-}O^-)]^{2+}$, reacts with molecular oxygen in a reversible manner, under cryogenic conditions, to give a superoxide-dicopper(II) complex, $[Cu^{II}_2(UN\text{-}O^-)(O_2^{\bullet-})]^{2+}$ (Figure 1c).[8] A closely related species, a peroxo analogue $[Cu^{II}_2(UN\text{-}O^-)(O_2^{2-})]^+$, was generated when the dicopper(I) precursor complex $[Cu^{I}_2(UN\text{-}O^-)]^+$ is (reversibly) oxygenated (Figure 1c). [9]

To carry out this study with biologically relevant copper ion, ligand design and adaption of low-temperature manipulations and characterization techniques have had to be applied. Here, motivated by the need for determining fundamentally important properties of metal-bound oxygen-derived species, we provide a rare case where an equilibrium constant and therefore reduction potential, plus a reorganization energy (Marcus theory lambda (λ) value) can be determined as the outer sphere electron-transfer interconversion of a superoxo and peroxo moiety bound to a dicopper center. The species involved are the metal bound μ-1,2- superoxide moiety in $[Cu^{II}_2(UN\text{-}O^{-})(O_2^{\bullet-})]^{2+}$ and the μ-1,2-peroxide ligand in complex $[Cu^{II}_2(UN\text{-}O^{-})(O_2^{2-})]^{+}$ (Figure 1c). Resonance Raman spectroscopic and DFT analysis also reveals that μ-1,2-$[Cu^{II}_2(UN\text{-}O^{-})(O_2^{\bullet-})]^{2+}$ is in fast equilibrium with a structural isomer, the μ-1,1-superoxide complex $[Cu^{II}_2(UN\text{-}O^{-})(O_2^{\bullet-})]^{2+}$ (Figure 1c).

EXPENRIMENTAL SECTION

General Instrumentations.

All materials purchased were of highest purity available from Sigma-Aldrich Chemicals, Strem Chemicals, or Tokyo Chemical Industries (TCI) and used as received, unless specified otherwise. Dichloromethane (CH_2Cl_2), acetonitrile (CH_3CN) and diethyl ether ($CH_3CH_2OCH_2CH_3$) were used after passing them through a 60 cm long column of activated alumina (Innovative Technologies, Inc.) under argon. Dioxygen was dried by passing through a short column of supported P_4O_{10} (Aquasorb, Mallinkrodt). Preparation and handling of air sensitive complex were performed in an MBraun Labmaster 130

nitrogen atmosphere drybox or under argon atmosphere using standard Schlenk techniques. Solvent deoxygenation was achieved by bubbling with argon for about 40 minutes through addition funnel connected to a receiving Schlenk flask. Elemental analysis was conducted by Columbia Analytical Services and air-sensitive samples were prepared in the glovebox and flame sealed outside using standard Schlenk Technique. UV-vis spectra were recorded with a Cary-50 Bio spectrophotometer equipped with a fiber optic coupler (Varian) and a fiber optic dip probe (Hellma: 661.202-QX-UV-1cm-for-low-temperature) and/or UnispeKs CoolSpeK N40P103410 cryostat controller and cell holder kit by Unisoku Scitific Instruments. NMR spectroscopy was performed on Bruker 300 and/or 400 MHz instruments with spectra calibrated to either internal tetramethylsilane (TMS) standard or to residual protio solvent. EPR measurements were performed on an X-Band Bruker EMX-plus spectrophotometer equipped with a dual mode cavity (ER 4116DM) or Bruker EMX CW EPR controlled with a Bruker ER 041 XG microwave bridge operating at the X band (~9 GHz). X-ray diffraction was performed at the X-ray diffraction facility at the Johns Hopkins University. The X-ray intensity data were measured on an Oxford Diffraction Xcalibur3 system equipped with a graphite monochromator and an Enhance (Mo) X-ray Source (λ = 0.71073Å) operated at 2 kW power (50 kV, 40 mA) and a CCD detector. The frames were integrated, scaled and corrected for absorption using the Oxford Diffraction CrysAlisPRO software package. Resonance Raman spectra were collected with a triple monochromator (Spex 1877 CP with 1200, 1800, and 2400 groves/mm holographic spectropgraph gratings) and a CCD (Andor Newton). Laser excitation (20 mW at the sample) was provided by an argon ion

laser (Innova Sabre 25/7) and a krypton ion laser (Coherent I90C-K). The $^{18}O_2$ gas was purchased from Icon Isotopes as 1L tank with 99% atom percentage. The mixed-isotope O_2 gas was purchased from Icon Isotopes as 25 ml glass bulb containing a statistical mixture of 1:2:1 of ^{16}O-^{16}O : ^{16}O-^{18}O : ^{18}O-^{18}O with 97% atom percentage. Stopped-flow kinetics measurements were performed on a Unisoku RSP-601 stopped-flow spectrometer equipped with a MOS-type highly sensitive photodiode array or a Hewlett-Packard 8453 photodiode-array spectrophotometer using a 10 mm quartz cuvette (10 mm path length) and a Unisoku thermostatted cell holder. The rates were determined through monitoring the decrease in spectral intensity at 510 nm corresponding to $[Cu^{II}_2(UNO^-)](O_2^{2-})(SbF_6)$. UV-vis absorption spectra were recorded on a Hewlett Packard 8453 spectrophotometer and Shimadzu UV-3100PC attached with a UNISOKU thermostat cell holder. DFT calculations were performed with the B3LYP functional with TZVP on copper, oxygen, and nitrogen atoms and SV on carbon and hydrogen with an ultrafine integration grid in dichloromethane as modeled by a Polarizable Continuum Model as implemented in Gaussian 09. Analytical frequency calculations were performed on all stationary points to verify that a local minimum (or transition state) had been found and for comparison to rR data. Low temperature infrared spectra were collected on a Bruker tensor 27 FT-IR spectrophotometer equipped with a liquid nitrogen chilled LN-MCT mid-range detector. A Remspec 619 single-crystal sapphire fiber probe (1100 cm^{-1} to 4000 cm^{-1}) was employed for its temperature endurance and the probe was submerged in a custom made Schlenk reaction tube with 2 side arms. Samples for the infrared studies were first prepared in the glovebox and then transferred to the reaction tube using a 5ml

Hamilton gastight syringe. Electrospray ionization mass spectrometry (ESI-MS) experiments were performed on a Thermo Finnigan LCQ Deca XP Plus spectrometer. GC-MS analysis was carried out on a Shimadzu GC-17A/GCMS0QP5050 gas chromatographs/mass spectrometer.

Synthetic Procedures.

Synthesis of complex $[Cu^{I}_2(UNO^-)](SbF_6)(CH_3CN)$.

The complex $[Cu^{I}_2(UNO^-)](PF_6)(CH_3CN)$ was previously synthesized and characterized.[9] The method employed here is to use $Cu^{I}(CH_3CN)_4(SbF_6)$ instead of the $Cu^{I}(CH_3CN)_4(PF_6)$ salt while other conditions are kept the same. The final product $[Cu^{I}_2(UNO^-)](SbF_6)(CH_3CN)$ was recrystallized with DCM/ether to give a 65% yield of light yellow air sensitive crystals. The purity of the complex was determined by elemental analysis and NMR spectroscopy and X-ray crystal structure in Figure 30, Chapter three. Mw = 961.6. Anal. Calcd for ($C_{37}H_{40}Cu_2F_6N_7OSb$): C, 46.21; H, 4.19; N, 10.20. Found: C, 46.05; H, 4.02; N, 9.93. ^{1}H-NMR (CD_3NO_2; 400MHz): 2.05 (s,3H), 2.45-2.71 (m, 8H), 2.85-2.95 (m,4H), 3.25-3.35 (m, 4H), 3.75 (s, 2H), 6.55 (t(d-d), 1H), 6.89 (d, 1H), 7.05 (t(d-d), 2H), 7.21 (t(d-d), 4H), 7.31 (d,1H), 7.41 (t(d-d), 2H), 7.71 (t(d-d), 2H), 7.79 (t(d-d), 2H), 7.95 (s, br,2H), 9.05 (d, 2H).

Synthesis of complex $[Cu^{II}_2(UNO^-)(OH)](SbF_6)_2$.

The complex $[Cu^{II}_2(UNO^-)(OH)](PF_6)_2$ was previously synthesized and characterized. The method employed here was to use $Cu^{I}(CH_3CN)_4(SbF_6)$ instead of the

$Cu^{I}(CH_3CN)_4(PF_6)$ salt while other conditions were kept the same. The final product $[Cu^{II}_2(UNO^{-})(OH)](SbF_6)_2$ was recrystallized with DCM/ether to give a 45% yield of green crystals. The purity of the complex was determined by elemental analysis and further examined by X-ray crystallography. Mw = 1132.3 Anal. Calcd for ($C_{35}H_{38}Cu_2F_{12}N_6O_2Sb_2$): C, 35.8; H, 3.3; N, 7.2. Found: C, 36.1; H, 3.2; N, 7.4.

Synthesis of complex $[Cu^{I}Cu^{II}(UNO^{-})(DMF)](SbF_6)_2$.

110 mg (0.114 mmol) of the $[Cu^{I}_2(UNO^{-})](SbF_6)(CH_3CN)$ complex charged in a clean vial inside a glovebox. 48 mg (0.114mmol) of $[(Cp)_2Fe]SbF_6$ was dissolved using 3 ml of degassed DMF solvent in the glovebox to obtain a dark blue solution. The $[(Cp)_2Fe]SbF_6$ solution was added dropwise to the vial charged with $[Cu^{I}_2(UNO^{-})](SbF_6)(CH_3CN)$ complex. The light yellow crystals gradually dissolved and the solution turned to a brownish green color, whereupon this solution was left to stir for an hour under a nitrogen atmosphere. Then, the contents of the vial was transferred to a wide neck bottle filled with 15 ml of degassed ether and these were leff to slowly diffuse and mix with the $[Cu^{I}Cu^{II}(UNO^{-})](SbF_6)_2$ solution. After two days, brownish green crystals of $[Cu^{I}Cu^{II}(UNO^{-})(DMF)](SbF_6)_2$ were obtained and the remaining solution turned yellow. Yield; ~70% (95 mg) after washing and drying under nitrogen. Mw =1229.6. Anal. Calcd for ($C_{38}H_{44}Cu_2F_{12}N_7O_2Sb_2$): C, 37.12; H, 3.61; N, 7.98. Found: C, 37.26; H, 3.73; N, 7.68.

Synthesis of complex $[Cu^{II}Cu^{II}(^{NO2}UN\text{-}O^{-})(Cl)](SbF_6)_2(CH_2Cl_2)_2$.

20 mg (0.021 mmol) of $[Cu^{I}Cu^{II}(UNO^{-})(DMF)](SbF_6)_2$ was dissolved in 10 ml of dichloromethane (DCM) solvent and charged into a 50 ml Schlenk flask. The flask was chilled in a dry-ice/acetone bath (-80 °C) under argon using standard Schlenk techniques. The solution was bubbled with excess O_2 for a few seconds and left to react for 1 hr. Then O_2 was removed by applying vaccum/purge (with Ar) cycles. The resulting solution was bubbled with excess $NO_{(g)}$ and let react for 20 mins. With slow warmup of the solution crystals of $[Cu^{II}Cu^{II}(^{NO2}UN\text{-}O^{-})(Cl)](SbF_6)_2(CH_2Cl_2)_2$ were directly obtained.

Synthesis and characterization of ferrocenium hexafluoroantimonate ($FcSbF_6$).

0.55g (1.6 mmol) of silver hexafluoroantimonate ($AgSbF_6$) was charged in a 20 ml vial wrapped with aluminum foil. Ferrocene (Fc. 0.30 g (1.6 mmol), dissolved with 10 ml of diethyl ether was placed in another 20 ml vial and this solution was gradually added to the vial containing $AgSbF_6$., whereupon the solution color changed to green. After stirring for 30 min, a dark green/blue precipitate formed on the bottom of the vial and the solution changed to a yellow color. That supernatant solution was removed with a Pasteur pipette and the solid remaining was redissolved using 10 ml of acetone. This solution was passed through a medium glass-fritted funnel layered with a short Celite column (1 inch) and 30 ml more of acetone was used as eluent to collect all the remaining compound in a round bottom flask (100 ml). This solution was concentrated by rotary evaporation, to about a total of 10 ml and then transferred to a 20 ml vial. This vial was placed into a wide neck bottle containing about 30 ml of diethyl ether at the bottom, and it was allowed to slowly diffuse to the vial with product complex. Royal blue crystals were formed after

~ 12 hours giving 0.4 g (~ 60 % yield). Anal. Calcd for ($C_{10}H_{10}FeSbF_6$): C, 28.5; H, 2.4. Found: C, 28.3; H, 2.5.

Synthesis and characterization of acetyl-ferrocenium hexafluoroantimonate ($AcFcSbF_6$).

0.55g (1.6mmol) of silver hexafluoroantimonate ($AgSbF_6$) was charged in a 50 ml with a 14/20 joint Schlenk flask with a glass stopcock. The flask was sealed with a rubber septum and wrap with aluminum foil. 0.36g (1.6mmol) of acetyl-ferrocene was dissolved in the 20 ml of ether solution in a 100 ml addition funnel. Deoxygenate the ether solution by rigorously bubbling argon for 20 mins. Gradually add the acetyl-ferrocene solution to react with $AgSbF_6$ for 30 mins. The solution gradually turned yellow with dark blue precipitate, then decant the yellow solution under argon, dissolve the precipitate with degassed DCM (remove oxygen by bubbling argon for 20 mins) and filtered through celite using a medium glass-fritted Schlenk funnel under argon and pass the solution to a receiving 100ml Schlenk flask. Add 80 ml of degassed ether to the solution and obtained blue crystal the next day. The yield is about 40% after drying and weight the product. The blue crystal is relatively stable under air when it is dry. Anal. Calcd for ($C_{12}H_{12}FeOSbF_6$): C, 31.1; H, 2.6. Found: C, 30.8; H, 2.7.

Synthesis and characterization of Dimethyl-ferrocenium hexafluoroantimonate (Me_2FcSbF_6).

0.55g (1.6mmol) of silver hexafluoroantimonate ($AgSbF_6$) was charged in a 20 ml vial and wrapped with aluminum foil. Dimethyl ferrocene (Me_2Fc) of 0.34g (1.6mmol) was dissolved with 10ml of diethyl ether in a 20 ml vial and the ferrocene solution was gradually added to the vial containing $AgSbF_6$ whereupon the solution turned into a greenish blue color and after stirring for 30 mins, dark green/blue precipitate was formed on the bottom of the vial and the supernatant solution changed to a yellow color. The supernatant was removed using a glass pipette and redissolve the remaining solid using 10 ml of acetone. This solution was passed through a medium glass-fritted funnel layered with short Celite column (1 inch) and 30 ml more of acetone was used as eluent to collect all the remaining compound in a round bottom flask (100 ml). The solution was concentrated using rotary evaporation, to about 10ml and then transferred to a 20 ml vial. This vial was placed in a wide neck bottle containing about 30 ml of diethyl ether at the bottom and it was allowed to slowly diffuse to the vial. Royal blue crystal was formed overnight and giving 0.42g of product which counts for 60% yield. Anal. Calcd for ($C_{12}H_{16}FeSbF_6$): C, 32.0; H, 3.1. Found: C, 32.2; H, 3.3.

Synthesis and characterization of diphenyl amine ferrocene (Ph_2NFc) and diphenyl amine ferrocenium hexafluoroantimonate ($Ph_2NFcSbF_6$).

Bromoferrocene (0.53g, 2mmol), CuI (0.40g, 2.1mmol), K_2CO_3 (0.55g, 4mmol), Diphenylamine (Ph_2NH) (0.37g, 2.2mmol) are measured respectively. In a 10 ml Schlenk flask charged with a magnetic stir-bar and 4ml of DMSO solvent, freeze and thaw using liquid nitrogen several cycles under vacuum and argon purging to remove air. While keep argon flowing, add the reagents Bromoferrocene, CuI, K_2CO_3 and Diphenylamine into the flask. Seal the flask with a 14/20 rubber septum (and secured with copper wire) and heat the solution to 90 ºC under argon using sand bath while keep stirring for 24 hours. Working up the product using a ½ inch by 8-inch column packed with silica gel and use pure hexane as eluent, the diphenyl amine ferrocene (Ph_2NFc) containing solution was collected and obtained a yield of 35% after drying. Anal. Calcd for ($C_{22}H_{19}FeN$): C, 74.8; H, 5.4. Found: C, 74.5; H, 5.6.

The diphenyl amine ferrocenium hexafluoroantimonate ($Ph_2NFcSbF_6$) was synthesized using the following preps. 0.1g (0.3mmol) of silver hexafluoroantimonate ($AgSbF_6$) was charged in a 20 ml vial wrapped with aluminum foil and dissolve with 5 ml of 90:10 of Dichloromethane: Acetonitrile mixture. 0.11g (0.3mmol) of diphenyl amine ferrocene (Ph_2NFc) was charged in a vial and slowly add the $AgSbF_6$ solution. The

solution was filtered and recrystallized using DCM/pentane to obtain red needle-like crystals. Anal. Calcd for ($C_{22}H_{19}F_6FeNSb$): C, 44.9; H, 3.2. Found: C, 44.6; H, 3.3. The UV-Vis absorption spectrum using various concentration for 1013.9nm band at 0.19mM, 0.095mM, 0.048mM and 0.019mM at -80ºC found to be 0.56, 0.31, 0.18 and 0.01. Therefore, the extinction coefficient at 1013.9 is 2675 M^{-1} cm^{-1}.

Cyclic Voltammetry (CV)

Reduction potentials of the ferrocenes and derivatives were measured using a BAS-100B potentiostat linked to a computer. The ferrocene and derivatives were each prepared as 10 mM solutions in DCM under a nitrogen atmosphere in a round bottom Schlenk flask equipped with 3 side arms sealed with 14/20 rubber septa. CVs were recorded at 25 ºC using a 100 mV/s scan rate. nBu_4NPF_6 (0.1 M) was employed as the supporting electrolyte. In a typical experiment, a standard three-electrode cell was used containing a glassy carbon working electrode, a platinum wire counter electrode, and a reference electrode consisting of a 10 mM solution of Ag/AgCl. The ferrocenium/ferrocene (Fc^+/Fc) couple was employed as external standard to calculate the reduction potentials for the ferrocenium derivatives, and the calculated reduction potentials versus Fc^+/Fc were further calibrated versus SCE and listed in Figure 11a.

Single Crystal X-ray Crystallography

All reflection intensities were measured at 110(2) K using a KM4/Xcalibur (detector: Sapphire3) with enhance graphite-monochromated Mo *K*α radiation (λ =

0.71073 Å) under the program CrysAlisPro (Versions 1.171.34.44/ 1.171.35.11 Oxford Diffraction Ltd., 2010). The same program was used to refine the cell dimensions and for data reduction. The structure was solved with the program SHELXS-2014/7 (Sheldrick, 2008) and was refined on F^2 with SHELXL-2014/7 (Sheldrick, 2008). Analytical numeric absorption corrections based on a multifaceted crystal model were applied using CrysAlisPro. The temperature of the data collection was controlled using the system Cryojet (manufactured by Oxford Instruments). The H atoms were placed at calculated positions using the instructions AFIX 23, AFIX 43 or AFIX 137 with isotropic displacement parameters having values 1.2 or 1.5 times *U*eq of the attached C atoms. For the structure of $[Cu^{II}Cu^{II}(UN\text{-}O^{-})(OH)](SbF_6)_2$, the H atom of the coordinated hydroxide was found from difference Fourier map, and the O–H distance was set to be refined to 0.84(3) Å using one DFIX restraint.

$[Cu^{I}Cu^{II}(UNO^{-})(DMF)](SbF_6)_2$: Fw = 1229.38, yellow-green lath, 0.47 × 0.17 × 0.04 mm^3, triclinic, *P*-1 (no. 2), a = 10.81274(18), b = 11.4439(2), c = 19.1353(3) Å, α = 78.4517(14), β = 78.6462(14), γ = 73.1423(15)°, V = 2195.72(6) $Å^3$, Z = 2, D_x = 1.859 g cm^{-3}, μ = 2.267 mm^{-1}, abs. corr. range: 0.499–0.926. 30479 Reflections were measured up to a resolution of $(\sin \theta/\lambda)_{max}$ = 0.62 $Å^{-1}$. 8625 Reflections were unique (R_{int} = 0.0549), of which 7365 were observed [$I > 2\sigma(I)$]. 634 Parameters were refined with 321 restraints. $R1/wR2$ [$I > 2\sigma(I)$]: 0.0276/0.0658. $R1/wR2$ [all refl.]: 0.0351/0.0682. S = 1.055. Residual electron density found between −0.62 and 0.57 e $Å^{-3}$. The asymmetric unit contains one molecule of Cu(I)–Cu(II) complex and two SbF_6^- counterions. The

structure is mostly ordered, except for one of the two counterions that is found to be disordered over two orientations [occupancy factor of the major component: 0.697(4)].

$[Cu^{II}Cu^{II}(^{NO2}UN\text{-}O^{-})(Cl)](SbF_6)_2\bullet (CH_2Cl_2)_2$: Fw = 1401.64, yellow plate, 0.42 × 0.33 × 0.05 mm^3, triclinic, *P*-1 (no. 2), *a* = 9.5t5(2), *b* = 13.8420(3), *c* = 20.1911(5) Å, α = 106.146(2), β = 93.216(2), γ = 107.792(2)°, *V* = 2402.75(9) Å^3, *Z* = 2, D_x = 1.937 g cm^{-3}, μ = 2.354 mm^{-1}, abs. corr. range: 0.440–0.893. 29451 Reflections were measured up to a resolution of (sin $\theta/\lambda)_{max}$ = 0.62 Å^{-1}. 9714 Reflections were unique (R_{int} = 0.0352), of which 8386 were observed [$I > 2\sigma(I)$]. 678 Parameters were refined using 207 restraints. *R*1/*wR*2 [$I > 2\sigma(I)$]: 0.0264/0.0636. *R*1/*wR*2 [all refl.]: 0.0339/0.0665. S = 1.048. Residual electron density found between −0.78 and 1.19 e Å^{-3}. The structure is mostly ordered, except for one of the two counteanions that is found to be disordered over two orientations [occupancy factor of the major component: 0.530(13)]. The crystal is a phase mixture, for which the major component has the nitrato group attached to C17 with an occupancy of 0.886(4). The minor component being that for which one H atom is attached to C17 (which was initially the expected ligand). After tackling the phase mixture problem, the refinement turned out to be problem free.

$[Cu^{II}Cu^{II}(UN\text{-}O^{-})(OH)](SbF_6)_2$: Fw = 1173.29, green lath, 0.58 × 0.16 × 0.10 mm^3, monoclinic, $P2_1/n$ (no. 14), *a* = 13.5404(4), *b* = 11.2264(4), *c* = 26.4611(11) Å, β = 90.054(3), *V* = 4022.3(3) Å^3, *Z* = 4, D_x = 1.937 g cm^{-3}, μ = 2.469 mm^{-1}, abs. corr. range: 0.399–0.840. 20865 Reflections were measured up to a resolution of (sin $\theta/\lambda)_{max}$ = 0.59

Å^{-1}. 6974 Reflections were unique (R_{int} = 0.0307), of which 6579 were observed [$I > 2\sigma(I)$]. 536 Parameters were refined using 1 restraint. $R1/wR2$ [$I > 2\sigma(I)$]: 0.0377/0.0892. $R1/wR2$ [all refl.]: 0.0410/0.0908. S = 1.040. Residual electron density found between −0.65 and 1.03 e Å^{-3}. The structure is ordered. The crystal was found to be twinned pseudo-merohedrally, and the twin relationship corresponds to a twofold axis found along the c direction. The twin law is described by the matrix: (-1 0 0 / 0 -1 0 / 0 0 1). The batch scale factor refines to 0.4973(9).

Titration Experiments for Superoxide and Peroxide Interconversion

$[Cu^{I}_2(UNO^{-})](SbF_6)(CH_3CN)$ (5.5 mg) was used to prepare a 25 ml stock solution using a 25 ml volumetric flask. From here, 10 ml (0.00231mmol) were transferred to a Schlenk flask and charged with a magnetic stir-bar in the inert-atmosphere box. The Schlenk flask was sealed using a septum and brought out of the glove-box and put into a Dewar filled with acetone/dry and allowed to equilibrate for 10 min. In the meantime, the side-arm of the Schlenk flask was attached to the Schlenk line under an Ar atmosphere. The top septum was removed and a UV-vis Dip-Probe was put into the Schlenk flask while keeping an Ar flow. After ~5 min, a spectrum was recorded for this complex $[Cu^{I}_2(UNO^{-})](SbF_6)$, as shown in Figure 12a (yellow line spectrum). Dioxygen gas was slowly bubbled into the solution for ~ 1 second which allowed for the full formation of $[Cu^{II}_2(UNO^{-})](O_2^{2-})(SbF_6)$ in Figure 12a (purple line spectrum), as evidenced by having no further increase in the intensity of the purple line spectrum after additional O_2-injection. Separately, $[(Cp)_2Fe]SbF_6$ (24 mg) was used to prepare a 5 ml stock solution

and 200 µl put into a 1 ml Hamilton gas-tight syringe. Initially, ¼ equiv (50 µl) of the $[(Cp)_2Fe]SbF_6$ solution was injected which led to the the first red line spectrum Figure 12a, that below the purple line spectrum. Further additions of half and then three-quarter equiv resulted in two more red line spectra, Figure 12a, with isosbestic conversion to the green line spectrum, which corresponds to a fully formed solution of $[Cu^{II}_2(UNO^-)](O_2^-)(SbF_6)_2$, as evidenced by the observation that additional one more equiv from the $[(Cp)_2Fe]SbF_6$ solution led to no change from the green spectrum.

The experiment was repeated several times using varying amounts of $[Cu^{I}_2(UNO^-)](SbF_6)(CH_3CN)$. With 4.4 mg of the $[Cu^{I}_2(UNO^-)](SbF_6)(CH_3CN)$ complex, similar steps were repeated as given by the procedures written just above (Figure 12b) where the purple line spectrum represents the fully formed $[Cu^{II}_2(UNO^-)](O_2^{2-})(SbF_6)$ complex and the green line spectrum was the fully formed superoxide complex $[Cu^{II}_2(UNO^-)](O_2^-)(SbF_6)_2$. Addition of one equivalent of $(Cp^*)_2Fe$ (decamethylferrocene) resulted in near complete ~ 90% regeneration of the $[Cu^{II}_2(UNO^-)](O_2^{2-})(SbF_6)$ which is the black spectrum regeneration of $[Cu^{II}_2(UNO^-)](O_2^{2-})(SbF_6)$ regeneration (Figure 12b; black line spectrum).

The diphenylamine ferrocenium complex (see above), made according to literature, was used and led to the generation of Figure 12c where the ferrocenium and the superoxide reached a equilibrium state and the redox potential was calculated using Nernst equation. The final spectrum is the red with 1 equiv of $Ph_2NFcSbF_6$.

Stopped-flow Kinetics of Superoxide Formation

60 *m*M solutions of $[Cu^{I}_2(UN\text{-}O^{-})](SbF_6)(CH_3CN)$ (1.4 mg in 25 mL) and of 60 mM dimethyl ferrocenium hexafluoroantimonate (Me_2FcSbF_6) (53.9 *m*g in 2 mL) in O_2-free 1,2-dichloroethane were prepared, separately, in a glove box and were placed into 50 mL Schlenk flasks equipped with rubber septa. In a typical experiment, the $[Cu^{II}_2(UN\text{-}O^{-})(O_2^{2-})]^{+}$ complex was formed by direct O_2 bubbling through a 24-inch needle (19-gauge) for 5 minutes into 1 mL of the 60 *m*M solution of $[Cu^{I}_2(UN\text{-}O^{-})]^{+}$, previously transferred in the stopped-flow pre-loading cell, equipped with a rubber septum (and previously flashed with argon gas), through a 2 mL Hamilton syringe equipped with a three-way high-pressure stopcock that allowed syringe flashing with argon gas. After transferring 1 mL of the 60 *m*M dimethyl ferrocenium in a separate pre-loading stopped-flow cell using the same procedure as used for $[Cu^{I}_2(UN\text{-}O^{-})]^{+}$, mixing of $[Cu^{II}_2(UN\text{-}O^{-})(O_2^{2-})]^{+}$ and dimethyl ferrocenium was allowed and UV-visible spectra were collected at various temperature ranging from -55°C to -80°C.

Resonance Raman Spectroscopy for the superoxide and peroxide.

A 2 mM stock solution of $[Cu^{I}_2(UNO^{-})](SbF_6)(CH_3CN)$ in DCM was prepared in the dry box using similar procedures as described above in section 10. Each tube for the Resonance Raman was charged with 500 μl of the stock solution and sealed with septum and parafilm. The tubes were immediately put into acetone/dry ice bath after bringing outside the glove box. A gas tight syringe with a three-way stopper was used for oxygenation. Firstly, the syringe was flushed with argon gas for several cycles, then pure

oxygen $^{16}O_2$ from a sealed Schlenk flask. Note (The O_2 containing Schlenk flask was prepared by vacuum/Ar purge for three cycles and keep under vacuum while sealed by a rubber septum and electrical/parafilm tapes. Then dry O_2 was introduced from a tank of $^{16}O_2$) was used to oxygenate some of the same tubes of dicopper(I) complex. Afterwards, the tube was flame sealed. Note: The sample solution was frozen under LN_2 and flame sealed under an active vacuum. The above steps were repeated in order to generate complexes with $^{18}O_2$. Repeat the above steps for the O^{18} and mixed-isotope oxygen (The O_2 containing Schlenk flask was prepared by vacuum/Ar purge for three cycles and keep under vacuum while sealed by a rubber septum and electrical/parafilm tapes. Then dry O_2 was introduced from a tank of $^{18}O_2$) The mixed-isotope oxygen bulb was connected to a glass adapter sealed with a rubber septum. The adapter and the gas tight three-way syringe were put under vacuum/Ar purge three cycles to remove O_2, respectively. Break the bulb with the metal bar inside the adapter and take the mixed-isotope oxygen with the gas-tight syringe.

Resonance Raman spectra were collected with a triple monochromator (Spex 1877 CP with 1200, 1800, and 2400 groves/mm holographic spectrograph gratings) and a CCD (Andor Newton). Laser excitation (20 mW at the sample) was provided by an argon ion laser (Innova Sabre 25/7) and a krypton ion laser (Coherent I90C-K). Samples in NMR tubes were placed in a liquid nitrogen finger dewar (Wilmad) in a ~135° backscattering configuration and spectra were collected for 5 minutes. The average spectra were baseline corrected with Peakfit Version 4 and individual transitions were fit with Gaussian bands.

Density Functional Theory Calculations.

DFT calculations of superoxide and peroxide were performed with the B3LYP functional with TZVP on copper, oxygen, and nitrogen atoms and SV on carbon and hydrogen with an ultrafine integration grid in dichloromethane as modeled by a Polarizable Continuum Model as implemented in Gaussian 09. Analytical frequency calculations were performed on all stationary points to verify that a local minimum (or transition state) had been found and for comparison to rR data. For all of the computed isomers of the superoxide the S =1/2 wave function was predicted to be lower in energy than the S = 3/2, in agreement with EPR spectroscopy (Figure 2(c)). For the peroxide, the S = 1 state was lower in energy than the S = 0, in agreement with the temperature dependent NMR data (*vide infra*). The Gibbs free energy of the various isomers was computed at -80 °C and contributions of spin contamination to the energy of the broken symmetry wave function (^{BS}E) of the superoxide was removed by computing the S = 3/2 energy (^{4}E) at the same molecular geometry to obtain the spin purified S = 1/2 energy (^{2}E)

While the structures of the superoxide and the peroxide supported by 8 potential isomers of the UN-O^{-} ligand were computed, only isomers that are within 5 kcal/mol are reported.

The reorganization energy of the various UN-O^{-} isomers of the μ-1,2 superoxo and μ-1,2 peroxo structures can be computed as determined previously. The energy of reorganization energy of the oxidized state (λ_{ox}) was determined from the energy difference of the oxidized state at the oxidized and reduced geometries. The

reorganization energy of the reduced state (λ_{red}) was determined in a similar fashion to compute the overall reorganization energy λ.

RESULTS AND DISCUSSION

Structural Characterization of the Mixed-Valent Complex

Synthesis and Crystal Structure of Mixed-Valent Complex $[Cu^{I}Cu^{II}(UN\text{-}O^{-})(DMF)]^{2+}$. After improving on previously developed procedures, the complex $[Cu^{I}Cu^{II}(UN\text{-}O^{-})(DMF)]^{2+}$ could be isolated as single crystal with one coordinated dimethylformamide (DMF) molecule, following the one-electron oxidation of the dicopper(I) complex $[Cu^{I}_{2}(UN\text{-}O^{-})]^{+}$ with ferrocenium hexafluoroantimonate ($FcSbF_6$). In this study, SbF_6^{-} is used as counter anion and dichloromethane (DCM) as solvent unless indicated otherwise (see Experimental Section). The two copper ions in $[Cu^{I}Cu^{II}(UN\text{-}O^{-})(DMF)]^{2+}$ differ in coordination number and geometry, Figure 2a (and see the Supporting Information (SI) for further structural details). Cu1 (Figure 2a) is assigned as the cuprous ion based on its lower coordination number and a Bond Valence Sum Analysis.

BVSA was first proposed by Thorp,[10] according to the equation $s = \exp[(r_0\text{-}r)/B]$ where s represents bond valences; r_0 and B (=0.37) are empirically determined values listed in Table 1. The r values are determined through the bond distances in the crystal structure (Figure 2 (a)). Employing $s = \exp[(r_0\text{-}r)/B]$ and values in Table 1, s(Cu1) = 1.12 and s(Cu2) = 2.16.[10]

Table 1: r and r0 values used to calculate the bond valences (s)

bond	r_0, Å [10]	bond	r, Å	bond	r, Å
Cu^{2+}-N	1.751	Cu1-N1	1.964	Cu2-N4	2.048
Cu^{2+}-O	1.679	Cu1-N2	2.129	Cu2-N5	2.024
Cu^{+}-N	1.595	Cu1-N3	1.989	Cu2-N6	2.180
Cu^{+}-O	1.523	Cu1-O1	2.169	Cu2-O1	1.942
				Cu2-O2	1.991

Cu2 is the oxidized cupric ion (also from BVSA) which is pentacoordinate with a distorted square pyramidal geometry, with $\tau = 0.39$ ($\tau = 1.0$ for trigonal bipyramidal and $\tau = 0.0$ for perfect square pyramidal coordination).[11] The DMF is coordinated to Cu2 *via* its carbonyl O-atom (O2), Figure 2a. The Cu^{I}-Cu^{II} distance in $[Cu^{I}Cu^{II}(UN\text{-}O^{-})(DMF)]^{2+}$ is found to be 3.65 Å.

The X-ray-determined structure with its unsymmetrical nature and assignment of copper ion oxidation states puts complex $[Cu^{I}Cu^{II}(UN\text{-}O^{-})(DMF)]^{2+}$ into the category of a Robin-Day Class I (localized) mixed-valent $Cu^{I}Cu^{II}$ complex.[12] We can conclude that the structure of $[Cu^{I}Cu^{II}(UN\text{-}O^{-})(DMF)]^{2+}$ is maintained in solution based on the observation of a typical (for a single Cu ion) four line Cu^{II} ($I = 3/2$) electron paramagnetic resonance (EPR) spectrum (Figure 2c) with $g_{\|} = 2.25$ at 77 K as previously reported.[8]

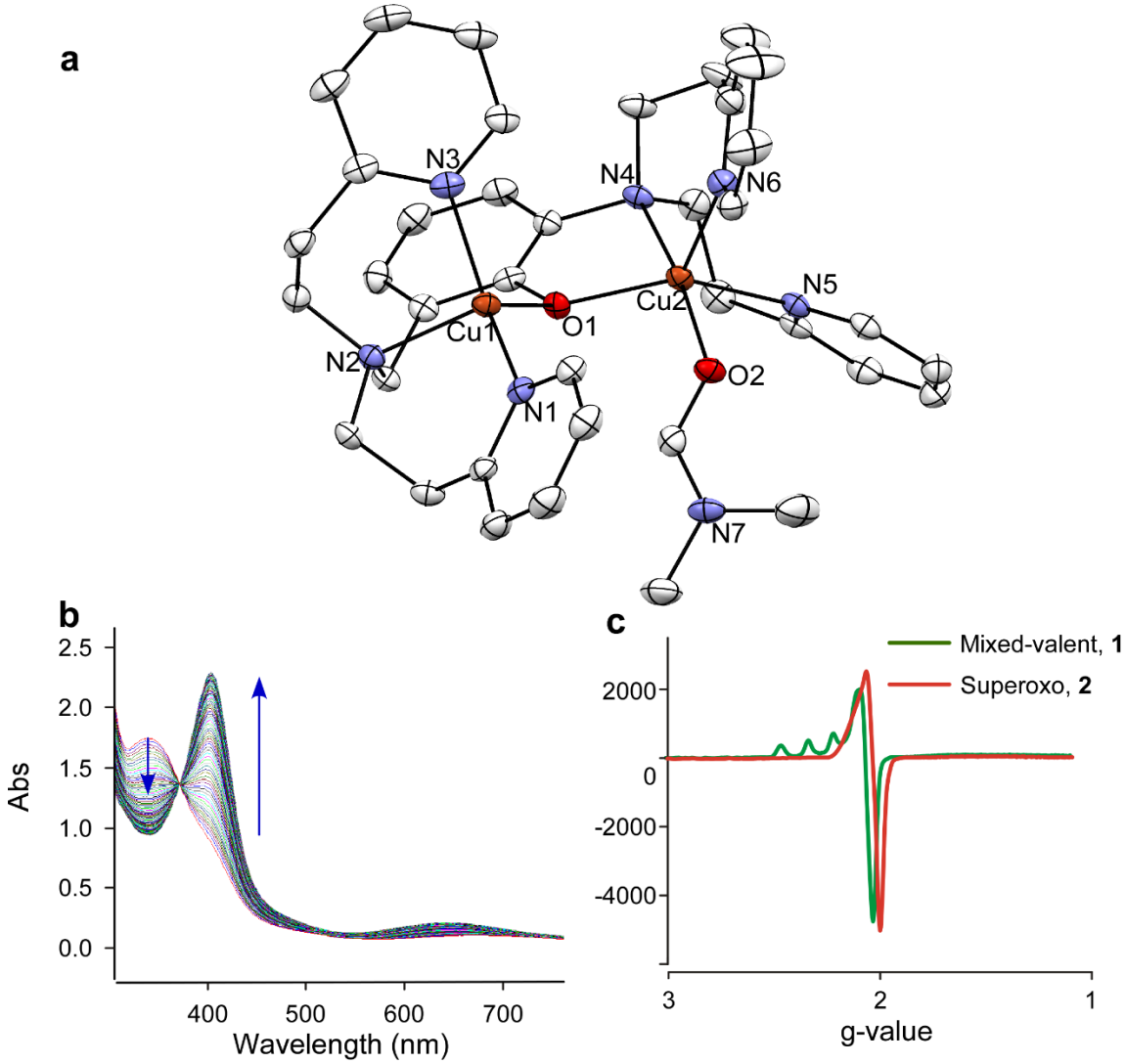

Figure 2. X-ray Structure of the mixed-valent complex, UV-Vis and EPR.

(a) Displacement ellipsoid plot (50% probability level) of the cationic part of the mixed-valent complex $[Cu^{I}Cu^{II}(UN\text{-}O^{-})(DMF)]^{2+}$ at 110(2) K, Cu-Cu = 3.65Å, hydrogen atoms are omitted for clarity. (b) UV-Vis spectral changes due to the formation of superoxide complex $[Cu^{II}_2(UN\text{-}O^{-})(O_2^{\bullet-})]^{2+}$ (λ_{max} = 404 nm) by oxygenation of $[Cu^{I}Cu^{II}(UN\text{-}O^{-})(DMF)]^{2+}$ (λ_{max} = 350 nm) in DCM solution at -80 °C; time period ~ 1

hour. (c) Frozen DCM solution (~ 77 K) EPR spectra of $[Cu^{I}Cu^{II}(UN\text{-}O^{-})(DMF)]^{2+}$ and $[Cu^{II}_{2}(UN\text{-}O^{-})(O_2^{\bullet-})]^{2+}$ (~ 9 GHz).

Table 2. Kinetic Parameters for Selected Ligand-Copper (LCu_n^{I}) Frameworks Leading to 1:1 Cu^{II}_{n}-(O_2) Adducts (n = 1, 2).

ligand	**solvent**	k_{on} **(M^{-1} s^{-1})**	$\Delta H^{\ddagger}$ **:kJ** mol^{-1} $\Delta S^{\ddagger}$ **: J** K^{-1} mol^{-1}	**ref**
UN-O^{-} [a]	DCM	$9.0 \pm 0.2 \times 10^{-2}$ [d]	31.1 ± 1.1 -99 ± 6	this work
XYL-O^{-} [b]	DCM	$> 1 \times 10^{6}$ [d]		13
TMPA [c]	THF	$1.5 \pm 0.1 \times 10^{8}$ [d]	7.62 -45.1	14
PV-TMPA [c]	MeTHF	$6.6 \pm 3.5 \times 10^{5}$ [d]	9 ± 1 -97 ± 7	15
TMG_3tren [c]	MeTHF	$2.1 \pm 1.0 \times 10^{6}$ [d]	10 ± 6 -70 ± 26	15
Me_6Tren [c]	EtCN	$9.5 \pm 0.4 \times 10^{4}$ [e]	17.0 ± 0.2 -68 ± 0.9	16
$HIPT_3$tren [c]	acetone	2.3 ± 0.2 [e]		17
L^{iPr} [c]	THF	$7.6 \pm 0.2 \times 10^{-1}$ [e]	24.4 ± 1.3 -110 ± 7	18
HMe_2L^{iPr2} [c]	THF	1560 ± 19 [f]	18 ± 2 -100 ± 10	19

[a]Binucleating ligand one electron reduced copper-oxygen adduct Cu^{II}_{2}-($O_2^{\bullet-}$). [b]Binucleating ligand two electron reduced copper-oxygen adduct Cu^{II}_{2}-(O_2^{2-}). [c]Mononucleating ligand one electron reduced copper-oxygen adduct Cu^{II}-($O_2^{\bullet-}$). [d] Kinetic data determined at 193 K. [e] Kinetic data determined at 183 K. [f] Kinetic data determined at 223K. See Figure 3 for drawings and full IUPAC names of the ligands.

Formation of Superoxide Complex.

The superoxide μ-1,2-$[Cu^{II}_2(UN\text{-}O^-)(O_2^{\bullet-})]^{2+}$ or μ-1,1-$[Cu^{II}_2(UN\text{-}O^-)(O_2^{\bullet-})]^{2+}$ isomers, where the two are in fast equilibrium based on mixed-isotope resonance Raman spectroscopic and DFT analysis (*vide infra*), can be achieved by directly injecting excess dioxygen into mixed-valent complex solution at -80 °C which is evident by formation of its distinct UV-Vis absorption bands at 404 nm (5400 M^{-1} cm^{-1}) and 635 nm (670 M^{-1} cm^{-1}) (Figure 2b). The superoxide species μ-1,2-$[Cu^{II}_2(UN\text{-}O^-)(O_2^{\bullet-})]^{2+}$ and μ-1,1-$[Cu^{II}_2(UN\text{-}O^-)(O_2^{\bullet-})]^{2+}$ mixture gives an EPR spectrum which whose fine-structure could not be resolved, with a *g* value close to 2.0 (Figure 2c), with no indication for coupling to copper ions. This indicates that the unpaired electron is localized at the superoxide $O_2^{\bullet-}$ center ($S = 1/2$ as ground state), as previously described.[8]

Kinetic data for oxygenation of $[Cu^ICu^{II}(UN\text{-}O^-)]^{2+}$ in DCM could be collected with benchtop UV-Vis Spectroscopy (Figure 2b). A second-order rate constant k_{on} has been calculated to be 9 x 10^{-2} M^{-1} s^{-1} (–80 °C, 193 K) (Table 3) based on k_{obs} data and using the value $[O_2]$ = 2.0 mM for oxygen saturated DCM solution at -80 °C.[13]Activation parameters could also be determined (Table 3), (Figure 4) for the Eyring plot.[15]

$$\ln\frac{k}{T} = -\frac{\Delta H^{\neq}}{R}\cdot\frac{1}{T} + \ln\frac{k_B}{h} + \frac{\Delta S^{\neq}}{R}$$

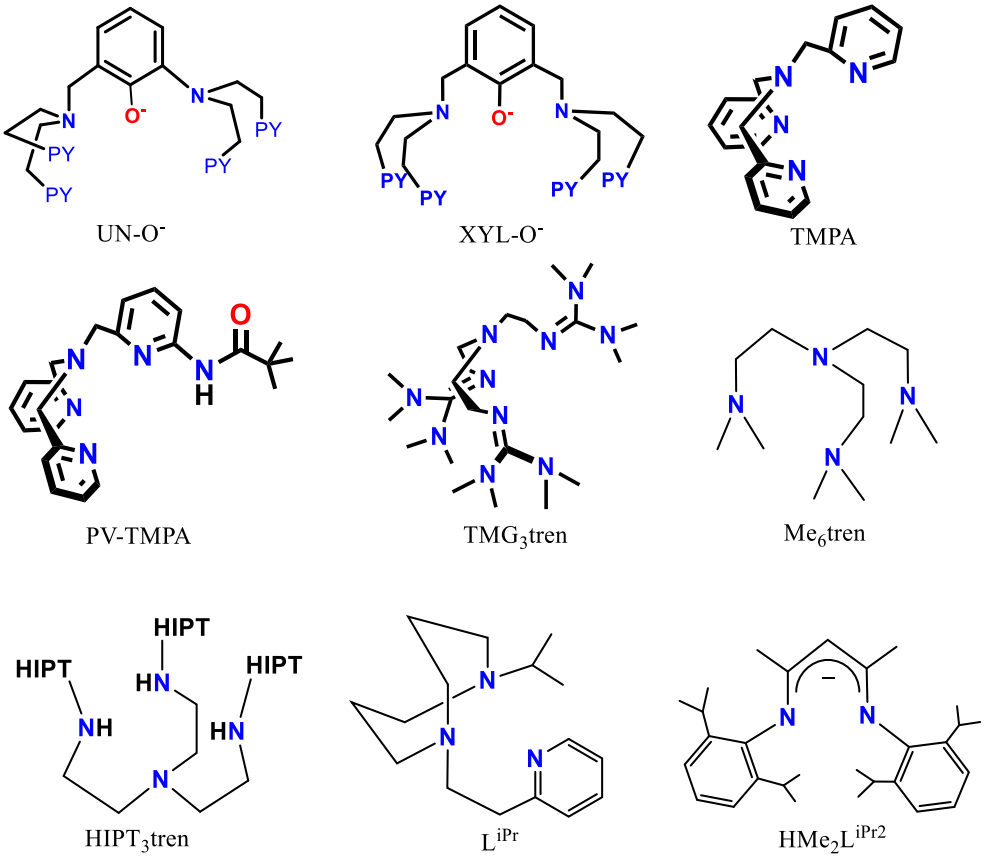

Figure 3. Drawings of the ligands listed in Table 2.

UN-OH = 2-(bis(2-(pyridin-2-yl)ethyl)amino)-6-((bis(2-(pyridin-2-yl)ethyl)amino)methyl)phenol; XYL-OH = 2,6-bis((bis(2-(pyridin-2-yl)ethyl)amino)methyl)phenol; TMPA = tris(2-methylpyridyl)amine; PV-TMPA = bis(pyrid-2-ylmethyl)[[6-(pivalamido)pyrid-2-yl]-methyl]amine; TMG_3tren = 1,1,1-tris-2-[N2-(1,1,3,3-tetramethylguanidino)]ethylamine); Me_6tren = tris(2-dimethylaminoethyl)amine; $HIPT_3$tren = tris(hexaisopropylterphenyl) amine; L^{iPr} = 1-isopropyl-5-[2-(2-pyridyl)ethyl]-1,5-diazacyclooctane; HMe_2L^{iPr2} = pentane-2,4-diylbis((2,6-diisopropylphenyl)-l2-azane), hydrogen salt.

Calculated value of the activation enthalpy and entropy as follows. $\Delta H^{\neq} = 31.1 \pm 1.1 kJ/mol, \quad \Delta S^{\neq} = -99.4 \pm 6.0 J/K \cdot mol$

The low-temperature rate constants for oxygenation of $[Cu^{I}Cu^{II}(UN\text{-}O^{-})(DMF)]^{2+}$, k_{on}, is small compared to many other ligand-Cu^{I}/O_2 reaction systems like those where TMPA, PV-TMPA, TMG_3tren, Me_6tren and $HIPT_3$tren (Table 2 and Figure 3) are all tripodal tetradentate N_4 ligands. All except $HIPT_3$tren are good donors and there is good steric access to the copper ion center; thus, the rate constants are very large, greater than 10^5 M^{-1} s^{-1}. The O_2-reaction with $[(Me_6tren)Cu^{I}]^{+}$ is slower because the solvent used was propionitrile, which is known to strongly compete with O_2 binding to the cuprous ion.[16] Reactions with the tridentate ligand-Cu(I) complexes (ligands, L^{iPr})[18] or the bidentate ligand-Cu(I) complex (L, HMe_2L^{iPr2}, a mono-anion)[19] are quite slow (Table 2), probably also for reasons of steric access to the copper ion, see drawings of the ligands in the Figure 3.

A contrasting reaction is the oxygenation of the dicopper(I) complex $[Cu^{I}_2(XYL\text{-}O^{-})]^{+}$ with dioxygen, involving a two-copper two-electron O_2-reduction to the peroxide dicopper(II) complex $[Cu^{II}_2(XYL\text{-}O^{-})(O_2^{2-})]^{+}$, which is exceedingly fast, too fast to be measured by stopped-flow kinetics-spectroscopy even at 193 K. This result is mentioned and tabulated here, because of the close analogy of the ligands XYL-O^{-} and UN-O^{-}, the former being a symmetric analog of the latter (Figure 3).

Table 3: Kinetics data for $[Cu^{II}_2(UNO^-)](O_2^-)(SbF_6)_2$ formation at various temperature

ln(k/T)	1/T (K^{-1})
-8.52	0.00546
-8.08	0.00532
-7.66	0.00518
-7.06	0.00505
-6.50	0.00492
-6.16	0.00481

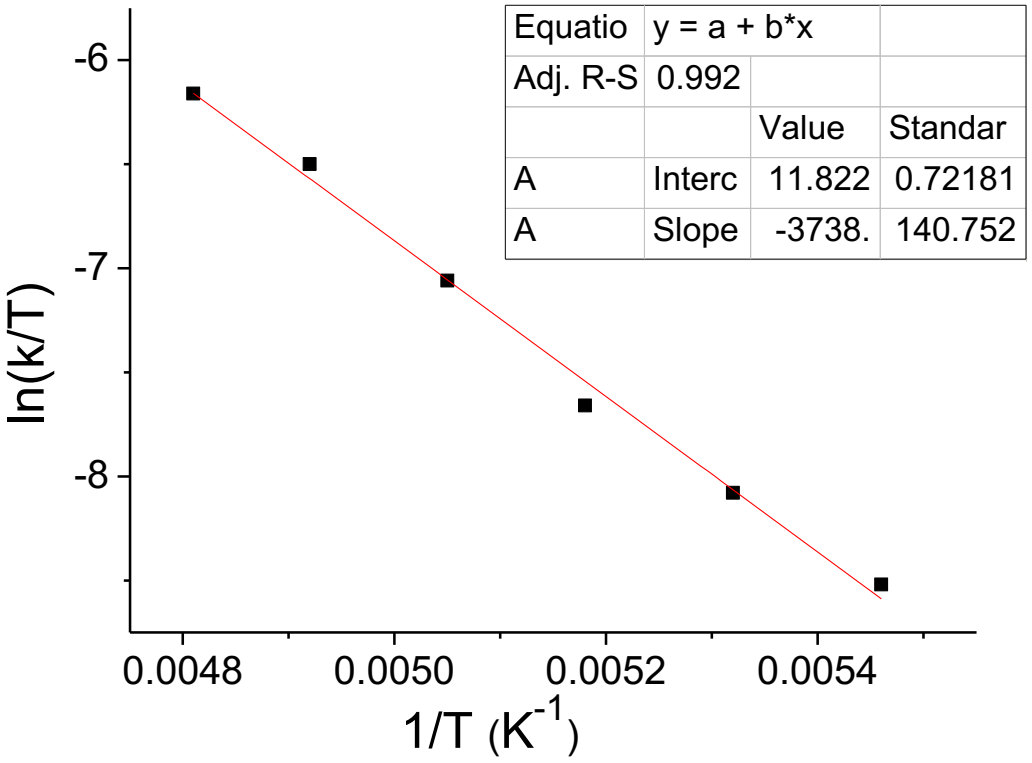

Figure 4. Eyring plot for kinetic results obtained on $[Cu^{II}_2(UNO^-)](O_2^-)(SbF_6)_2$

rRaman and DFT Analysis the Superoxide Complex.

Laser excitation of frozen solutions of the superoxo complex consisting of μ-1,2-$[Cu^{II}_2(UN\text{-}O^{-})(O_2^{\bullet-})]^{2+}$ and μ-1,1-$[Cu^{II}_2(UN\text{-}O^{-})(O_2^{\bullet-})]^{2+}$ (*vide infra*) at 407 nm yield rR spectra that confirm the presence of a copper superoxide complex (Figure 5, bottom). The presence of two oxygen isotope sensitive features (1144 cm^{-1} $\Delta^{18}O_2$ = -61 cm^{-1} and 1120 cm^{-1} $\Delta^{18}O_2$ = -65 cm^{-1}) corresponds to two superoxide O–O stretches indicating the presence of two, distinct superoxide isomers. Additionally, two oxygen isotope sensitive Cu–O stretches are observed at lower energy (478 cm^{-1} $\Delta^{18}O_2$ = –22 cm^{-1} and 383 cm^{-1} $\Delta^{18}O_2$ = -26 cm^{-1}, note the $^{18}O_2$ feature at 367 cm^{-1} is split into two features due to a Fermi resonance). Experimental evidence to distinguish between potential superoxide binding modes (μ-1,1- vs μ-1,2-) in $[Cu^{II}_2(UN\text{-}O^{-})(O_2^{\bullet-})]^{2+}$ could be obtained from preparing rR samples with mixed isotope dioxygen (a 1:2:1 statistical mixture of $^{16}O_2$:$^{16,18}O_2$:$^{18}O_2$). This spectrum (green, Figure 5, top) does not indicate the presence of an intermediate Cu–O stretch (Figure 5, top and Figure 7). As for the analysis of an end-on bound superoxo-copper(II) mononuclear complex,[20] these considerations indi-cate that the observed Cu–O vibrations originate from *m*-1,1- superoxide isomers since only a single oxygen atom is coordinated to both Cu(II) ions. In contrast, the mixed isotope sample of a μ-1,2-isomer would yield a Cu–O stretch with energy approximately half way between the corresponding $^{16}O_2$ and $^{18}O_2$ vibrations since both oxygen atoms are coordinated to the Cu(II) ions. Insight into the origin of the multiple superoxide isomers observed in the rR spectra was determined from a comparison of the ligand geometry

over a number of new crystal structures containing the UN-O^{-} dicopper framework; [Cu$^{II}_2$(^{NO2}UN-O^{-})(Cl)]$^{2+}$ and

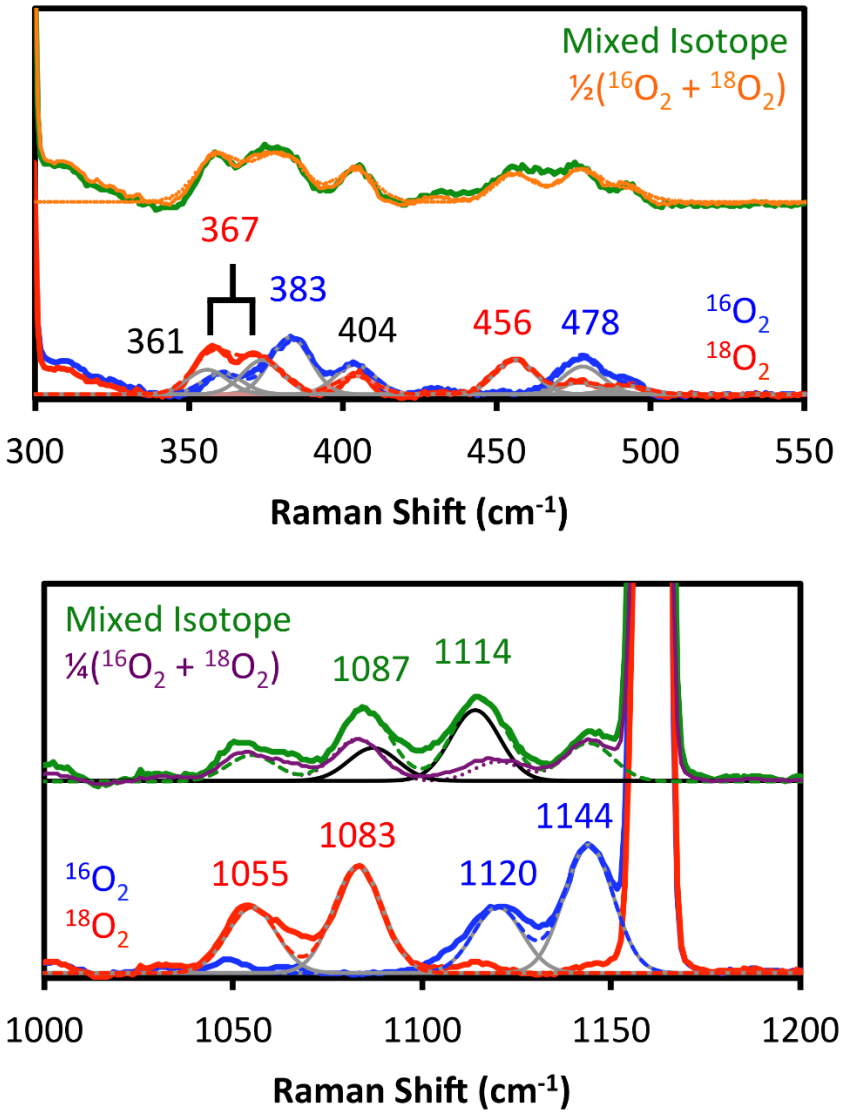

Figure 5. Resonance Raman of the superoxide.

(a) Resonance Raman spectra of [Cu$^{II}_2$(UN-O^{-})(O$_2^{\bullet-}$)]$^{2+}$ with 407 nm excitation; $^{16}O_2$ (blue), $^{18}O_2$ (red), mixed isotope (a 1:2:1 mixture of $^{16}O_2$:$^{16,18}O_2$:$^{18}O_2$ green), ¼($^{16}O_2$ + $^{18}O_2$) (purple), and ½($^{16}O_2$ + $^{18}O_2$) (orange) and Gaussian fits (individual transitions are

grey for $^{16}O_2$ and $^{18}O_2$ and black for mixed isotope while the Gaussian sum for each spectrum is shown as a dashed curve).

$[Cu^{II}_2(UN\text{-}O^-)(OH)]^{2+}$ possess a phenolato O-atom bridge, plus either a μ-chloride or μ-hydroxide anion. In these complexes, the UN-O^- ligand adopts a number of different conformations depending on the crystallization conditions and the anion coordinating to the copper. To gather additional insights into the structure of $[Cu^{II}_2(UN\text{-}O^-)(O_2^{\bullet-})]^{2+}$, density functional theory (DFT) calculations were performed on a number of these ligand conformations (Figure 7). A number of μ-1,1-superoxide isomers were found to have a similar energy and Cu…Cu distances in the range of 3.27-3.28 Å, very reasonable for a single atom bridging the two copper(II) ions, as the same Cu…Cu distance is observed for the structural analogues μ-chloride complexes 3.25 Å.

The computed O–O stretching frequencies of the isomers are predicted to be within 10 cm^{-1} of each other. Thus, due to the large experimental difference between the observed O–O frequencies (24 cm^{-1}), the solution likely also has a different type of isomer, a μ-1,2-superoxo form.

As a result, we considered the possibility of a μ-1,2-superoxide species being present in solution. DFT calculations of a μ-1,2- isomer (Table 5-7) indicate a number of potential structures with a similar energy (all of the isomers in Tables 4-6 are within 5 kcal/mol of each other) and Cu...Cu distances average about 3.47 Å (Table 5-7). In addition, the O–O stretch of the μ-1,2- isomers are predicted to be similar and ~ 25 cm^{-1} higher than the O–O stretch of the μ-1,1-isomers, in good agreement with the experimental data, and also supporting the results above.

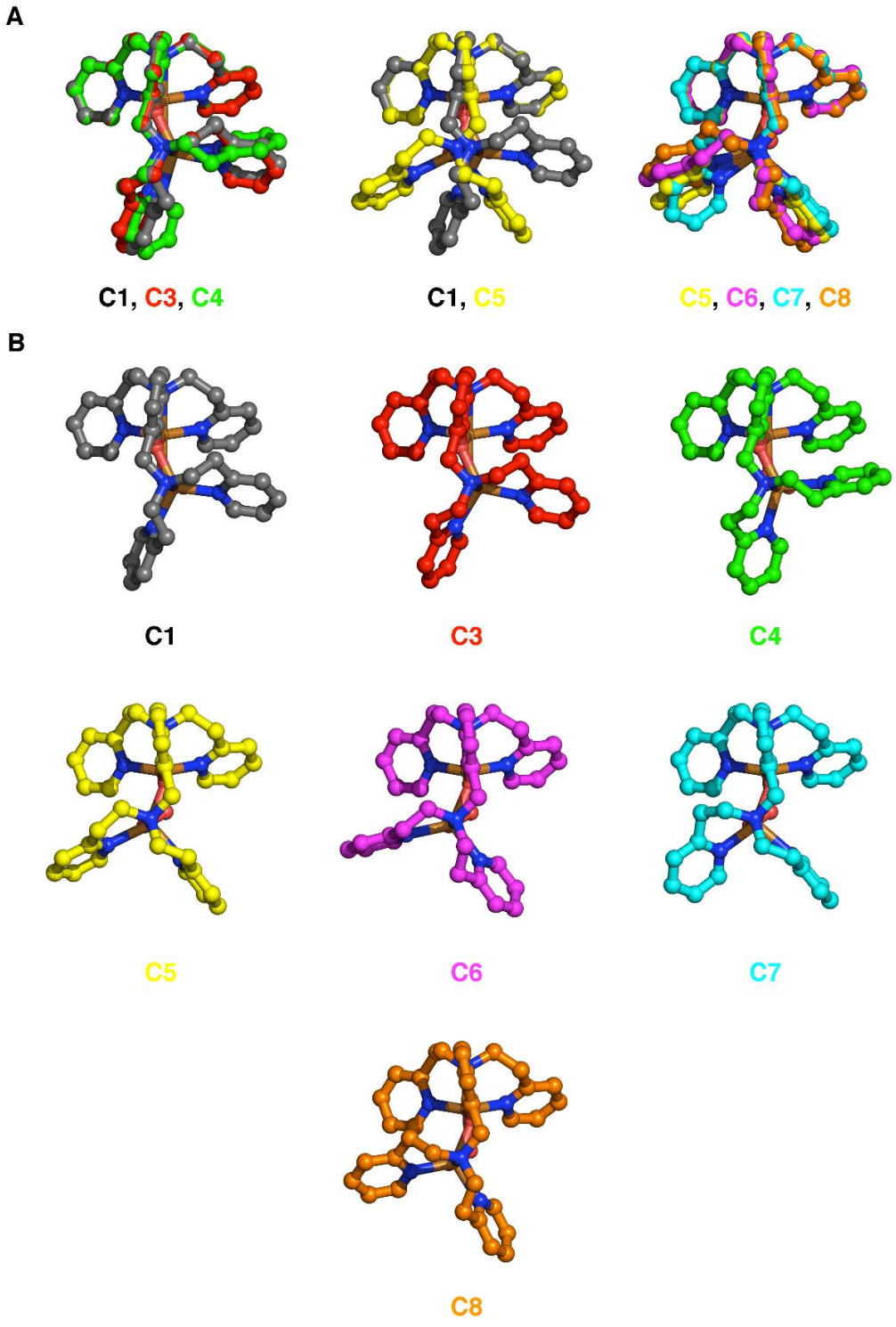

Figure 6. DFT determined UN-O- ligand conformations.

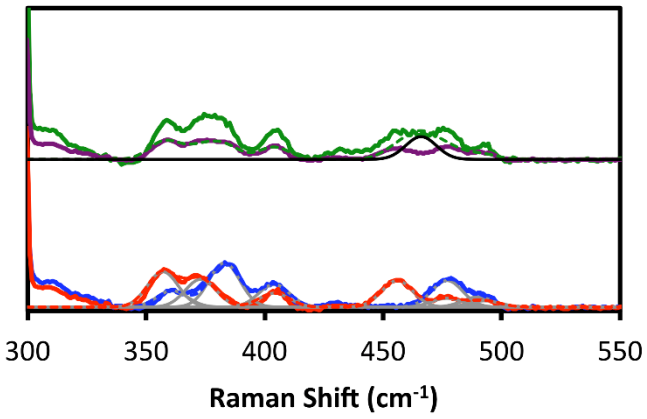

Figure 7. Resonance Raman (Cu-O) spectra of the superoxide.

407 nm excitation; $^{16}O_2$ (blue), $^{18}O_2$ (red), mixed isotope (a 1:2:1 mixture of $^{16}O_2$:$^{16,18}O_2$:$^{18}O_2$ green), and ¼($^{16}O_2$ + $^{18}O_2$) (orange) and Gaussian fits (individual transitions are grey for $^{16}O_2$ and $^{18}O_2$ and black for mixed isotope while the Gaussian sum for each spectrum is shown as a dashed curve). Attempts to fit the mixed isotope spectrum (green) with an intermediate Cu–O stretch at ~ 467 cm^{-1} yield a spectral shape (dashed green curve) that is in poor agreement with the experimental data.

Table 4: Computational details for the lowest energy μ-1,1-superoxo isomers of $[Cu^{II}_2(UNO^-)](O_2^-)(SbF_6)_2$

	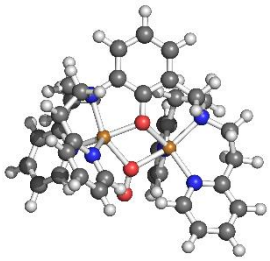	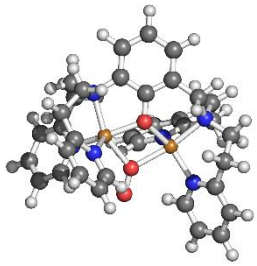	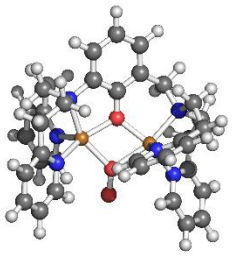
	μ-1,1-S^{C1}	**μ-1,1-S^{C4}**	**μ-1,1-S^{C5}**
Functional	UB3LYP	UB3LYP	UB3LYP
Basis Set	TZVP (Cu, O, N) SV (C, H)	TZVP (Cu, O, N) SV (C, H)	TZVP (Cu, O, N) SV (C, H)
Charge	2	2	2
Multiplicity	2	2	2
Point Group	C_1	C_1	C_1
Solvation	PCM in dichloromethane	PCM in dichloromethane	PCM in dichloromethane
Integral Grid	Ultrafine	Ultrafine	Ultrafine
SCF Energy (a.u.)	-5189.84381744	-5189.84585763	-5189.84391736
S^2	1.6426	1.6307	1.6476
ΔG (kcal, -80° C)	4.8	2.4	4.6
$\nu_{O\text{-}O}$ (cm^{-1})	1206	1211	1210
	Selected Metrical Parameters		
Cu_N•••Cu_{Me} (Å)	3.286	3.272	3.283
O–O (Å)	1.292	1.292	1.295
Cu_N–O (Å)	2.116	2.075	2.101
Cu_{Me}–O (Å)	2.072	2.145	2.149
Cu_N–$O_{PhO\text{-}}$ (Å)	1.964	1.990	1.991
Cu_{Me}–$O_{PhO\text{-}}$ (Å)	2.095	1.996	1.975
Cu_N–N (Å)	2.013, 2.109, 2.203	2.028, 2.123, 2.188	2.053, 2.086, 2.217
Cu_{Me}–N (Å)	2.110, 2.121, 2.131	2.026, 2.111, 2.249	2.013, 2.113, 2.242
	Selected Spin Densities		
Cu_N	-0.57	0.53	0.53
Cu_M	0.51	-0.56	-0.57
O_2	0.44, 0.69	0.42, 0.67	0.42, 0.66

Table 5: Computational details for the lowest energy *μ*-1,2-superoxo isomers of $[Cu^{II}_2(UNO^-)](O_2^-)(SbF_6)_2$

	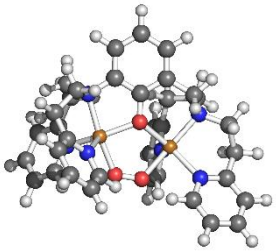	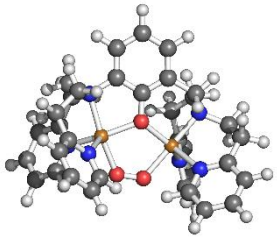	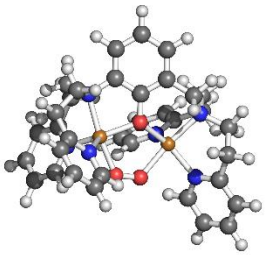
	μ-1,2-S^{C1}	**μ-1,2-S^{C3}**	**μ-1,2-S^{C4}**
Functional	UB3LYP	UB3LYP	UB3LYP
Basis Set	TZVP (Cu, O, N) SV (C, H)	TZVP (Cu, O, N) SV (C, H)	TZVP (Cu, O, N) SV (C, H)
Charge	2	2	2
Multiplicity	2	2	2
Point Group	C_1	C_1	C_1
Solvation	PCM in dichloromethane	PCM in dichloromethane	PCM in dichloromethane
Integral Grid	Ultrafine	Ultrafine	Ultrafine
SCF Energy (a.u.)	-5189.84854879	-5189.84658507	-5189.85132448
S^2	1.6667	1.6734	1.6679
ΔG (kcal, -80° C)	1.7	3.0	0.0
$\nu_{O\text{-}O}$ (cm^{-1})	1238	1235	1231
	Selected Metrical Parameters		
Cu_N•••Cu_{Me} (Å)	3.486	3.460	3.473
O–O (Å)	1.292	1.295	1.293
Cu_N–O (Å)	2.019	2.026	2.013
Cu_{Me}–O (Å)	2.040	2.035	2.080
Cu_N–$O_{PhO\text{-}}$ (Å)	2.003	2.002	2.020
Cu_{Me}–$O_{PhO\text{-}}$ (Å)	2.068	2.044	2.013
Cu_N–N (Å)	2.078, 2.102, 2.216	2.074, 2.101, 2.222	2.091, 2.100, 2.192
Cu_{Me}–N (Å)	2.080, 2.132, 2.175	2.055, 2.083, 2.242	2.066, 2.101, 2.247
∠Cu_N–O–O–Cu_M (°)	-14.4	-8.7	8.4
	Selected Spin Densities		
Cu_N	0.55	0.53	0.54
Cu_M	-0.57	-0.56	-0.57
O_2	0.43, 0.61	0.42, 0.66	0.46, 0.62

Table 6: Computational details for the lowest energy *μ*-1,2-superoxo isomers of $[Cu^{II}_2(UNO^-)](O_2^-)(SbF_6)_2$

	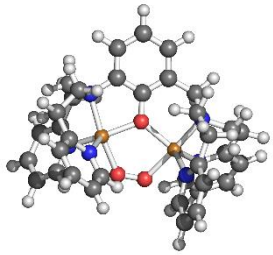	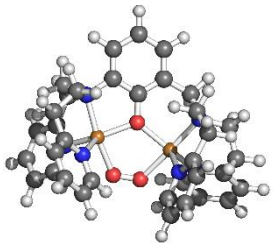
	μ-1,2-S^{C5}	**μ-1,2-S^{C6}**
Functional	UB3LYP	UB3LYP
Basis Set	TZVP (Cu, O, N) SV (C, H)	TZVP (Cu, O, N) SV (C, H)
Charge	2	2
Multiplicity	2	2
Point Group	C_1	C_1
Solvation	PCM in dichloromethane	PCM in dichloromethane
Integral Grid	Ultrafine	Ultrafine
SCF Energy (a.u.)	-5189.84560258	-5189.84577736
S^2	1.6855	1.6818
ΔG (kcal, -80° C)	4.0	4.3
$\nu_{O\text{-}O}$ (cm^{-1})	1232	1231
	Selected Metrical Parameters	
Cu_N•••Cu_{Me} (Å)	3.485	3.499
O–O (Å)	1.296	1.295
Cu_N–O (Å)	2.024	2.023
Cu_{Me}–O (Å)	2.034	2.047
Cu_N–$O_{PhO\text{-}}$ (Å)	1.989	2.002
Cu_{Me}–$O_{PhO\text{-}}$ (Å)	2.050	2.031
Cu_N–N (Å)	2.080, 2.101, 2.217	2.094, 2.104, 2.212
Cu_{Me}–N (Å)	2.009, 2.180 2.207	2.048, 2.100, 2.253
∠Cu_N–O–O–Cu_M (°)	0.7	4.3
	Selected Spin Densities	
Cu_N	0.55	0.55
Cu_M	-0.58	-0.58
O_2	0.44, 0.62	0.45, 0.61

Table 7: Computational details for the lowest energy μ-1,2-superoxo isomers of $[Cu^{II}_2(UNO^-)](O_2^-)(SbF_6)_2$

	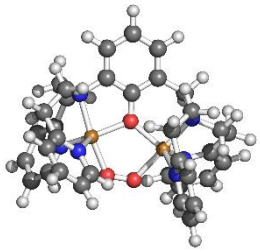	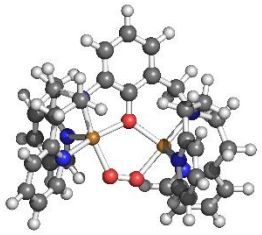
	μ-1,2-S^{C7}	**μ-1,2-S^{C8}**
Functional	UB3LYP	UB3LYP
Basis Set	TZVP (Cu, O, N) SV (C, H)	TZVP (Cu, O, N) SV (C, H)
Charge	2	2
Multiplicity	2	2
Point Group	C_1	C_1
Solvation	PCM in dichloromethane	PCM in dichloromethane
Integral Grid	Ultrafine	Ultrafine
SCF Energy (a.u.)	-5189.84610235	-5189.84712413
S^2	1.6787	1.6783
ΔG (kcal, -80° C)	3.3	2.9
$\nu_{O\text{-}O}$ (cm^{-1})	1232	1238
Selected Metrical Parameters		
Cu_N•••Cu_{Me} (Å)	3.452	3.500
O–O (Å)	1.294	1.293
Cu_N–O (Å)	2.023	2.029
Cu_{Me}–O (Å)	2.045	2.036
Cu_N–$O_{PhO\text{-}}$ (Å)	2.008	1.987
Cu_{Me}–$O_{PhO\text{-}}$ (Å)	2.033	2.061
Cu_N–N (Å)	2.105, 2.110, 2.172	2.041, 2.092, 2.262
Cu_{Me}–N (Å)	2.051, 2.088, 2.206	2.096, 2.122, 2.171
∠Cu_N–O–O–Cu_M (°)	7.6	7.6
Selected Spin Densities		
Cu_N	0.55	-0.58
Cu_M	-0.58	0.54
O_2	0.45, 0.62	0.45, 0.63

Table 8. Select vibrations for μ-1,1-S^{C4} and their predicted isotope shift (cm^{-1}).

	^{16}O–^{16}O	^{16}O–^{18}O	^{18}O–^{18}O
$\nu_{O\text{–}O}$	1211	1177, 1175	1144
Sym $\nu_{Cu\text{–}O}$	466	464, 431	430
Antisym $\nu_{Cu\text{–}O}$	280	280, 249	247

Table 9. Select vibrations for μ-1,2-S^{C4} and their predicted isotope shift (cm^{-1}).

	^{16}O–^{16}O	^{16}O–^{18}O	^{18}O–^{18}O
ν_{O-O}	1230	1197, 1197	1161
Sym ν_{Cu-O}	469	455, 452	443
Antisym ν_{Cu-O}	321	317, 314	312

Table 10: Computational details for the interconversion of μ-1,1-S^{C4} and μ-1,2-S^{C4}.

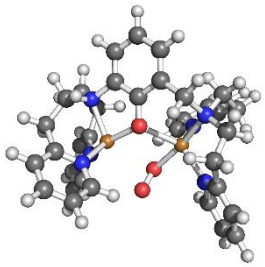

	TS-S^{C4}
Functional	UB3LYP
Basis Set	TZVP (Cu, O, N) SV (C, H)
Charge	2
Multiplicity	2
Point Group	C_1
Solvation	PCM in dichloromethane
Integral Grid	Ultrafine
SCF Energy (a.u.)	-5189.83473963
S^2	1.7378
ΔG (kcal, -80° C)	9.8
Imaginary Frequencies	1
Selected Metrical Parameters	
Cu_N•••Cu_{Me} (Å)	3.514
O–O (Å)	1.288
Cu_N–O (Å)	2.679, 2.827
Cu_{Me}–O (Å)	2.034, 2.845
Cu_N–O_{PhO-} (Å)	1.923
Cu_{Me}–O_{PhO-} (Å)	2.243
Cu_N–N (Å)	1.984, 2.103, 2.109
Cu_{Me}–N (Å)	2.100, 2.145, 2.153
$\angle Cu_N$–O–O–Cu_M (°)	92.7
Selected Spin Densities	
Cu_N	-0.59
Cu_M	0.44
O_2	0.65, 0.73

Hence, these calculations are able to reproduce two sets of O–O stretching frequencies that experimentally differ by 24 cm^{-1} being a mixture of μ-1,1- and a μ-1,2-superoxide isomers. From these structures, the observed rRaman features can be assigned where the 1144 cm^{-1} feature corresponds to the O–O stretch of the μ-1,2- isomer while the 1120 cm^{-1} stretch results from the μ-1,1-isomer. From the mixed isotope spectrum, the 478 cm^{-1} and 383 cm^{-1} features must result from the μ-1,1-isomer and correspond to symmetric and antisymmetric Cu–O stretching frequencies (Tables 8-9). The mixed isotope experiments conclusively demonstrate that the origin of these features are from a μ-1,1-adduct because of lack of observation of a peak "in the middle" of the 16O−Cu and 18O−Cu features, which would result from a μ-1,2 adduct at the average of the two stretches. Within the quality of our data, we are unable to locate a Cu−O stretch from the μ-1,2 component, which suggests that it must have either or both a weak intensity and/or is underneath the isotope sensitive bands we are observing. The increased intensity of the O−O could be linked to a decreased intensity of the Cu−O. However, this level of analysis is not possible given (1) the quality of the data as these are all weak features, and (2) the complications from all the different ligand conformational isomers. Five batches of samples were used, and the experimental results were in agreement. Thus, we choose to not speculate on this point in the manuscript, as the O−O region is diagnostic regarding the presence of μ-1,1 and μ-1,2 superoxide. DFT calculations also indicate that a transition state with a low barrier (less than or equal to 5 kcal/mol) connects these two superoxide-dicopper(II) structural isomers (Table 10), suggesting that they are able to rapidly interconvert in solution. Another line of supporting evidence comes from when

the superoxide $[Cu^{II}_2(UN\text{-}O^{-})(O_2^{\bullet-})]^{2+}$ rR samples are prepared from oxidation of the peroxide $[Cu^{II}_2(UN\text{-}O^{-})(O_2^{2-})]^{+}$ using one equivalent of $AgSbF_6$. Then, the same spectrum containing both μ-1,2-$[Cu^{II}_2(UN\text{-}O^{-})(O_2^{\bullet-})]^{2+}$ and μ-1,1-$[Cu^{II}_2(UN\text{-}O^{-})(O_2^{\bullet-})]^{2+}$ are recorded. Since the oxidation of $[Cu^{II}_2(UN\text{-}O^{-})(O_2^{2-})]^{+}$ would directly generate μ-1,2-$[Cu^{II}_2(UN\text{-}O^{-})(O_2^{\bullet-})]^{2+}$ (*vide infra*), the additional presence of μ-1,1-$[Cu^{II}_2(UN\text{-}O^{-})(O_2^{\bullet-})]^{2+}$ proves that the two isomers are interconvertible, in agreement with DFT predictions.

rRaman and DFT analysis of peroxide complex conformations.

The peroxide species $[Cu^{II}_2(UN\text{-}O^{-})(O_2^{2-})]^{+}$ can be generated by direct oxygenation of the (LCu^{I}_2) species through injecting excess oxygen to the copper DCM solution at -80 °C, which has characteristic UV-Vis absorption at 392 nm (3400 M^{-1} cm^{-1}), 510 nm (5300 M^{-1} cm^{-1}), 642 nm (2700 M^{-1} cm^{-1}). The peroxide complex $[Cu^{II}_2(UN\text{-}O^{-})(O_2^{2-})]^{+}$ is also prepared by reduction of the superoxide complex $[Cu^{II}_2(UN\text{-}O^{-})(O_2^{\bullet-})]^{2+}$ with one equivalent of decamethylferrocene (vide infra). The two sets of samples give rise to the same rRaman spectra.

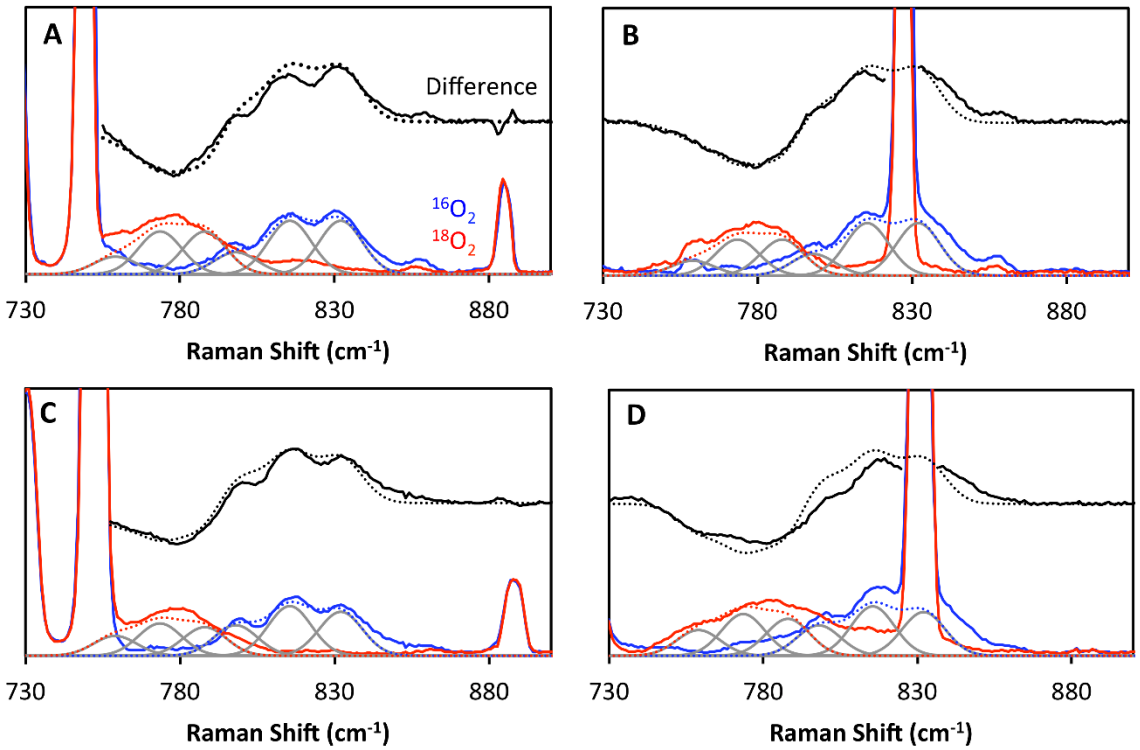

Figure 8. Resonance Raman spectra of the peroxide complex

Resonance Raman spectra of $[Cu^{II}_2(UN\text{-}O^{-})(O_2^{2-})]^{+}$; $^{16}O_2$ (blue), $^{18}O_2$ (red), difference (black), and Gaussian fits (individual transitions are grey while the sum and difference are shown as a dashed curve). 530 nm excitation (**A**, **B**) and 568 nm excitation (**C**, **D**) for samples in CH_2Cl_2 (**A**, **C**) and CD_2Cl_2 (**B**, **D**).

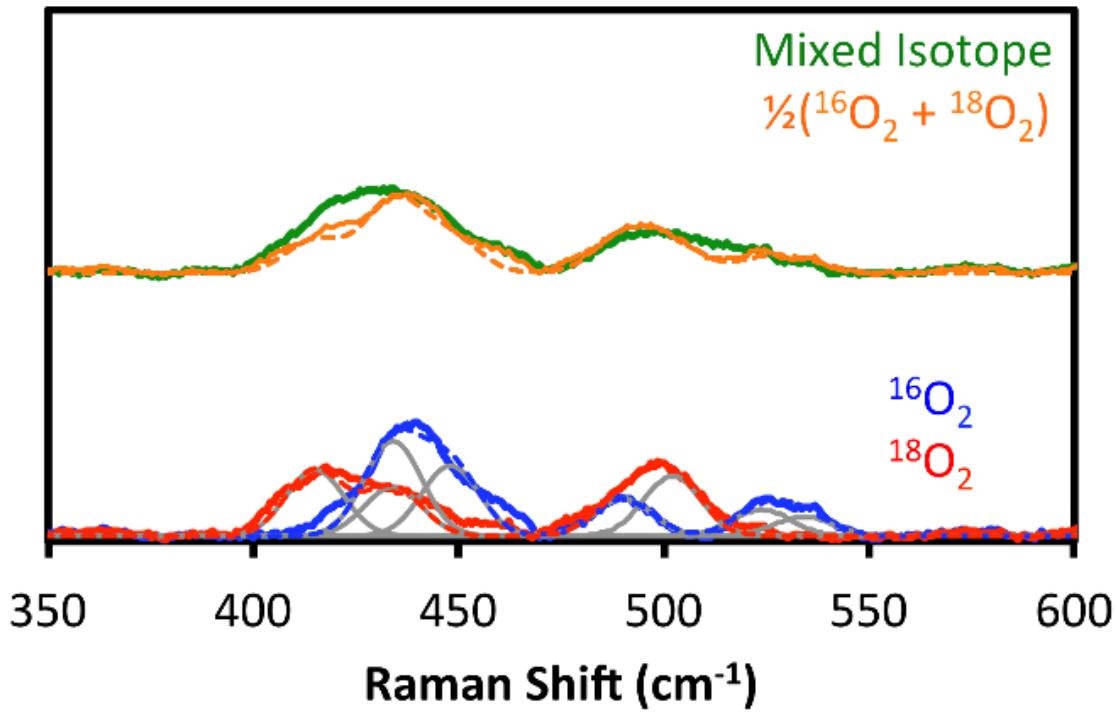

Figure 9. Resonance Raman spectra of Cu-O in the peroxide complex

Resonance Raman spectra of $[Cu^{II}_2(UN\text{-}O^{-})(O_2^{2-})]^{+}$ with 530 nm excitation; $^{16}O_2$ (blue), $^{18}O_2$ (red), mixed isotope (a 1:2:1 mixture of $^{16}O_2$:$^{16,18}O_2$:$^{18}O_2$ green), and ½($^{16}O_2$ + $^{18}O_2$) (orange) with 530 nm excitation. Fitting the mixed isotope data with equal contributions of the $^{16}O_2$ and $^{18}O_2$ spectra poorly reproduce the mixed isotope spectrum indicating the presence of intermediate Cu–O stretches.

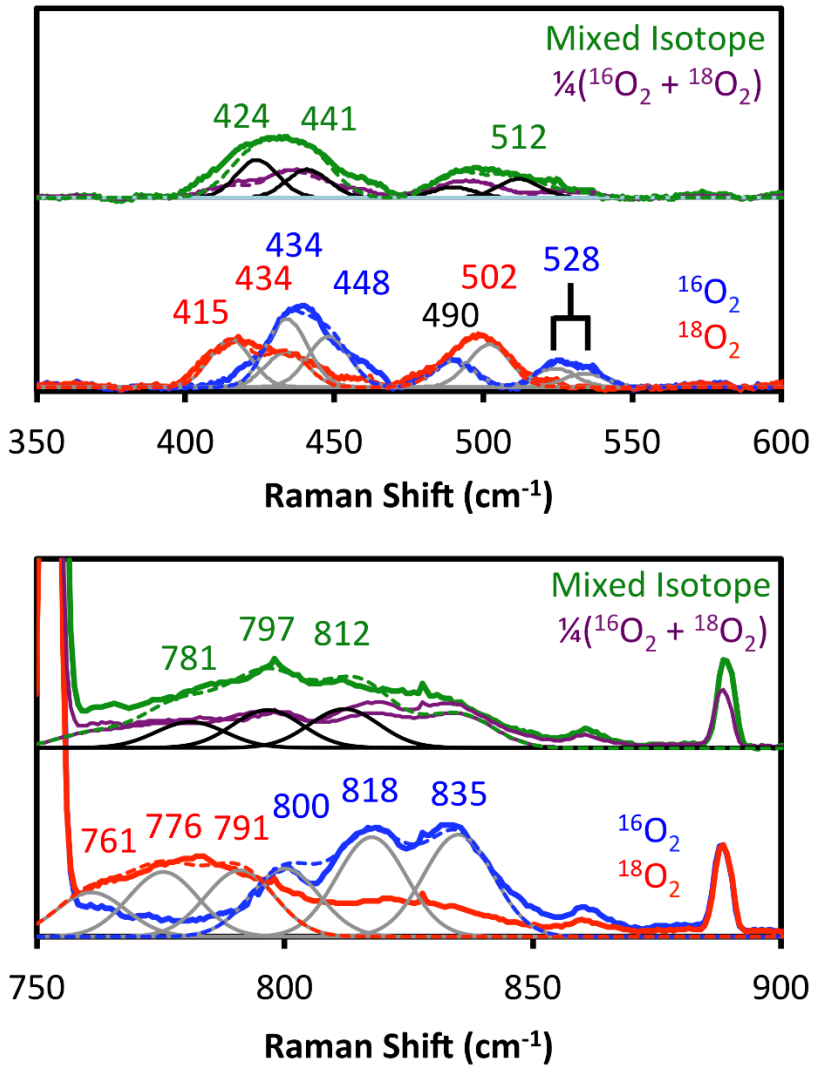

Figure 10. Resonance Raman spectra of the peroxide complex with Gaussian fit.

Resonance Raman spectra of $[Cu^{II}_2(UN\text{-}O^{-})(O_2^{2-})]^{+}$ with 530 nm excitation; $^{16}O_2$ (blue), $^{18}O_2$ (red), mixed isotope (a 1:2:1 mixture of $^{16}O_2$:$^{16,18}O_2$:$^{18}O_2$ green), and ¼($^{16}O_2$ + $^{18}O_2$) (purple) and Gaussian fits (individual transitions are grey for $^{16}O_2$ and $^{18}O_2$ and black for mixed isotope while the Gaussian sum for each spectrum is shown as a dashed curve).

Laser excitation of samples of $[Cu^{II}_2(UN\text{-}O^{-})(O_2^{2-})]^{+}$ at 530 nm yield rR spectra that confirm the presence of a dicopper peroxo complexes (Figure 8-10). The presence of multiple peroxide O–O stretches and more than two Cu–O stretches indicate multiple distinct isomers are present in solution. Laser excitation at 568 nm indicates that the three bands in the $^{16}O_2$ spectrum vary with excitation energy and are best fit by three, distinct Gaussians (Figure 8). Similarly, information about the geometry of $[Cu^{II}_2(UN\text{-}O^{-})(O_2^{2-})]^{+}$ can be determined from the mixed isotope rR spectrum. For $[Cu^{II}_2(UN\text{-}O^{-})(O_2^{2-})]^{+}$, an intermediate Cu–O stretch (Figure 9, Figure 10, top) with an intermediate frequency, that occurs in between the pure Cu-^{16}O and Cu-^{18}O vibrations (given by the purple average), is observed for each Cu–O stretch, indicating that these vibrations result from μ-1,2-peroxo isomers.

Table 11: Computational details for the lowest energy μ-1,2-peroxo isomers of $[Cu^{II}_2(UN\text{-}O^{-})(O_2^{2-})]^{+}$.

	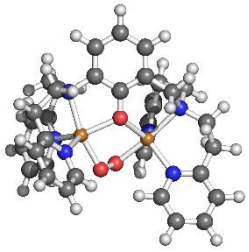	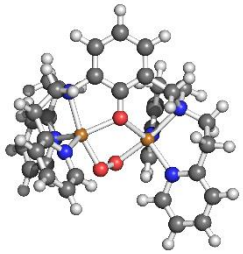	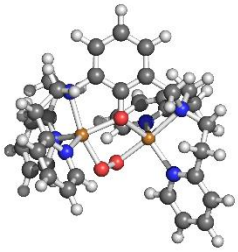
	μ-1,2-P^{C1}	**μ-1,2-P^{C3}**	**μ-1,2-P^{C4}**
Functional	UB3LYP	UB3LYP	UB3LYP
Basis Set	TZVP (Cu, O, N) SV (C, H)	TZVP (Cu, O, N) SV (C, H)	TZVP (Cu, O, N) SV (C, H)
Charge	1	1	1
Multiplicity	3	3	3
Point Group	C_1	C_1	C_1
Solvation	PCM in dichloromethane	PCM in dichloromethane	PCM in dichloromethane
Integral Grid	Ultrafine	Ultrafine	Ultrafine
SCF Energy (a.u.)	-5190.02630026	-5190.02415405	-5190.02711184
S^2	2.0096	2.0094	2.0098
ΔG (kcal, -80° C)	0.7	1.8	0.0
$\nu_{O\text{-}O}$ (cm^{-1})	938	934	941
Selected Metrical Parameters			
Cu_N•••Cu_{Me} (Å)	3.441	3.443	3.449
O–O (Å)	1.360	1.362	1.356
Cu_N–O (Å)	1.973	1.968	1.972
Cu_{Me}–O (Å)	1.988	1.982	1.998
Cu_N–$O_{PhO\text{-}}$ (Å)	2.076	2.079	2.079
Cu_{Me}–$O_{PhO\text{-}}$ (Å)	2.110	2.117	2.111
Cu_N–N (Å)	2.141, 2.147, 2.213	2.142, 2.148, 2.209	2.144, 2.149, 2.205
Cu_{Me}–N (Å)	2.153, 2.171, 2.217	2.160, 2.195, 2.200	2.137, 2.219, 2.231
∠Cu_N–O–O–Cu_M (°)	71.9	73.0	72.6
Selected Spin Densities			
Cu_N	0.44	0.44	0.43
Cu_M	0.41	0.42	0.40
O_2	0.46, 0.46	0.45, 0.46	0.47, 0.47

Table 12: Computational details for the lowest energy μ-1,2-peroxo isomers of $[Cu^{II}_2(UN\text{-}O^{-})(O_2^{2-})]^{+}$.

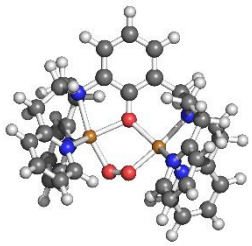

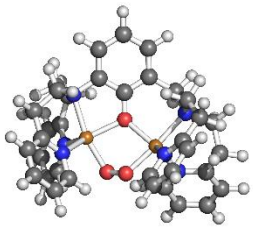

	μ-1,2-P^{C5}	**μ-1,2-P^{C6}**
Functional	UB3LYP	UB3LYP
Basis Set	TZVP (Cu, O, N) SV (C, H)	TZVP (Cu, O, N) SV (C, H)
Charge	1	1
Multiplicity	3	3
Point Group	C_1	C_1
Solvation	PCM in dichloromethane	PCM in dichloromethane
Integral Grid	Ultrafine	Ultrafine
SCF Energy (a.u.)	-5190.02304723	-5190.02338503
S^2	2.0086	2.0090
ΔG (kcal, -80° C)	2.9	2.6
$\nu_{O\text{-}O}$ (cm^{-1})	918	923
Selected Metrical Parameters		
Cu_N•••Cu_{Me} (Å)	3.451	3.461
O–O (Å)	1.376	1.371
Cu_N–O (Å)	1.957	1.964
Cu_{Me}–O (Å)	1.950	1.972
Cu_N–$O_{PhO\text{-}}$ (Å)	2.073	2.061
Cu_{Me}–$O_{PhO\text{-}}$ (Å)	2.110	2.110
Cu_N–N (Å)	2.154, 2.159, 2.207	2.156, 2.178, 2.200
Cu_{Me}–N (Å)	2.107, 2.221, 2.246	2.131, 2.169, 2.265
∠Cu_N–O–O–Cu_M (°)	-68.6	-69.3
Selected Spin Densities		
Cu_N	0.45	0.45
Cu_M	0.47	0.44
O_2	0.39, 0.42	0.42, 0.43

Table 13: Computational details for the lowest energy μ-1,2-peroxo isomers of $[Cu^{II}_2(UN\text{-}O^{-})(O_2^{2-})]^{+}$.

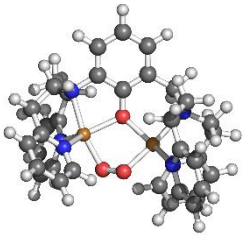

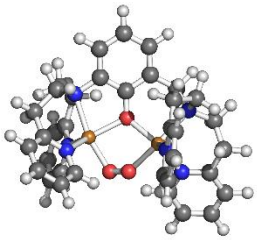

	μ-1,2-P^{C7}	**μ-1,2-P^{C8}**
Functional	UB3LYP	UB3LYP
Basis Set	TZVP (Cu, O, N) SV (C, H)	TZVP (Cu, O, N) SV (C, H)
Charge	1	1
Multiplicity	3	3
Point Group	C_1	C_1
Solvation	PCM in dichloromethane	PCM in dichloromethane
Integral Grid	Ultrafine	Ultrafine
SCF Energy (a.u.)	-5190.02304661	-5190.02545227
S^2	2.0091	2.0094
ΔG (kcal, -80° C)	2.4	1.3
$\nu_{O\text{-}O}$ (cm^{-1})	913	928
Selected Metrical Parameters		
Cu_N•••Cu_{Me} (Å)	3.422	3.444
O–O (Å)	1.374	1.366
Cu_N–O (Å)	1.960	1.965
Cu_{Me}–O (Å)	1.959	1.981
Cu_N–$O_{PhO\text{-}}$ (Å)	2.089	2.085
Cu_{Me}–$O_{PhO\text{-}}$ (Å)	2.085	2.111
Cu_N–N (Å)	2.152, 2.154, 2.209	2.152, 2.165, 2.207
Cu_{Me}–N (Å)	2.130, 2.167, 2.229	2.149, 2.172, 2.209
∠Cu_N–O–O–Cu_M (°)	-66.7	-70.3
Selected Spin Densities		
Cu_N	0.44	0.44
Cu_M	0.46	0.43
O_2	0.41, 0.42	0.44, 0.44

Table 14: Computational details for the lowest energy mixed valent μ-1,1-superoxo and η^1-superoxo isomers of $[Cu^{II}_2(UN\text{-}O^-)(O_2^{2-})]^+$.

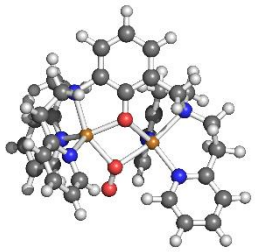
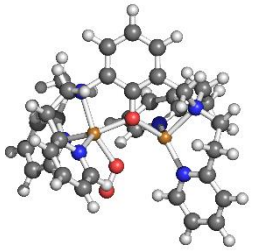
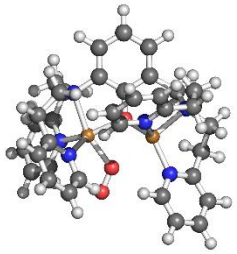

	μ-1,1-MV-S^{C1}	**η^1-MV-S^{C4}**	**η^1-MV-S^{C5}**
Functional	UB3LYP	UB3LYP	UB3LYP
Basis Set	TZVP (Cu, O, N) SV (C, H)	TZVP (Cu, O, N) SV (C, H)	TZVP (Cu, O, N) SV (C, H)
Charge	1	1	1
Multiplicity	3	3	3
Point Group	C_1	C_1	C_1
Solvation	PCM in dichloromethane	PCM in dichloromethane	PCM in dichloromethane
Integral Grid	Ultrafine	Ultrafine	Ultrafine
SCF Energy (a.u.)	-5190.01713136	-5190.01908120	-5190.01789552
S^2	2.0135	2.0111	2.0111
ΔG (kcal, -80° C)	5.9	3.7	4.5
$\nu_{O\text{-}O}$ (cm^{-1})	1131	1189	1206
Selected Metrical Parameters			
Cu_N•••Cu_{Me} (Å)	3.319	3.538	3.693
O–O (Å)	1.298	1.288	1.281
Cu_N–O (Å)	2.151	2.045	2.054
Cu_{Me}–O (Å)	2.187	2.728	3.574
Cu_N–$O_{PhO\text{-}}$ (Å)	2.057	2.031	2.024
Cu_{Me}–$O_{PhO\text{-}}$ (Å)	2.110	2.164	2.152
Cu_N–N (Å)	2.072, 2.181, 2.225	2.097, 2.182, 2.206	2.098, 2.213, 2.233
Cu_{Me}–N (Å)	2.128, 2.143, 2.216	2.042, 2.087, 2.189	2.026, 2.063, 2.200
Selected Spin Densities			
Cu_N	0.29	0.42	0.42
Cu_M	0.25	0.03	0.00
O_2	0.65, 0.63	0.67, 0.71	0.70, 0.72

Table 15. Select vibrations for **μ-1,2-P^{C4}** and their predicted isotope shift (cm^{-1}).

	^{16}O–^{16}O	^{16}O–^{18}O	^{18}O–^{18}O
$\nu_{O\text{–}O}$	941	919, 918	892
Sym $\nu_{Cu\text{–}O}$	415	412, 402	395
Antisym $\nu_{Cu\text{–}O}$	383	374, 365	363

Additional insights into the structures of $[Cu^{II}_2(UN\text{-}O^-)(O_2^{2-})]^+$ can be obtained from DFT calculations on the various ligand conformations of UN-O$^-$ (Figure 7). A

number of μ-1,2-peroxo isomers are found to have a similar energy (Tables 11-13) which vary by 28 cm^{-1} across the range of the isomers, in reasonable agreement with the experimental data which exhibits several closely spaced spectral features (Figure 10, bottom). Attempts to compute the possible μ-1,1-peroxo isomers yielded structures of a mixed valent complex coordinated by a superoxide ion (Table 14). Therefore, one can conclude that the absence of an oxygen isotope sensitive vibration corresponding to a superoxide O–O stretch and the intermediate Cu–O stretches observed in the mixed isotope spectrum indicate that the structure of $[Cu^{II}_2(UN\text{-}O^{-})(O_2^{2-})]^{+}$ is best described by three μ-1,2-peroxo conformational isomers. It should also be noted that the calculated DFT structures give a Cu…Cu distance averaging 3.44 Å (Tables 11-13); this is in reasonable agreement with an older EXAFS-derived value (but on an isolated solid) of ~3.3 Å.[9]

Reduction Potential Determination.

As mentioned in the introduction, superoxide and peroxide complexes $[Cu^{II}_2(UN\text{-}O^{-})(O_2^{\bullet-})]^{2+}$ and $[Cu^{II}_2(UN\text{-}O^{-})(O_2^{2-})]^{+}$ are interconvertible. These reactions can be carried out using a series of ferrocene or ferrocenium derivatives, in DCM as solvent, Figure 11a.[21] With deca- or octa-methyl ferrocene, a titration can be carried out, showing that only one equiv of reductant is required to fully convert superoxide complex $[Cu^{II}_2(UN\text{-}O^{-})(O_2^{\bullet-})]^{2+}$ to peroxide complex $[Cu^{II}_2(UN\text{-}O^{-})(O_2^{2-})]^{+}$, Figure 12b. For the opposite reaction, addition of one equiv ferrocenium hexafluoroantimonate derivatives (the parent unsubstituted ferrocenium salt, and either acetyl or dimethyl ferrocenium) to

solutions of peroxide complex $[Cu^{II}_2(UN\text{-}O^{-})(O_2^{2-})]^{+}$ results in complete oxidation of the peroxide complex to superoxide species $[Cu^{II}_2(UN\text{-}O^{-})(O_2^{\bullet-})]^{2+}$. Such a titration (adding ¼ equiv oxidant for each recorded spectrum) is shown in Figure 11b, for dimethylferrocenium as oxidant. Following completion of this reaction, re-addition of one equiv decamethylferrocene reductant gave back the peroxo complex $[Cu^{II}_2(UN\text{-}O^{-})(O_2^{2-})]^{+}$ in 90% yield (–80 °C, as determined from spectrophotometry, see Figure 12b). In either direction of the reaction, the transformations are consistently fast, i.e., the reactions were complete immediately following benchtop addition of the redox reagent and recording of UV-vis spectrum, suggesting that an outer-sphere electron transfer mechanism is operative.

By choosing the right oxidizing reagent, in particular diphenylamine ferrocenium (Figure 11a) we could achieve an equilibrium condition, where all oxidant and reductant pairs are present in amounts that could be quantified by spectrophotometry. This oxidant possesses a formal reduction potential close to that of the superoxide/peroxide pair, in fact, complex $[Cu^{II}_2(UN\text{-}O^{-})(O_2^{\bullet-})]^{2+}$ is present in greater amounts than peroxide species $[Cu^{II}_2(UN\text{-}O^{-})(O_2^{2-})]^{+}$; most but not all of peroxide species $[Cu^{II}_2(UN\text{-}O^{-})(O_2^{2-})]^{+}$ becomes oxidized, Figure 11c. The amount of diphenylamine ferrocenium ion present can be directly quantitated by its known absorption at 1014 nm (e = 2675 M^{-1} cm^{-1}) (Figure 11c and Figure 12). The Nernst equation (**eq. 3**) could be directly applied to this system which is at equilibrium, as λ_{max} and absorptivity (ε) values are known for both $[Cu^{II}_2(UN\text{-}O^{-})(O_2^{\bullet-})]^{2+}$ and $[Cu^{II}_2(UN\text{-}O^{-})(O_2^{2-})]^{+}$; by direct measurement of the concentration of diphenylamine ferrocenium**,** the amount of diphenylferrocene was determined by

difference. Thus, the electron-transfer equilibrium constant (K_{et}) was determined to be K_{et} = 5.3. The DFT calculations suggest there may be seven μ-1,2-peroxide conformers with small ligand conformation changes and energies different from 0.7 to 2.9 kcal/mol (determined at −80 °C) compared to the one with lowest energy, tables 11−13. There are also three μ-1,1- superoxide and seven μ-1,2-superoxide species, which differ by only small ligand conformation changes and which possess energy differences of between 1.7 to 4.8 kcal/mol (tables 4−7). Therefore, we consider the energy differences between the μ-1,1-superoxide and μ-1,2- superoxide isomers are on the same order of magnitude for different ligand conformation changes and thus has very small if any influence on the overall superoxide/peroxide equilibrium constant or the reduction potential. By employing this value along with our experimentally measured reduction potential of the diphenylamine ferrocenium/ferrocene pair, the $E°$ value for the superoxide/peroxide pair is calculated to be +130 mV vs SCE.

$$E(\text{peroxide/superoxide}) = E_{ox} + (RT/F)\ln K_{et} \qquad \textbf{(eq. 3)}$$

or

$$0 = E^{o}_{et} - \frac{RT}{nF}\ln K_{et}, E^{o}_{et} = E^{o}\left(\frac{Ph_2NFc^{+}}{Ph_2NFc}\right) - E^{o}\left(\frac{Superoxide}{Peroxide}\right)$$

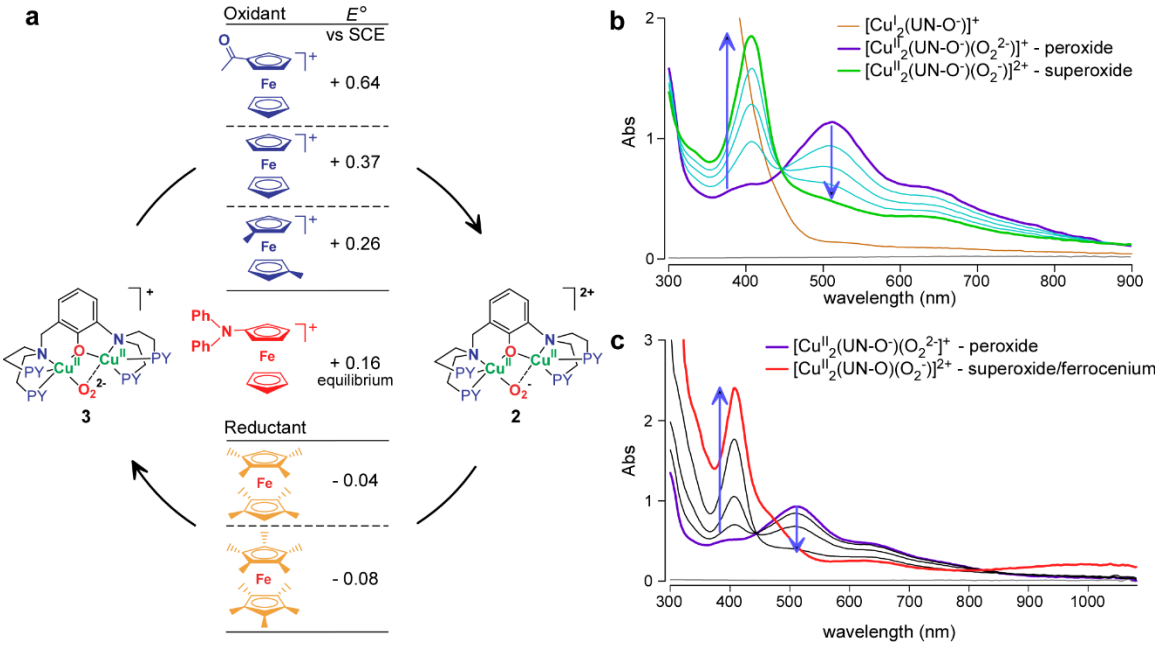

Figure 11. UV-Vis spectroscopy of the redox equilibrium.

(a) E° values for the oxidants used to convert $[Cu^{II}_2(UN\text{-}O^{-})(O_2^{2-})]^{+}$ to $[Cu^{II}_2(UN\text{-}O^{-})(O_2^{\bullet-})]^{2+}$ and for the reductants used to convert $[Cu^{II}_2(UN\text{-}O^{-})(O_2^{\bullet-})]^{2+}$ to $[Cu^{II}_2(UN\text{-}O^{-})(O_2^{2-})]^{+}$ and. (b) Oxidation of $[Cu^{II}_2(UN\text{-}O^{-})(O_2^{2-})]^{+}$ to $[Cu^{II}_2(UN\text{-}O^{-})(O_2^{\bullet-})]^{2+}$ using dimethylferrocenium ion. (c) Diphenylamine ferrocenium as oxidant used to reach an equilibrium state between $[Cu^{II}_2(UN\text{-}O^{-})(O_2^{2-})]^{+}$ and $[Cu^{II}_2(UN\text{-}O^{-})(O_2^{\bullet-})]^{2+}$.

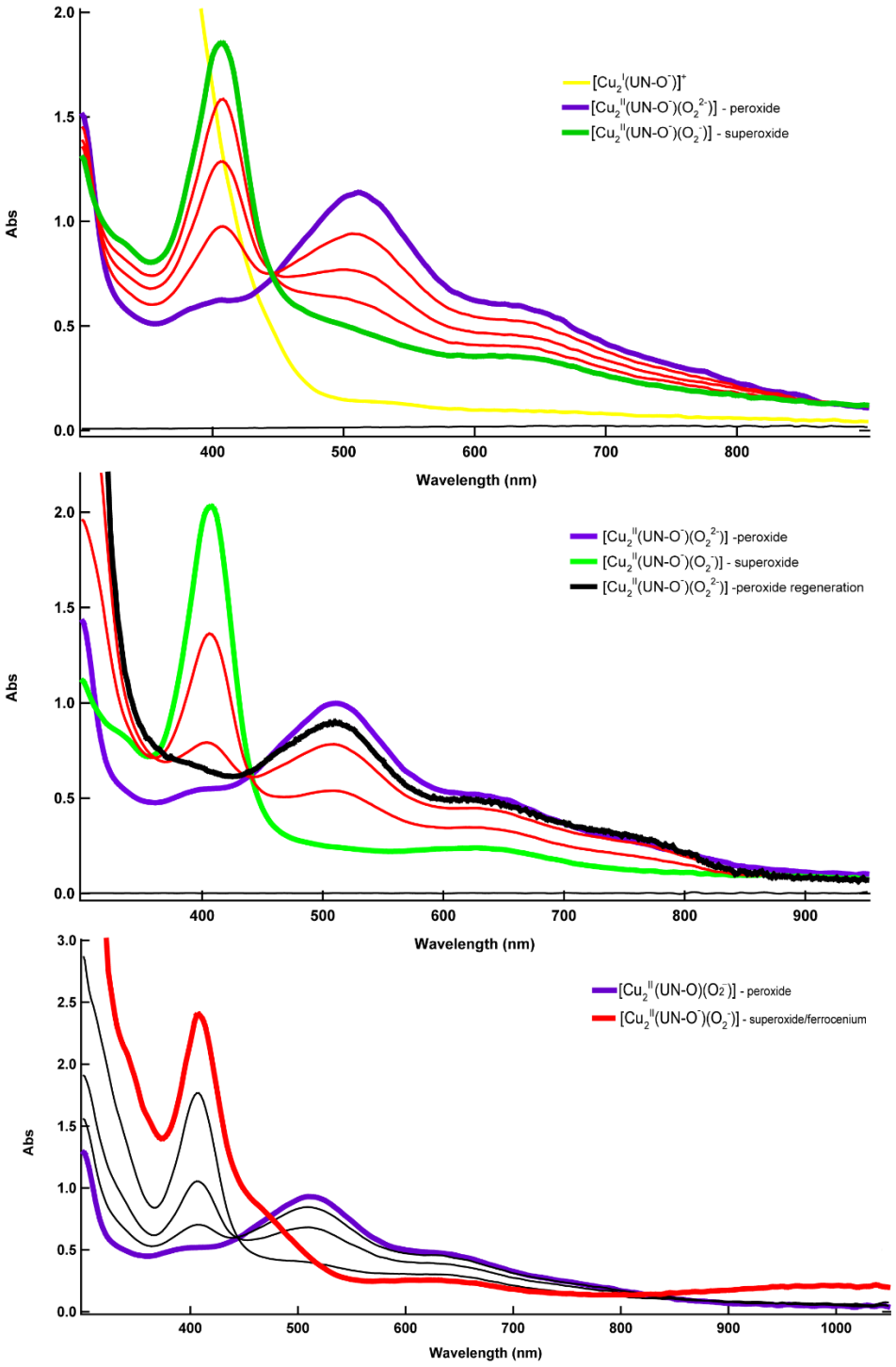

Figure 12. Peroxide and superoxide interconversion.

Reduction potential of superoxide/peroxide compared to other systems.

Given that this is the first determination of a copper coordinated dioxygen-derived fragment reduction potential (**eq. 4**; $E°$ = +130 mV vs SCE), comparison to the literature is constructive.

$$[Cu^{II}_2(UN\text{-}O^-)(O_2^{\bullet-})]^{2+} + e^- \longrightarrow [Cu^{II}_2(UN\text{-}O^-)(O_2^{2-})]^+ \qquad E° = +\,0.13\ V\ (\textbf{eq. 4})$$

Perhaps closely related comparisons can be made with the well-known superoxo- and peroxo-bridged dicobalt(III) complexes. One example comes from complexes employing a phenolato-bridged binucleating ligand pbpb$^-$ ((2,6-bis(N,N-bis(2-pyridyl-methyl)aminomethyl)-4-tert-butylphenolate)),[22] somewhat similar to our own UN-O$^-$ ligand (Table 16). Superoxo-to-peroxo dicobalt(III) complex reduction potentials (see Table 16 (in acetone vs. SCE)) are far more positive (i.e., favorable). Likely this is due to the higher charged cobalt(III) ion, compared to copper(II). It should be noted that one cannot generally compare standard reduction potentials ($E°$) in different solvents; however, for potentials measured for the ferrocenium/ferrocene (Fc^+/Fc) couple,[21] and $E°$ values determined for a variety of other kinds of organic or inorganic compounds that are electrochemically active, there are only quite small differences in the $E°$ value in DCM vs acetonitrile (ACN) vs acetone vs dimethylformamide (DMF).[23]

Table 16. List of Redox Pairs of Interest for Comparisons

redox pair	solvent	E^o (mV) [a]	ref
$[Co_2(bpbp^-)(CCl_3CO_2^-)(O_2^{\bullet-})]^{3+}$/ $[Co_2(bpbp^-)(CCl_3CO_2^-)(O_2^{2-})]^{2+}$	Acetone	1060	22a
$[Co_2(bpbp^-)(CH_3CO_2^-)(O_2^{\bullet-})]^{3+}$/ $[Co_2(bpbp^-)(CH_3CO_2^-)(O_2^{2-})]^{2+}$	Acetone	880	22a
$[Co_2(NH_3)_{10}(\mu\text{-}O_2^{\bullet-})]^{5+}$/ $[Co_2(NH_3)_{10}(\mu\text{-}O_2^{2-})]^{4+}$/	Water	708 [b]	24
$[(C_6F_5)_3B]_2O_2^-$/ $[(C_6F_5)_3B]_2O_2^{2-}$	DCM	540	25
Fc^+/Fc	DCM	370	22
$[Co_2(NH_3)_8(\mu\text{-}O_2^{\bullet-}, NH_2)]^{4+}$/ $[Co_2(NH_3)_8(\mu\text{-}O_2^{2-}, NH_2)]^{3+}$	Water	358	24
Me_2Fc^+/Me_2Fc	DCM	260	this work
$[Cu^{II}_2(UN\text{-}O^-)(O_2^{\bullet-})]^{2+}/[Cu^{II}_2(UN\text{-}O^-)(O_2^{2-})]^+$	DCM	130	this work
Cyt *c*	ACN	3	26
$iAscH^{\bullet-}/iAscH^-$	ACN	–30	27
$[HTrip\ldots O_2] + 2H^+$/ $[HTrip + H_2O_2]$ [c]	PhCN	[-40, 260] [d]	28
$TMG_3trenCu^{II}(O_2^{\bullet-}) + H^+$/ $TMG_3trenCu^{II}OOH$	MeTHF	[-40, 260] [d]	29
Me_8Fc^+/Me_8Fc	DCM	–40	this work
$Me_{10}Fc^+/Me_{10}Fc$	DCM	–80	this work
$[Co_2(CN)_{10}(\mu\text{-}O_2^{\bullet-})]^{5-}$/ $[Co_2(CN)_{10}(\mu\text{-}O_2^{\bullet-})]^{6-}$	Water	-182	24
$[(O_2^{\bullet-})\subset mBDCA\text{-}5t\text{-}H_6]^-$/ $[(O_2^{2-})\subset mBDCA\text{-}5t\text{-}H_6]^{2-}$	DMF	–520	30

[a] Standard reduction potential $E°$ (vs SCE) [b] Value determined at neutral pH; for pH < 1 $E°$ ~ 470 mV vs SCE. [c] Two electron reduction process. [d] Standard reduction potential $E°$ bracketed between -40 mV and 260 mV. $iAscH^{\bullet-}$; as 5,6-isopropylidiene

ascorbyl anion/radical. Cyt *c*; Cytochrome *c*. HTrip; [14]triphyrin(2.1.1). TMG_3tren; see Figure 3. mBDCA-5t-H_6; *tert*-butyl-substituted hexacarboxamide cryptand.

Within this dicobalt set, the complex supported by a better donor ancillary ligand, acetate compared to trichloroacetate, leads to a less favorable superoxide-to-peroxide reduction. The better donor would destabilize (in a relative sense) reductive conversion to the more negatively charged di-anionic peroxide ligand; conversely the trichloroacetate ligand can help stabilize some of the extra negative charge of the peroxide complex.

Data on other dicobalt(III) complexes also reveal interesting findings. For the classical dicobalt(III) compound with a single bridging superoxide ligand, $[Co_2(NH_3)_{10}(m\text{-}O_2^{\bullet-})]^{5+}$, the reduction potential is over 300 mV more oxidizing than the closely related doubly-bridged complex $[Co_2(NH_3)_8(m\text{-}O_2^{\bullet-},NH_2)]^{4+}$ (Table 16), likely because of the difference in overall charge of the complexes. Still, both these complexes and that dicobalt compound with the $pbpb^-$ ligand containing species (see discussion above) have $E°$ values significantly more positive than that for our $[Cu^{II}_2(UN\text{-}O^-)(O_2^{\bullet-})]^{2+}$ / $[Cu^{II}_2(UN\text{-}O^-)(O_2^{2-})]^+$ redox couple (Table 16). The grossly more negative $E°$ value for $[Co_2(CN)_{10}(m\text{-}O_2^{\bullet-})]^{5-}$, is ~900 mV less oxidizing than the ammonia ligand containing analog, the explanation for this observation being that the complex has a vastly altered overall charge of 5–.[24a]

Interestingly, recent synthetic advances allowed for the stabilization of three peroxide dianion moieties, by using various organic 'hosts'.[25,30-31] For two of these, superoxide-to-peroxide reduction potentials were obtained by cyclic voltammetry (CV),

see Table 16. In one example by Agapie and coworkers[25] the O_2^{2-} fragment was captured by $B(C_6F_5)_3$ as a Lewis acid, giving the species $[(C_6F_5)_3B–O\text{-}O–B(C_6F_5)_3]^{2-}$: a quasi-reversible oxidation wave (CV) occurred at + 0.54 V vs SCE (Table 16). By comparison, this is more than 400 mV higher than that found for our complex with superoxide or peroxide are dicopper(II) coordinated. This may be ascribed to the very strong Lewis acidity of the $B(C_6F_5)_3$ moieties. Another example is provided by Cummins, Nocera and coworkers[30]where corresponding superoxide or peroxide moieties are encapsulated in a hexacarboxamide cryptand through hydrogen bonding networks. A standard reduction potential measured in this case, in DMF solvent is $E°$ = –520 mV vs SCE. Solvent variations in $E°$ or not, this value is quite low compared to the Superoxide/Peroxide couple; apparently the extensive cryptand H-bonding is sufficient to stabilize the O_2^{2-} fragment, but it is not nearly as effective as our dicopper(II) or the $B(C_6F_5)_3$ bound peroxide.

In further comparison, we previously were able to bracket the reduction potential associated with a protonated superoxo species, $TMG_3trenCu^{II}(O_2^{\bullet-})H^+$ conversion to the corresponding hydroperoxide complex $TMG_3trenCu^{II}OOH$, Table 16, to be found within the range between Me_2Fc^+/Me_2Fc and Me_8Fc^+/Me_8Fc. Notably, the same is true for our $[Cu^{II}_2(UN\text{-}O^-)(O_2^{\bullet-})]^{2+}/[Cu^{II}_2(UN\text{-}O^-)(O_2^{2-})]^+$ couple. Also worth mentioning is a recent study by Fukuzumi and coworkers[28] where they bracketed the two-electron two-proton reduction potentials of O_2 in the presence of an organic macrocycle Htrip and $HClO_4$ to also fall in the range between Me_2Fc and Me_8Fc reagents (Table 16).

To further put our results (**eq. 4**) and the others carried out in organic solvents (discussed just above) in context, we can compare to $E°$ values for biologically relevant reductants, those determined in ACN solvent. The heme protein cytochrome *c* and an organic soluble ascorbate analog also possess standard reduction potentials that lie between those of the Me_2Fc^+/Me_2Fc and Me_8Fc^+/Me_8Fc couples (Table 16). We can conclude, that our study and the others, do possess biological relevance, in that the reduction potentials lie in a range within or close to those occurring in biochemistry; perhaps, cytochrome *c* or ascorbate could reduce $[Cu^{II}_2(UN\text{-}O^-)(O_2^{\bullet-})]^{2+}$ to $[Cu^{II}_2(UN\text{-}O^-)(O_2^{2-})]^+$. We extend the argument to say that our work with copper or dicopper bound O_2-derived reduced fragments can and will provide useful if not important information in the biological context.

Also, it is well known and clear from literature data that there is a considerable importance for the role of protons in the reduction of O_2-derived fragments. Protonation and formation of very strong O–H bonds greatly enhances reactions (i.e., protons usually accompany electrons). For example, the addition of an electron to the P450 monoxygenase heme-superoxo (i.e., $Fe^{III}\text{-}O_2^{\bullet-}$) species, a neutral entity, to give the corresponding reduced peroxide anion, is extremely uphill, **eq. 5**.[5b] The process switches over to being highly favorable if a proton is involved, **eq. 6** at pH 7.0.[32]

$$P450\text{-}Fe^{III}(O_2^{\bullet-})^{2+} + e^- \longrightarrow P450\text{-}Fe(O_2^{2-})^+ \quad E°' \leq -1.0\ V \quad \textbf{(eq. 5)}$$

P450-Fe($O_2^{\bullet-}$)$^{2+}$ + H^+ + e^-

——> P450-Fe($^-$OOH)$^{2+}$ $E°'$ = + 0.80 V (vs. SCE) (**eq. 6**)

It will be of considerable future interest to determine the thermodynamics for the reduction *and* protonation of [Cu^{II}_2(UN-O^-)($O_2^{\bullet-}$)]$^{2+}$ to give the hydroperoxide complex [Cu^{II}_2(UN-O^-)($^-$OOH)]$^{2+}$; the latter has been separately characterized and is known to have a μ-1,1-hydroperoxo structure.[33] Knowledge of such thermodynamic parameters would be of interest in comparing with the values in **eqs. 5** and **6** or other known cases.[4,5b,32]

Stopped-flow Kinetics.

In order to obtain further mechanistic insights, the electron-transfer kinetics of the oxidation of peroxo complex [Cu^{II}_2(UN-O^-)(O_2^{2-})]$^+$ by the dimethylferrocenium ion (Me_2Fc^+) were followed by the low-temperature (–80 °C) stopped-flow method. With an excess of Me_2Fc^+ (i.e., under pseudo-first-order conditions) the oxidation of the peroxide [Cu^{II}_2(UN-O^-)(O_2^{2-})]$^+$ is too fast to observe instrumentally. Therefore, we employed a one-to-one ratio for the peroxide [Cu^{II}_2(UN-O^-)(O_2^{2-})]$^+$ and dimethylferrocenium at low concentration to observe the second-order decay of the peroxide-to-superoxide [Cu^{II}_2(UN-O^-)(O_2^{2-})]$^+$ → [Cu^{II}_2(UN-O^-)($O_2^{\bullet-}$)]$^{2+}$ (as from **eq. 7**); an example of the data obtained is shown in Figure 13 and k_{et} values could be determined from a plot of [[Cu^{II}_2(UN-O^-)(O_2^{2-})]$^+$]$^{-1}$ vs time (Table 17).

$$d[[Cu^{II}_2(UN\text{-}O^-)(O_2^{2-})]^+]/dt = -k_{et}[[Cu^{II}_2(UN\text{-}O^-)(O_2^{2-})]^+]^2 \quad \textbf{(eq. 7)}$$

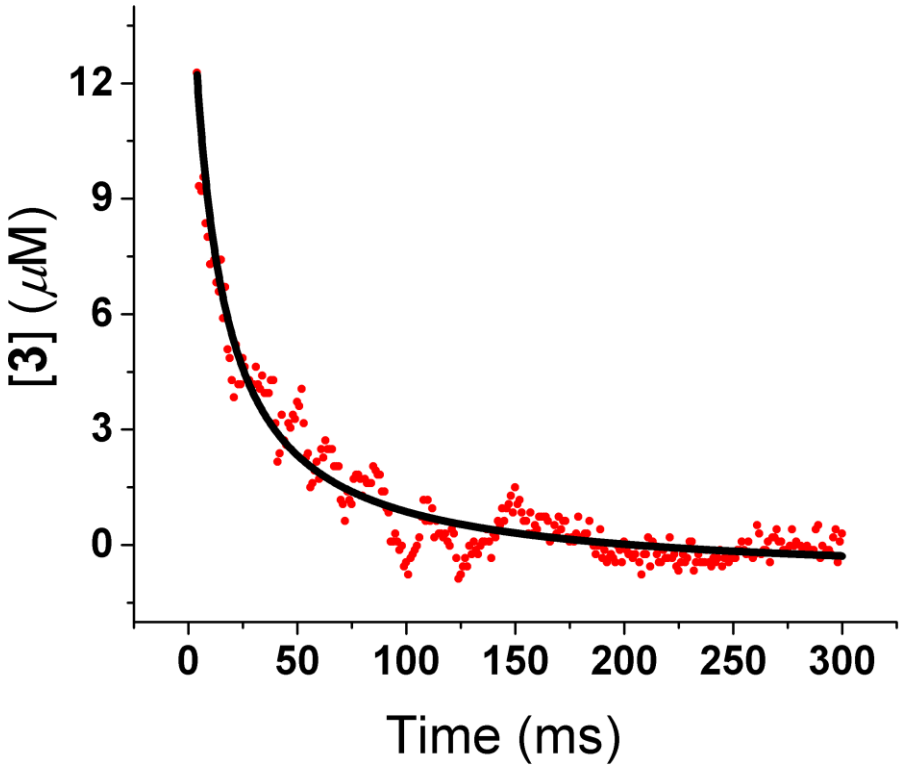

Figure 13. Stopped-flow kinetics trace of peroxide oxidation

Time course for the electron transfer from $[Cu^{II}_2(UN\text{-}O^{-})(O_2^{2-})]^{+}$ to Me_2Fc^{+} to produce $[Cu^{II}_2(UN\text{-}O^{-})(O_2^{\bullet-})]^{2+}$ in DCM solvent at -80 °C.

Calculation of the reorganization energy λ.

Using k_{et} values determined as above, and given in Table 17 at various temperatures, a plot of ln k_{et} vs T^{-1} (Figure 14) gives rise to activation free enthalpy and entropy values (**eq. 8**) for the conversion peroxide-to-superoxide ($[Cu^{II}_2(UN\text{-}O^{-})(O_2^{2-})]^{+}$ + Me_2Fc^{+} → μ-1,2-$[Cu^{II}_2(UN\text{-}O^{-})(O_2^{\bullet-})]^{2+}$+ Me_2Fc), $\Delta H^{\ddagger}$ = (17 ± 3) kJ mol^{-1} and $\Delta S^{\ddagger}$ = (-

16 ± 16) J K^{-1} mol^{-1}, respectively. According to the classic Marcus theory for intermolecular electron transfer,[34] the activation free energy, $\Delta G^{\ddagger}$, is given by **eq. 9**,

$$\Delta G^{\ddagger} = \Delta H^{\ddagger} - T\Delta S^{\ddagger} \qquad \textbf{(eq. 8)}$$

$$\Delta G^{\ddagger} = (\lambda + \Delta G^{o})^2/4\lambda \qquad \textbf{(eq. 9)}$$

$$DG^{o} = -nF[E^{o}(Me_2Fc^{+/0}) - E^{o}((\textbf{Sup})/(\textbf{Per})] = -12.5 \text{ kJ/mol} \qquad \textbf{(eq. 10)}$$

where $\Delta G°$ (**eq. 10**) is the difference of the reduction potential of the dimethylferrocenium ion/dimethylferrocene couple (Me_2Fc^{+}/Me_2Fc = + 260 mV vs SCE) and that of the superoxide/peroxide complexes $[Cu^{II}_2(UN\text{-}O^{-})(O_2^{\bullet-})]^{2+}/[Cu^{II}_2(UN\text{-}O^{-})(O_2^{2-})]^{+}$ (+ 130 mV vs SCE). Then, the reorganization energy, λ, for the electron transfer is calculated to be 1.1 ± 0.2 eV (see diagram below); this is the first measurement of such a fundamentally important parameter for the redox chemistry of interconverting superoxide anion and peroxide dianion ligated to a dicopper(II) center.

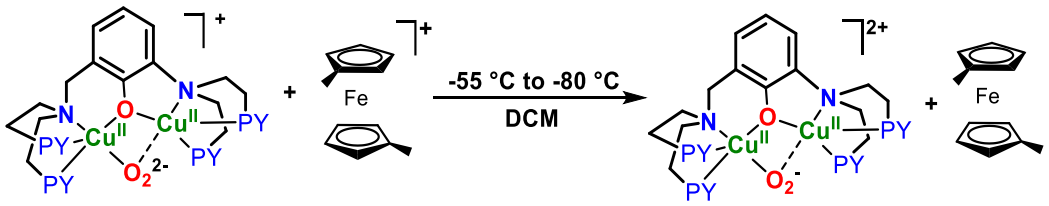

$\lambda = \lambda_{ET}$ = overall reorganization energy = 1.1 ± 0.2 eV

In order to further confirm the value mentioned above, the reorganization energy for the electron transfer was also estimated using **eq. 11**, considering the second-order

rate constant and the superoxo-peroxo reduction potential, both measured at –80 °C in this work:

$$k_{ET} = Z \exp[- (\lambda + \Delta G^0)^2 / 4\lambda RT)] \qquad \textbf{(eq. 11)}$$

where Z is the frequency factor, taken as 1 x 10^{11} M^{-1} s^{-1} at 298 K and ΔG^0 is from **eq. 10**. The value found using this method is 0.84 ± 0.02 eV which is consistent with 1.1 ± 0.2 eV.

This experimentally determined reorganization energy λ = 1.1 eV is the total reorganization energy of the system, composed of the average of the sum of the bond reorganization energies of the (Peroxide/Superoxide) and (Me_2Fc^+/Me_2Fc) pairs (λ_{inner}), plus the solvent reorganization energy (λ_{outer}).

Table 17. Rate Constants for the Electron Transfer from 3 to Me2Fc+ Determined at Various Temperatures.

T (°C)	k_{et} ($M^{-1}s^{-1}$)
-55	$(6.0 \pm 2.0) \cdot 10^7$
-60	$(3.3 \pm 1.1) \cdot 10^7$
-65	$(2.3 \pm 1.2) \cdot 10^7$
-70	$(2.2 \pm 0.9) \cdot 10^7$
-75	$(2.0 \pm 0.8) \cdot 10^7$
-80	$(1.2 \pm 0.3) \cdot 10^7$

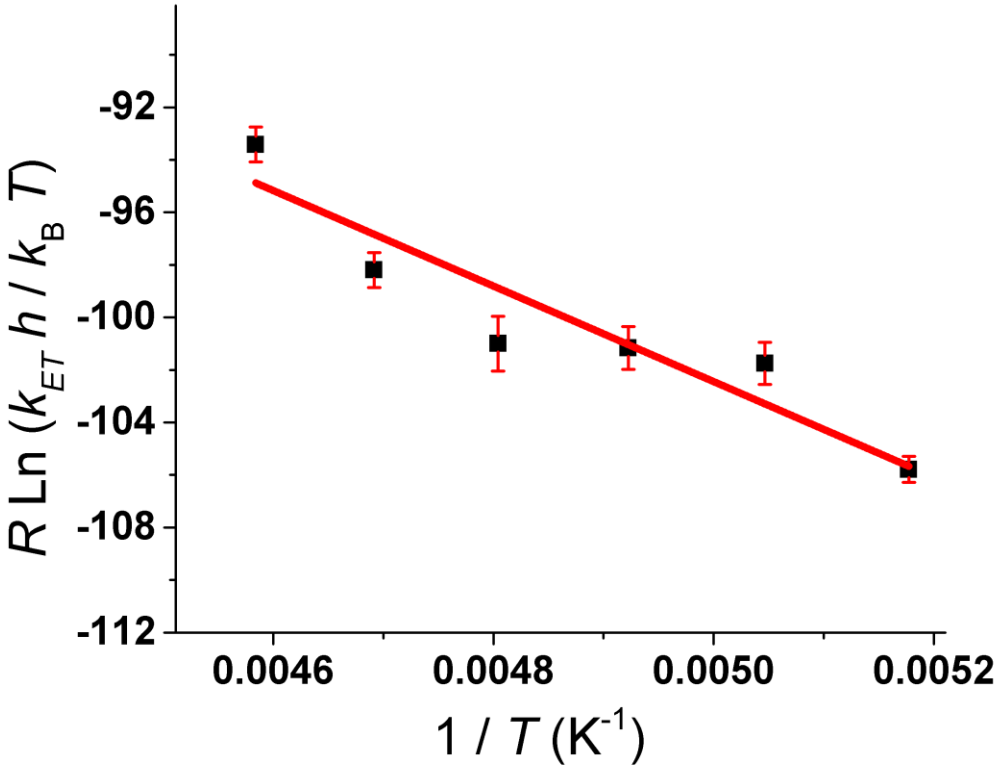

Figure 14. Eyring plot of peroxide oxidation at different temperatures.

Plot of ln k_{et} vs T^{-1} for the electron transfer from $[Cu^{II}_2(UN\text{-}O^{-})(O_2^{2-})]^{+}$ to Me_2Fc^{+} in DCM solvent.

The inner sphere reorganization energy for the electron transfer between the μ-1,2-superoxo and μ-1,2-peroxo isomers could be computed for each ligand conformation from DFT structures on superoxide $[Cu^{II}_2(UN\text{-}O^{-})(O_2^{\bullet-})]^{2+}$ and $[Cu^{II}_2(UN\text{-}O^{-})(O_2^{2-})]^{+}$ complexes. A small inner sphere reorganization energy of ~ 0.4 eV was predicted which results from the small geometric perturbation between the superoxo and peroxo structure

of the complexes (see Table 18). Specifically, in the DFT optimized structures the peroxo O—O bond decreases from 1.356 Å to 1.293 Å in the superoxo complex ($\Delta_{O—O}$ = 0.063Å) and there is an increase in the average Cu-O from 1.985 Å to 2.047 Å. This change is small compared to that calculated by DFT for oxidation of an isolated peroxide dianion, wherein the O—O distance decreases from 1.607 Å to 1.354 Å ($\Delta_{O—O}$ = 0.208 Å) yielding a λ_{inner} of 0.76 eV using identical methodology. (see Table 19)

Table 18: DFT computed electronic inner sphere reorganization energies for the μ-1,2-peroxo and μ-1,2-superoxo isomers.

Confirmation	Reorganization Energy (eV)
C1	0.37
C3	0.42
C4	0.38
C5	0.44
C6	0.43
C7	0.39
C8	0.44

To calibrate these calculations, the λ_{total} for Fc^{+}/Fc self-exchange was determined by DFT. This value serves as a useful benchmark for crosschecking our calculations because the value is well-known in the literature and is roughly invariant for a number of solvents such as acetone, acetonitrile and methanol.[35] First, λ_{inner} for Fc was calculated analogously as above, and was determined to be 0.102 eV which is reasonable considering the negligible change in structure upon oxidation of Fc, that seen from our calculations (Table 19). Next, λ_{outer} was estimated using a dielectric continuum model (**eq. 12**):[36]

$$\lambda_{outer} = (\Delta e)^2 \left[\frac{1}{2a_1} + \frac{1}{2a_2} - \frac{1}{r}\right]\left[\frac{1}{D_{optical}} - \frac{1}{D_{static}}\right] \qquad \textbf{(eq. 12)}$$

where the radius of ferrocene $a_1 = a_2 = 0.406$ nm, $r = 0.812$ nm, and $D_{optical}$ and D_{static} are defined as the optical and static dielectric constants of the solvent, which for acetonitrile are 1.806 and 37.5 respectively. This estimation yielded a λ_{outer} of 0.934 eV, for an overall λ_{total} of 1.036 eV. This value compares well to 1.06 eV measured experimentally in acetonitrile.[35]

DFT calculations of inner and outer sphere reorganization energy

The radii of ferrocene and the UN-O isomers (a1 and a2) for use in the Marcus-Sutin outer sphere electron transfer equation were approximated by averaging the distances between most distant protons plus van der Walls radii along each cartesian axis and dividing in half. The distance between redox centers (r) was taken as the sum of the individual radii (a1 + a2). Ferrocene structure is calculated by DFT (b3lyp/tzvp,sv int=ultrafine) and λ_{inner} is calculated using equation (2) and Table 19.

Table 19. DFT calculated energy for the ferrocene moiety

Neutral optimization	-1650.448056	Hartree
Cation at neutral geom	-1650.210707	Hartree
Cation optimization	-1650.214804	Hartree
Neutral at cation geom	-1650.444644	Hartree
λox	0.00409735	Hartree
λred	0.00341206	Hartree
Average	0.102170776	eV

Marcus and Sutin[36] described the outer sphere reorganization as a function of molecular radii, distance and amount of charge transferred, and polarity of the solvent as follows:

$$\lambda_{outer} = (\Delta e)^2 \left[\frac{1}{2a_1} + \frac{1}{2a_2} - \frac{1}{r}\right]\left[\frac{1}{D_{optical}} - \frac{1}{D_{static}}\right]$$

where λ_{outer} is the outer sphere reorganization energy, Δe is the change in charge, a_1 and a_2 are the molecular radii, r is the distance, $D_{optical}$ is the dynamic dielectric constant (frequently approximated as the square of the refractive index), D_{static} is the normal dielectric constant of the solvent.

a1 = a2 (ferrocene radius) = 0.406 nm (this was found by taking the optimized structure farthest two protons, adding the VDW radii of the protons (1.2Å) and dividing in half)

$D_{optical}$ (acetonitrile) = 1.806

D_{static} (acetonitrile) = 37.5

$\Delta e = \sqrt{(1.4399764\ \text{MeV}\bullet\text{fm})}$

λ_{outer} is 0.934 eV in acetonitrile

By this method, $\lambda = \lambda_{inner} + \lambda_{outer}$ = 1.036 eV. This compares well to 1.06 eV measured experimentally in acetonitrile.[35]

In DCM solvent, λ_{outer} for the following reaction can be calculated in similar fashion:

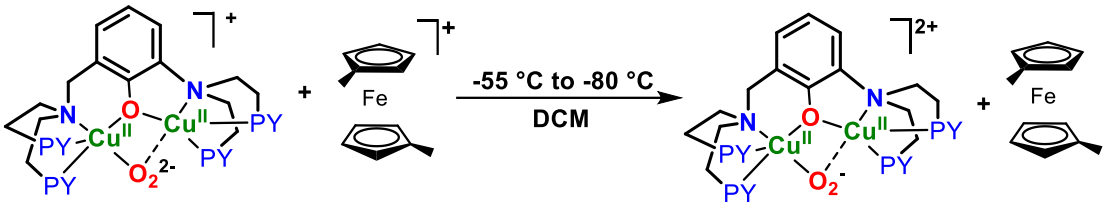

radii of peroxo 0.6775 nm

radii of dimethylferrocene –use the radius of ferrocene as an approximation (0.406 nm)

$D_{optical}$ (DCM) = 2.03

D_{static} (DCM) = 9.08

peroxide particularly strongly donating much greater pi* donation which lowers reorganization energy scale that down by the distortion squared, distributing that over mode centers, since it goes as the distortion squared, it dramatically lowers the reorganization energy

λ_{outer} to be 0.574 eV

As comparison to Table 18

Inner sphere reorganization (λ_{inner}) energy of free superoxide/peroxide is also calculated as follows using equation 12 and data in Table 20. The calculated λ_{inner} is hence 0.76 eV.

Table 20. DFT calculated energy for free superoxide/peroxide moieties

peroxo opt	-150.0925648	
peroxo at superoxo geom	-150.0658226	
superoxo opt	-150.3926457	
superoxo at peroxo opt	-150.3633128	
λox	0.02674217	hartrees
λred	0.02933291	hartrees
Average	0.762940688	eV

To determine the λ_{outer} contribution to the ferrocenyl reduction of the superoxide dicopper complex in DCM, the dielectric continuum model was used again with the radius of $[Cu^{II}_2(UN\text{-}O^{-})(O_2^{\bullet-})]^{2+}$ estimated to be 0.678 nm (calculated, see SI), ferrocene 0.406 nm, and the $D_{optical}$ and D_{static} of DCM as 2.03 and 9.08 which yielded a λ_{outer} of 0.56 eV. Thus, the calculations yielded a λ_{total} of 0.81 eV, which is in reasonable agreement with the Eyring plot derived value of 1.1 ± 0.2 eV, i.e., its lower side value (1.1 – 0.2 = 0.9 eV), but in excellent agreement with the value of 0.84 ± 0.02 eV derived from the experimentally determined electron transfer rate at -80 °C using **eq. 11**.

Kinetic data on the electron-transfer reduction of some superoxo-dicobalt(III) complexes have also provided λ value information. Thus, for the $[Co_2(NH_3)_{10}(m\text{-}O_2^{\bullet-})]^{5+}$ (Table 16) reduction by the cobalt(II) outer-sphere reducing agent, $[Co(terpyridine)_2]^{2+}$ [24a] or ascorbate, λ_{total} values of 2.9 eV and ~ 2.0 eV, respectively, could be determined from the cross-reaction rate constant and known thermodynamics for the redox partners involved. These reactions proceed reasonably fast with log k_{12} = 3-5 at RT for reactions with driving forces of ΔE = 0.5-0.7 V. While our detailed kinetic study is on the oxidation of $[Cu^{II}_2(UN\text{-}O^{-})(O_2^{2-})]^{+}$, when we carry out the reduction of superoxo complex

$[Cu^{II}_2(UN\text{-}O^{-})(O_2^{\bullet-})]^{2+}$, with Me_8Fc, the reaction is very fast, immediate by benchtop observation, at –80 °C, where the thermodynamic driving force ΔE_{rx} is only ~ 0.1 V. One can conclude that the reorganization energy for our dicopper superoxo/peroxo electron-transfer interconversion is far smaller than that for the dicobalt analogs. In support of this and perhaps a better comparison is that when $[Ru(bpy)_3]^{3+}_{(aq)}$ oxidizes $[Co_2(NH_3)_8(\mu\text{-}O_2^{2-}, NH_2)]^{3+}$ log k_{12} = –6 (RT, aqueous) where $\Delta E°_{rx}$ is ~ 0.5 V.[37] Thus, a thermodynamically very favorable oxidation of the bridged dicobalt(III) peroxo compound is exceedingly slow when compared to our extremely fast analogous reaction involving copper, $[Cu^{II}_2(UN\text{-}O^{-})(O_2^{2-})]^{+}$ + Me_2Fc^{+} → $[Cu^{II}_2(UN\text{-}O^{-})(\mu\text{-}1,2\text{-}O_2^{\bullet-})]^{2+}$ + Me_2Fc (at –80 °C); again, this is consistent with our finding of a very small λ_{total} (and λ_{inner}) for dicopper, but the presence of an unfavorable large reorganization energy for the dicobalt system.

Similarly, for an aqueous dirhodium[38] superoxide complex, $[(H_2O)_4(OH)Rh^{III}(O_2)Rh^{III}(OH)(H_2O)_4]^{3+}$, reduction to its peroxide counterpart occurs with a large thermodynamic driving force (> 1 V) when strong reducing agents such as $V^{2+}_{(aq)}$ and $Eu^{2+}_{(aq)}$ are elected, the reaction only shows moderately fast kinetics, log k_{12} ~ 5. Therefore, a large reorganization energy is operative for the reduction of this dirhodium superoxo complex.

Cummins, Nocera and co-workers,[39] with their hexacarboxamide cryptand encapsulated peroxide or superoxide anion (see above), also determined a reorganization energy of 1.5 eV by using photoexcited ruthenium(II) complexes as oxidants for the conversion of the peroxide dianion to superoxide anion (**eq. 13**).[39] The inner-sphere

reorganization energy portion of that was determined to be 0.9 eV based on DFT calculations.

$^{-}$O–O^{-} (H-bonding cryptand) – e^{-}

—> O–O$^{\bullet-}$ (H-bonding cryptand) (**eq. 13**)

It serves to be emphasized, that in the present study, the reorganization energy of the $[Cu^{II}_2(UN\text{-}O^{-})(O_2^{\bullet-})]^{2+}$ —> $[Cu^{II}_2(UN\text{-}O^{-})(O_2^{2-})]^{+}$ transformation is small compared to the cryptand and isolated dianion, which suggests a sizable metal complex (i.e., dicopper) contribution in decreasing the magnitude of the reorganization. To elucidate the nature of the contributions, we analyzed the donation of the peroxide/superoxide to the copper in the frontier molecular orbitals using a Mullikan population analysis. The oxygen character in the unoccupied Cu orbitals (186α and 186β) were 42.2 % and 44.9 % in the peroxide complex, whereas in the superoxide complex, the O_2 π^* contributions were 34.4 % and 11.1% (185β and 186α). Thus, the peroxide has a much greater π^* donation. This enhanced donation is reflected in the Mayer bond order, where the Cu-O bonds were 0.75 (average) in the peroxide compared to 0.517 (average) in the superoxide. (Table 21) The average Cu-O bond lengths also increased from 1.985 Å in the peroxide to 2.047 Å in the superoxide, while the Cu-N distances slightly contracted. The significantly better covalency in the peroxide complex thus distributes the distortion over more centers, and as the reorganization energy goes by the square of the distortion,[36] by

distribution the distortion over more centers the reorganization energy is dramatically lowered.

Mullikan population analysis

Mulliken populations were tabulated using QMForge. [Tenderholt, A. L. QMForge, Version 2.1; Stanford University: Stanford, CA, 2007]

Table 21. Mullikan population analysis

Peroxo C4

orbital	level	occ	E(eV)	Cu	O_2	rest
186α	Cu_A d – O_2 π^*	0	-4.279	45.5	42.2	12.3
186β	Cu_B d – O_2 π^*	0	-4.344	41.9	44.9	13.2
		charge		0.49, 0.53	-0.30, -0.27	
		spin density		-0.43, 0.39	0.10, -0.19	

Peroxo Mayer B.O. Cu_A-O_2 0.766 (0.624 + 0.142)

Peroxo Mayer B.O. Cu_B-O_2 0.734 (0.148 + 0.586)

Peroxo Mayer B.O. O-O 0.921

Selected Metrical Parameters	
Cu_N•••Cu_{Me} (Å)	3.449
O–O (Å)	1.356
Cu_N–O (Å)	1.972
Cu_{Me}–O (Å)	1.998
Cu_N–O_{PhO-} (Å)	2.079
Cu_{Me}–O_{PhO-} (Å)	2.111
Cu_N–N (Å)	2.144, 2.149, 2.205
Cu_{Me}–N (Å)	2.137, 2.219, 2.231
∠Cu_N–O–O–Cu_M (°)	72.6

Cu-O-O: 113.0°, 104.8°

Superoxo C4

orbital	level	occ	E(eV)	Cu	O_2	rest
185β	Cu_A d – O_2 π^*	0	-4.068	46.2	34.4	19.4
186α	Cu_B d – O_2 π^*	0	-4.251	59.7	11.1	29.1
186β	O_2 π^*	0	-3.961	14.3	78.1	7.6
		charge		0.47, 0.56	-0.16, -0.15	
		spin density		0.54, -0.57	0.46, 0.62	

Superoxo Mayer B.O. Cu_A-O_2 0.579 (0.500 + 0.079)

Superoxo Mayer B.O. Cu_B-O_2 0.455 (0.054 + 0.401)

Superoxo Mayer B.O. O-O 1.24

Selected Metrical Parameters	
Cu_N•••Cu_{Me} (Å)	3.473
O–O (Å)	1.293
Cu_N–O (Å)	2.013
Cu_{Me}–O (Å)	2.080
Cu_N–O_{PhO-} (Å)	2.020
Cu_{Me}–O_{PhO-} (Å)	2.013
Cu_N–N (Å)	2.091, 2.100, 2.192
Cu_{Me}–N (Å)	2.066, 2.101, 2.247
∠Cu_N–O–O–Cu_M (°)	8.4

Cu-O-O: 123.9°, 120.1° → 11% reduction in overlap from sin θ

Thus, the low reorganization energy for reduction of superoxo complex $[Cu^{II}_2(UN\text{-}O^{-})(O_2^{\bullet-})]^{2+}$ to peroxo species $[Cu^{II}_2(UN\text{-}O^{-})(O_2^{2-})]^{+}$, in fact experimentally determined by ferrocenium oxidations of $[Cu^{II}_2(UN\text{-}O^{-})(O_2^{2-})]^{+}$, occurs with no change in copper oxidation state, little if any change in the overall coordination geometry and only small changes in O–O and Cu–O bond distances. We can further compare the *l* value of 1.1 eV with situations where complexes with Cu(II) are reduced to Cu(I). A λ value of 1.6 eV [40]is found for ferrocenyl (Me_2Fc and Fc) reductions of the dicopper(II) complex $[Cu^{II}_2(N3)]^{4+}$ to its dicopper(I) analog (N3 is a binucleating ligand possessing bis(2-

pyridylethyl)amine (PY2) tridentate moieties connected by a $–(CH_2)_3–$ linker); the Cu(II) coordination environments include four or five ligand donors,[41]whereas the Cu(I) ligation to the PY2 tridentate moieties are three coordinate or sometimes a fourth exogenous ligand binds.[41a,42]With copper ion in a tetradentate tris(2-pyridylmethyl)-amine (tmpa) environment, the Cu(II) to Cu(I) reorganization energy is smaller, λ = 1.29 eV, also using ferrocenyl redox reagents, where both Cu(II) and Cu(I) tmpa complexes tend to be pentacoordinate with a solvent molecule as fifth ligand.[43]

Another value for comparison is λ = 2.2 eV found for the electron transfer from $Me_{10}Fc$ and Me_8Fc to the peroxo complex $[Cu^{II}_2(N3)(O_2^{2–})]^{2+}$.[40]This very large λ value has its origin in the fact that O-O bond cleavage occurs upon electron-transfer reduction. In contrast to this, for the electron-transfer reduction of superoxo complex $[Cu^{II}_2(UN\text{-}O^–)(O_2^{\bullet –})]^{2+}$ to peroxo species $[Cu^{II}_2(UN\text{-}O^–)(O_2^{2–})]^+$, no O-O cleavage occurs and a smallish change in O-O bond distance is expected, $O\text{-}O_{superoxide}$ ~ 1.29 Å and $O\text{-}O_{peroxide}$ ~ 1.36 Å. As mentioned above, the ferrocenyl reduction of $[Cu^{II}_2(UN\text{-}O^–)(O_2^{\bullet –})]^{2+}$ to $[Cu^{II}_2(UN\text{-}O^–)(O_2^{2–})]^+$ occurs with λ = 1.1 eV (experimentally derived) while the internal electron-transfer reorganization energy could be calculated to be ~ 0.4 eV (*vide supra*).

As we are emphasizing metal-bound oxygen derived species, high-valent metal-oxo complexes are of great biological and chemical interest, as strong electron-transfer oxidants or oxygen-atom transfer reagents.[44] Heme-containing horseradish peroxidases effect electron-transfer oxidations when the active species generated are Compound I $[(P^{\bullet +})Fe^{IV}=O]$ or Compound II $[(P)Fe^{IV}=O]$ (where $P^{\bullet +}$ is a porphryinate radical cation); for these one-electron reduction reactions, reorganization energies have been calculated

to be 1.3 and 1.6 eV, respectively.[45] A smaller λ value is associated with a more reactive species, i.e., the activation energy for reaction is lower, *cf* **eq. 9**. Some high-valent macrocycle-Mn^{V}=O or Mn^{IV}=O complexes have been shown to possess similar *l* values, 1.5 and 1.7 eV respectively.[46]However, non-heme high-valent Fe^{IV}=O complexes, important in biochemistry and in synthetic chemical systems, have higher reorganization energies for $Fe^{IV/III}$ transformations, in the range of 2.0 to 2.7 eV, due to a significantly greater flexibility of their supporting ligands.[44]

There is some data available for a dioxygen (molecular oxygen) reduction to superoxide anion reorganization energies. In aqueous media the total reorganization energy, λ, has been determined to be 1.97 eV.[47] In a calculation by Fukuzumi, based on thermodynamic data available, a Cu^{I}-O_2 species where dioxygen is hypothetically bound to copper(I) prior to electron-transfer), the internal (inner-sphere) electron-transfer from the copper(I) to the O_2 to give a cupric-superoxide product (that species which is observed) gives a calculated λ (total) value of 1.74 eV.[43b] A related calculation indicates that free dioxygen binds to a porphryinate-cobalt(II) complex to give the Co(III)-superoxide species with λ = 1.89 eV.[43b] An interesting finding and analysis by Roth and Klinman[48]is that for glucose oxidase, reduction of O_2 to give superoxide is rate-limiting but is made to be quite fast because of an enzyme adaption which lowers the reorganization energy by ~ 0.8 eV, *via* generation of a positive charge from His protonation.

Again, to overview, this small λ value for the reduction of $[Cu^{II}_2(UN\text{-}O^{-})(O_2^{\bullet -})]^{2+}$ to $[Cu^{II}_2(UN\text{-}O^{-})(O_2^{2-})]^{+}$ may possess further biological relevance since low *l* values are

estimated in many enzyme catalyzed reactions.[49] In 'blue' electron-transfer copper proteins, the copper ion ligand environment is essentially fixed for both copper ion oxidation states, in order for that biologically efficient redox chemistry to occur; *l* values in such proteins are as low as 0.6 eV.[50] For the heme protein cytochrome *c*, Warshel and coworkers[49c] have estimated the solvent (water) reorganization to be between 0.4 to 0.65 eV and the protein contribution to be 0.35 to 0.45 eV. Gray & Winkler[49b] have made similar findings, and including still other redox proteins, low reorganization energies in the range of 0.5 – 1.2 eV exist.

CONCLUSIONS

For the first time, a dicopper ion-bound superoxide/peroxide electron-transfer equilibrium has been observed, that for the pair of dicopper(II) complexes $[Cu^{II}_2(UN\text{-}O^{-})(O_2^{\bullet-})]^{2+}$ and $[Cu^{II}_2(UN\text{-}O^{-})(O_2^{2-})]^{+}$, providing a superoxide-to-peroxide reduction potential of $E°$ = + 0.13 V vs SCE, in dichloromethane as solvent. The binucleating ligand UN-O^{-} facilitated such chemistry, stabilizing both superoxide and peroxide entities (Figure 15). These synthetic complexes or related ones have the potential to serve as models for certain O_2-activating copper proteins with known or putative dicopper active sites. These include tyrosinase,[51] *particulate*-methane monooxygenase (pMMO)[51-52] and possibly even human dopamine β-hydroxylase.[53] As discussed, the one-electron reduction potential for the superoxo/peroxo redox pair found here falls into the biologically relevant region when comparing this value with the existing literature (Table 16), even though solvent and other conditions are different.

The small inner sphere reorganization energy λ_{in} of the peroxo complex $[Cu^{II}_2(UN\text{-}O^-)(O_2^{2-})]^+$ oxidation to the superoxo complex $[Cu^{II}_2(UN\text{-}O^-)(O_2^{\bullet-})]^{2+}$, calculated to be 0.4 eV, suggests the interconversion of $[Cu^{II}_2(UN\text{-}O^-)(O_2^{\bullet-})]^{2+}$ and $[Cu^{II}_2(UN\text{-}O^-)(O_2^{2-})]^+$ to be highly favorable pathway during electron transfer (Figure 15). The superoxo μ-1,2-$[Cu^{II}_2(UN\text{-}O^-)(O_2^{\bullet-})]^{2+}$ and μ-1,1-$[Cu^{II}_2(UN\text{-}O^-)(O_2^{\bullet-})]^{2+}$ forms are considered to be in fast equilibrium based on mixed-isotope rRaman analysis and DFT calculations.

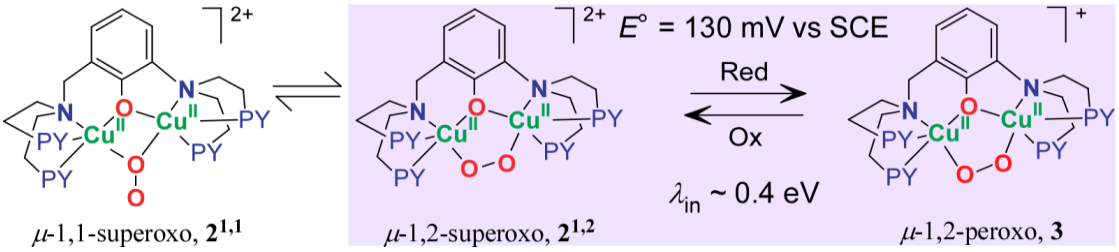

Figure 15. Superoxide and peroxide interconversion and equilibrium.

Interconversion of the μ-1,2-peroxide $[Cu^{II}_2(UN\text{-}O^-)(O_2^{2-})]^+$, and the μ-1,2-superoxide $[Cu^{II}_2(UN\text{-}O^-)(O_2^{\bullet-})]^{2+}$, and equilibrium of μ-1,2-superoxide and μ-1,1-superoxide complexes.

The total reorganization energy for the cross reaction, as an oxidation, $[Cu^{II}_2(UN\text{-}O^-)(O_2^{2-})]^+ + Me_2Fc^+ \rightarrow \mu$-1,2-$[Cu^{II}_2(UN\text{-}O^-)(O_2^{\bullet-})]^{2+} + Me_2Fc$, is determined to be 1.1 ± 0.2 eV with a small driving force $\Delta G^o \sim -0.1$ eV. This low λ value and a small thermodynamic driving force make this system quite interesting compared to more complex redox enzymes that typically have electron transfer reorganization energy $\lambda \leq$ 1.0 eV and rather small thermodynamic driving forces, $\Delta G^o \leq -0.3$ eV.[49]

The thermodynamics of metal-bound superoxo-peroxo interconversion reactions are important to determine for fundamental reasons. How with ligand design can we use coordination chemistry to control reduction potentials and subsequent reactivity? Do reduction potentials even correlate to reactivity, or the type of chemistry involved, e.g., H-atom abstraction, proton-coupled electron transfer (PCET) or atom transfer (oxo-transfer)?[54] Does the metal-superoxide to metal-peroxide (without or with a proton) reduction potential relate or correlate to the facility towards subsequent reductive O–O bond cleavage, as required and occurring in biological oxidases or fuel-cells? Is a metal ion bound peroxide moiety a necessary intermediate to pass on to an O-O reductive cleavage step? If it is, to what metalation and/or protonation state of the O_2^{2-} fragment required.

The fundamental thermodynamics and electron-transfer properties of these dicopper(II) peroxo and superoxo complexes, with $E°$ = +130 mV vs SCE and a reorganization energy of 1.1 eV makes this system biologically relevant in the sense that these compounds or others may be useful in understanding redox processes in more complex biological systems. Expansion of such investigations, for example to situations with a single copper ion (and not in a binuclear complex) is certainly required for us to fully understand important reactions involving O_2 and its reduced derivatives, which critically apply to our societal energy outlook.

Intended to be blank.

CHAPTER TWO

A Peroxynitrite Dicopper Complex: Formation via Cu-NO and Cu-O_2 Intermediates and Reactivity via O–O Cleavage Chemistry

INTRODUCTION

Over 10^{13} oxygen molecules (dioxygen; O_2) are consumed in a single human cell per day,[55] about 1% of which become free (unbound) radicals i.e. reactive oxygen species (ROS) and/or reactive nitrogen species (RNS) including superoxide, hydroxyl radical, and peroxynitrite (PN; $^{-}$OON=O).[55b] In biology, PN is commonly proposed to be responsible for tyrosine nitration, which may lead to loss of protein function and/or other deleterious consequences.[56] PN may be generated from the very fast coupling of superoxide radical ($O_2^{\bullet-}$) with nitric oxide (NO; nitrogen monoxide);[57] the latter itself plays a key role in a variety of biological processes, including signaling, neural transmission and the immune system.[58] Superoxide concentrations in cells are limited by superoxide dismutases (Zn/CuSOD and MnSOD), converting $2O_2^{\bullet-}$ to H_2O_2 and O_2, therefore suppressing PN production.[59]

Extensive biomolecule (e.g., protein Tyr residues, lipids) nitration and/or oxidation is associated with Alzheimer's disease (AD), quite possibly arising from imbalances in metal ion (e.g., Fe and Cu) homeostasis.[55c,60] Oxidative and/or nitrosative "stress" may in fact be attributed to the association of copper ion with amyloid beta (Aβ) peptides which are crucially involved in AD,[61] as they aggregate and deposit as amyloid plaques and neurofibrillary tangles that are found between damaged neurons in AD patient's brains.[62] The N-terminus of the Aβ peptides is a copper binding region (which includes His6, His13 and His 14)[55c,60f,63] and it has lately been shown that nitration of amino acid Tyr-10 may greatly enhance Aβ aggregation.[62c,64] A recent computational study shows that Aβ bound to Cu^{2+} ion could generate PN in the presence of ascorbate,

nitric oxide and dioxygen.[65] In fact, this proposal has separate experimental backing, in that ligand-copper complexes have in the last few years been shown to be able to form LCu($^{-}$OON=O) species,[66] with reactions of Cu^{I} with $O_{2(g)}$[66a] and then $NO_{(g)}$ or Cu^{I}-NO with $O_{2(g)}$ (Scheme 1).[66b-e]

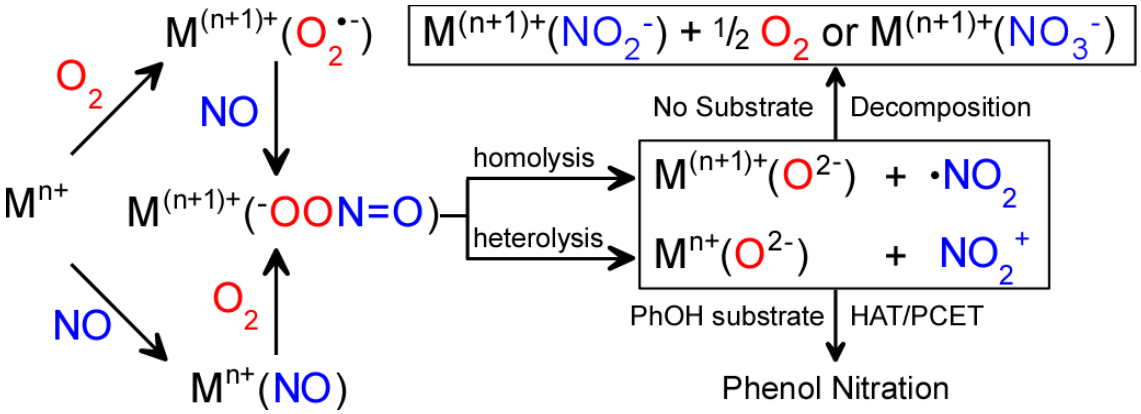

Scheme 1. Transition metal bound peroxynitrite ($^{-}$OON=O) chemistry.

Bioinspired chemical systems have shown that coordination complexes with a number of different metal ions, along with sources of $NO_{(g)}$ and $O_{2(g)}$ can lead to the generation of metal bound PN species. Koppenol and coworkers[67] reported the first isolated PN-complex of cobalt(III), from reaction of a pentacyano-cobalt(III) superoxide compound reacting with $NO_{(g)}$ to give $[Co^{III}(CN)_5(^{-}OON=O)]^{3-}$ (Scheme 1). Kurtikyan and coworkers[68] have more recently published on porphyrinate Co^{III}-PN complexes, thoroughly characterized by IR spectroscopy and DFT calculations. A heme-PN complex was implicated to form from a heme-superoxo species reacted with $NO_{(g)}$, as it led to a nitrato heme $Fe^{III}(NO_3^{-})$ species, by isomerization (Scheme 1).[69] In aqueous chemistry,

PN rapidly isomerizes to nitrate in ~90% yield,[70] in fact, the application of this reaction to PN decomposition catalysis has been a subject of intense research.[71] Such catalysts have been shown to exhibit highly favorable biological effects.[56g,72]

Peroxynitrite-metal complexes may also form as intermediates in the oxygenation of metal-nitrosyl complexes,[73] such as first reported by Basolo,[74] ultimately giving nitrite products (Scheme 1). For two cases involving copper-peroxynitrite complexes,[66a,66b] LCu^{II}-PN complexes thermally transform to give LCu^{II}-nitrite products plus dioxygen. This seems to also correspond to known aqueous chemistry; peroxynitrite decomposes through various pathways,[57c,75] including where it degrades according to $2\ ^{-}OON{=}O \rightarrow O_2 + 2\ NO_2^-$ under basic conditions and relatively high concentration,[75b,75d,75e] and such reactivity has even been observed in aqueous chemistry with copper ion.[76] Similarly, Nam and coworkers reported formation of macrocyclic ligand bound metal-PN complexes, for example, LCr^{III}-PN[77] and nonheme-Fe^{III}-PN[78] species, generated from precursor M-O_2 adducts reacting with $NO_{(g)}$ (Scheme 1). A novel case is where a macrocyclic ligand (L)Co-nitrosyl complex reacts with potassium superoxide (KO_2) leading to LCo^{III}-nitrite + ½ $O_{2(g)}$ products, all proceeding through putative Co-PN intermediates (Scheme 1).[79]

Following the now known M-$O_{2(g)}$ + $NO_{(g)}$ biological and chemical examples to give peroxynitrite and subsequent reactions, plus the likely importance of copper in chemical or biological systems,[55c,66f,6,61,9] we report here on a new system involving binuclear copper species, which gives rise to chemistry not previously observed, and providing new insights. In the past, we performed extensive studies concerning the

binucleating ligand UN-O$^-$ [9,80] where a phenolate O-atom bridges two copper ions. In this work, we report on the formation of a peroxynitrite moiety bound to this binuclear dicopper(II) framework, $[Cu^{II}_2(UN\text{-}O^-)(^-OON{=}O)]^{2+}$ (Chart 1).

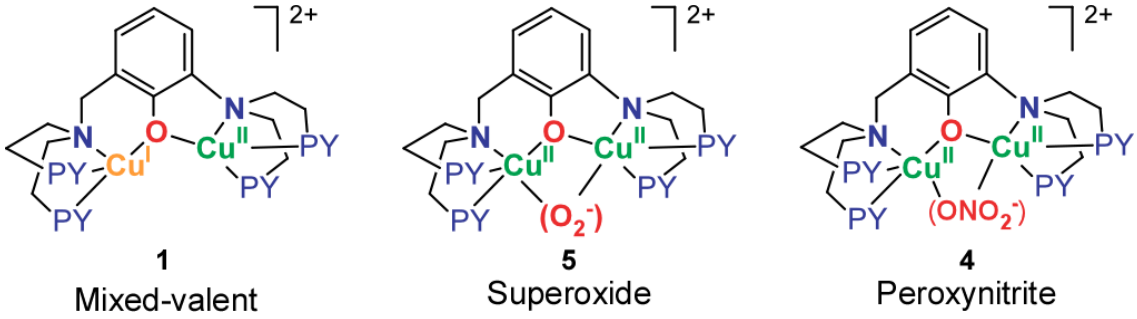

Chart 1. Mixed-valent dicopper complex $[Cu^{I,II}_2(UN\text{-}O^-)]^{2+}$, superoxide dicopper(II) complex $[Cu^{II}_2(UN\text{-}O^-)(O_2^{\bullet-})]^{2+}$ and peroxynitrite dicopper(II) complex $[Cu^{II}_2(UN\text{-}O^-)(^-OON{=}O)]^{2+}$.

Peroxynitrite complex $[Cu^{II}_2(UN\text{-}O^-)(^-OON{=}O)]^{2+}$ can be generated by both pathways discussed, (a) $M^{n+} + O_{2(g)} + NO_{(g)}$ or (b) $M^{n+} + NO_{(g)} + O_{2(g)}$ (Scheme 1, but where M^{n+} is a mixed-valent Cu^ICu^{II} complex **1** and $M^{n+} + O_{2(g)}$ gave rise to the fully characterized superoxide dicopper(II) complex $[Cu^{II}_2(UN\text{-}O^-)(O_2^{\bullet-})]^{2+}$, ν(O-O) = 1120 or 1140 cm^{-1}.[80]) Here, using low-temperature infrared (IR) spectroscopy, we report on a dicopper nitrosyl complex and intermediates involved metal-peroxynitrite $[Cu^{II}_2(UN\text{-}O^-)(^-OON{=}O)]^{2+}$ formation. Further, $[Cu^{II}_2(UN\text{-}O^-)(^-OON{=}O)]^{2+}$ is able to facilitate aromatic ring nitration chemistry, including an exogenously 2,4-di-^{t}Bu-phenol (DTBP) substrate, as a biological tyrosine substrate surrogate.

EXPERIMENTAL SECTION

Materials and Instrumentations.

All chemicals were purchased from Sigma-Aldrich Co. in the highest available quality unless otherwise specified. Preparation and handling of air sensitive compounds were achieved using either standard Schlenk line techniques under an argon atmosphere or in an MBraun Labmaster 130 nitrogen atmosphere glovebox with $O_{2(g)}$ and $H_2O_{(g)}$ levels < 1 ppm. HPLC grade dichloromethane (DCM), acetonitrile (ACN) and diethyl ether (Et_2O) were passed through a 60 cm long column of activated alumina under an argon atmosphere before use (Innovative Technologies, Inc.). 2-methyltetrahydrofuran (MeTHF) was distilled over sodium benzophenone under an argon atmosphere prior to use. Solvent deoxygenation was achieved by bubbling argon through the solvent for 30 mins in an addition funnel connected to a receiving Schlenk flask. Deoxygenated solvents were stored in the glovebox inside amber glass bottles and further dried over activated 3 or 4 Å molecular sieves. Dioxygen was dried by passing the gas through a short column of Drierite prior to usage. Nitric oxide was purchased from Matheson Gases and purified according to a literature method.[69a] UV-Vis absorption spectra were recorded on a Cary-50 Bio spectrophotometer using 10 mm path length Schlenk quartz cuvettes. The reaction temperature maintained by a UnispeKs CoolSpeK cryostat controller and a cell holder kit by Unisoku Scientific Instruments. EPR samples were prepared in 5mm O.D. quartz sample tubes (Wilmad-LabGlass) and spectra recorded on an X-band Bruker EMX-plus spectrophotometer equipped with a dual mode cavity (ER 4116DM) Bruker EMX CW EPR controller with a Bruker ER 041 XG microwave bridge operating at the X band (~9

GHz). Low temperature infrared spectra were collected on a Bruker TENSOR 27 FT-IR spectrophotometer equipped with a liquid nitrogen chilled LN-MCT mid-range detector using a Remspec 619 single-crystal sapphire fiber probe (1100 cm^{-1} to 4000 cm^{-1}). Samples were analyzed in a custom made Schlenk tube with two sidearms and an airtight joint from which the optical probe is inserted. In a typical infrared experiment, samples were first prepared in the glovebox and then transferred to the reaction tube using a 5 ml *Hamilton* gastight syringe. Electrospray ionization mass spectrometry(ESI-MS) experiments were performed on a Thermo Finnigan LCQ Deca XP Plus spectrometer. GC-MS analysis was carried out on a Shimadzu GC-17A/GCMS0QP5050 gas chromatograph/mass spectrometer. Synthesis and characterization of the mixed-valent complex $[Cu^{I,II}_2(UN\text{-}O^{-})(DMF)](SbF_6)_2$, M_w = 1229.6 following previously published procedures.[80]

Low-temperature infrared spectroscopy (LT-IR) characterization.

Preparation of LT-IR samples of mixed-valent complex $[Cu^{I,II}_2(UN\text{-}O^{-})(DMF)](SbF_6)_2$ were conducted as follows: 36.8 mg (0.03 mmol) of $[Cu^{I,II}_2(UN\text{-}O^{-})(DMF)](SbF_6)_2$ as a brownish green crystalline solid was added to 3 ml of dichloromethane (DCM) in the glovebox. 43.1 mg (0.06 mmol) of potassium tetrakis(pentafluorophenyl)borate (KBArF, M_w=718.3) was added to the mixture to help fully dissolve the solid compound through anion exchange. The DCM solution was filtered and the resulting clear solution was transferred to a 5 ml *Hamilton* gastight syringe. The LT-IR optical probe was placed inside a custom made reaction tube

equipped with two side arms and airtight joint from which the optical probe is inserted. One of the arms was connected to the Schlenk line and controlled by a glass stopcock while the other arm was sealed with a rubber septum. An inert atmosphere was established by 5 successive vacuum and argon purge cycles. To the reaction tube 3 ml of $[Cu^{I,II}_2(UN\text{-}O^{-})(DMF)](SbF_6)_2$ solution was syringed in through the rubber septum and the probe was submerged under the added solution. The tube was then placed in a dry ice/acetone bath to maintain the temperature at -80 °C. After waiting ten minutes for the temperature to equilibrate, the LT-IR spectrum for the $[Cu^{I,II}_2(UN\text{-}O^{-})(DMF)](SbF_6)_2$ solution was recorded over 20 scans (1100 cm^{-1} to 4000 cm^{-1}) using the OPUS software interface.

Formation of $[Cu^{I,II}_2(UN\text{-}O^{-})(\mu\text{-}\bullet NO)](SbF_6)_2$ monitored by LT-IR. Purified nitric oxide gas, $NO_{(g)}$, was collected in a 250 ml round bottom flask and secured with a clamp inside a fume hood. The pressure of the flask was adjusted to approximately 1 atmosphere using a gas bubbler. A 10 ml *Hamilton* gastight syringe equipped with a three-way high pressure stopcock, containing a stainless steel Luer fitting attached to a Schlenk line, and 12 in. stainless steel needle was prepared. The syringe was evacuated and purged with argon gas five times, before the needle was inserted into the flask containing the purified $NO_{(g)}$, and 5 ml of $NO_{(g)}$ (about 7 eqiv) was withdrawn. $NO_{(g)}$ was gradually added to the solution of $[Cu^{I,II}_2(UN\text{-}O^{-})(DMF)](SbF_6)_2$ by puncturing the septa on the side arm of the reaction tube with the 3-way syringe. The solution "trapped" in the window of the optical probe does not mix very well with the bulk solution in the reaction tube; therefore, the solution was "manually" mixed using the gastight syringe to

withdraw and then quickly inject solution back into the reaction tube to achieve better mixing. The solution was then left to equilibrate at -80 °C for a few additional minutes, after which the LT-IR spectrum of $[Cu^{I,II}_2(UN\text{-}O^{-})(\mu\text{-}\bullet NO)](SbF_6)_2$ was monitored and recorded.

Formation of $[Cu^{II}_2(UN\text{-}O^{-})(\bullet NO)(O_2^{\bullet-})](SbF_6)_2$ (Method 1) monitored by LT-IR. $[Cu^{I,II}_2(UN\text{-}O^{-})(\mu\text{-}\bullet NO)](SbF_6)_2$ solution was put under vacuum and subsequently and purged with argon gas. This process was repeated five times to remove excess $NO_{(g)}$ in the solution. A 10 ml *Hamilton* gastight syringe was equipped with a three-way high pressure stopcock, containing a stainless steel Luer fitting attached via rubber tubing directly to the regulator of dioxygen gas tank, and 12 in. stainless steel needle was prepared. The syringe was evacuated and purged with dioxygen gas. About 5 ml of $O_{2(g)}$ was injected, through the septum sealed side arm of the reaction tube, into the solution of $[Cu^{I,II}_2(UN\text{-}O^{-})(\mu\text{-}\bullet NO)](SbF_6)_2$ and over the course of five minutes, the intermediate $[Cu^{II}_2(UN\text{-}O^{-})(\bullet NO)(O_2^{\bullet-})](SbF_6)_2$ was formed and IR spectrum was recorded at -80 °C.

Formation of $[Cu^{II}_2(UN\text{-}O^{-})(^{-}OON{=}O)](SbF_6)_2$ (Method 1) monitored by LT-IR. The solution of $[Cu^{II}_2(UN\text{-}O^{-})(\bullet NO)(O_2^{\bullet-})](SbF_6)_2$ was mixed several times using a gastight syringe, *vide supra*. Over the course of 20 minutes at -80 °C, the LT-IR spectral features of $[Cu^{II}_2(UN\text{-}O^{-})(\bullet NO)(O_2^{\bullet-})](SbF_6)_2$ decreased and new features corresponding to $[Cu^{II}_2(UN\text{-}O^{-})(^{-}OON{=}O)](SbF_6)_2$ grew in.

Formation of $[Cu^{II}_2(UN\text{-}O^{-})(O_2^{\bullet-})](SbF_6)_2$ monitored by LT-IR. 36.8 mg (0.03 mmol) of $[Cu^{I,II}_2(UN\text{-}O^{-})(DMF)](SbF_6)_2$ as a crystalline solid was dissolved in 3 ml of DCM, and anion exchange was performed *vide supra*. 5 ml of $O_{2(g)}$ was added using a 3-

way syringe into the solution of $[Cu^{I,II}_2(UN\text{-}O^-)(DMF)](SbF_6)_2$ and mixed using a gastight syringe, *vide supra*. The solution was left to equilibrate for 10 minutes and a spectrum was recorded at -80 °C. The $[Cu^{II}_2(UN\text{-}O^-)(O_2^{\bullet-})](SbF_6)_2$ solution was put under vacuum and purged with argon gas. This process was repeated five times to remove excess $O_{2(g)}$ in the solution.

Formation of $[Cu^{II}_2(UN\text{-}O^-)(\bullet NO)(O_2^{\bullet-})](SbF_6)_2$ (Method 2) monitored by LT-IR. 5 ml of $NO_{(g)}$ was added in solution of $[Cu^{II}_2(UN\text{-}O^-)(O_2^{\bullet-})](SbF_6)_2$ using a gastight syringe, *vide supra*. Over the course of 5 minutes, $[Cu^{II}_2(UN\text{-}O^-)(\bullet NO)(O_2^{\bullet-})](SbF_6)_2$ was formed and the LT-IR spectrum was recorded at -80 °C.

Formation of $[Cu^{II}_2(UN\text{-}O^-)(^-OON{=}O)](SbF_6)_2$ (Method 2) monitored by LT-IR. The solution of $[Cu^{II}_2(UN\text{-}O^-)(\bullet NO)(O_2^{\bullet-})](SbF_6)_2$ was mixed several times using a gastight syringe, *vide supra*. Over the course of 20 minutes at -80 °C, the LT-IR spectral features of $[Cu^{II}_2(UN\text{-}O^-)(\bullet NO)(O_2^{\bullet-})](SbF_6)_2$ decreased and new features corresponding to $[Cu^{II}_2(UN\text{-}O^-)(^-OON{=}O)](SbF_6)_2$ grew in.

$^{15}NO_{(g)}$ isotope labeled LT-IR experiments were carried out in the same fashion as with $^{14}NO_{(g)}$, *vide supra*. Spectrum for each complex was recorded, respectively.

UV-Vis characterization of each complex.

The UV-Vis spectrum of superoxide $[Cu^{II}_2(UN\text{-}O^{-})(O_2^{\bullet-})](SbF_6)_2$ formation by reacting $[Cu^{I,II}_2(UN\text{-}O^{-})(DMF)](SbF_6)_2$ with excess $O_{2(g)}$ was previously published.[80] 1.1 mg (0.0009 mmol) of $[Cu^{I,II}_2(UN\text{-}O^{-})(DMF)](SbF_6)_2$ as a green color crystalline solid was dissolved in 6 ml of DCM in the glove box to give 6 ml of 0.15 mM stock solution. 3 ml of the stock solution was transferred to a custom made 1 cm path length Schlenk cuvette and sealed with a rubber septum before bringing the cuvette out of the glovebox. The cuvette was placed inside the cell holder of the cryostat and cooled down to -80 °C. The cuvette was left to equilibrate at -80 °C for 10 minutes, after which excess $O_{2(g)}$ was added to give a green spectrum corresponding to $[Cu^{II}_2(UN\text{-}O^{-})(O_2^{\bullet-})](SbF_6)_2$ in Figure 26b, *vide supra*.

UV-Vis spectrum of $[Cu^{II}_2(UN\text{-}O^{-})(^{-}OON{=}O)](SbF_6)_2$. The solution containing $[Cu^{II}_2(UN\text{-}O^{-})(O_2^{\bullet-})](SbF_6)_2$ was put under vacuum and purged with argon gas five times to remove excess $O_{2(g)}$. 0.2 ml of $NO_{(g)}$ (about 20 equiv) was gradually added to the solution using a 3-way gastight syringe and UV-Vis spectra changes were followed.

UV-Vis spectrum of $[Cu^{I,II}_2(UN\text{-}O^{-})(\mu\text{-}{\bullet}NO)](SbF_6)_2$. The remaining 3 ml of the $[Cu^{I,II}_2(UN\text{-}O^{-})(DMF)](SbF_6)_2$ stock solution was transferred to a second 1 cm path length Schlenk cuvette and sealed with a rubber septum before bringing the cuvette out of the glovebox. The cuvette was placed inside the cell holder of the cryostat and cooled down to -80 °C. The cuvette was left to equilibrate at -80 °C for 10 minutes then 0.2 ml of $NO_{(g)}$ (about 20 equiv) was added to the solution, *vide supra* and UV-Vis spectrum was recorded.

UV-Vis spectrum of $[Cu^{II}_2(UN\text{-}O^-)(^-OON{=}O)](SbF_6)_2$ prepared using Method 2. The $[Cu^{I,II}_2(UN\text{-}O^-)(\mu\text{-}\bullet NO)](SbF_6)_2$ solution was put under vacuum and subsequently purged with argon gas. This process was repeated five times to remove excess $NO_{(g)}$. 1 ml of $O_{2(g)}$ was added to the solution and distinct change in the UV-Vis spectra was observed. The final spectrum of $[Cu^{II}_2(UN\text{-}O^-)(^-OON{=}O)](SbF_6)_2$ was recorded at -80 °C.

UV-Vis spectrum of $[Cu^{II}_2(UN\text{-}O^-)(OH)](SbF_6)_2$ from the reaction of $[Cu^{II}_2(UN\text{-}O^-)(^-OON{=}O)](SbF_6)_2$ with DTBP. The peroxynitrite complex $[Cu^{II}_2(UN\text{-}O^-)(^-OON{=}O)](SbF_6)_2$ can be generated using two methods in DCM, *vide supra*. In either method, adding 1 equiv. of DTBP to the peroxynitrite solution at -80 °C results in the same spectral change to give $[Cu^{II}_2(UN\text{-}O^-)(OH)](SbF_6)_2$ as the final product , and recorded by UV-Vis spectrometry.

UV-Vis spectrum of $[Cu^{II}_2(UN\text{-}O^-)(^-OON{=}O)](SbF_6)_2$ formation and decay in 2-methyltetrahydrofuran (MeTHF) as solvent. 1.2 mg (0.001 mmol) of green color crystalline solid $[Cu^{I,II}_2(UN\text{-}O^-)(DMF)]$ $(SbF_6)_2$ was put in 6 ml of MeTHF in the glovebox. 1.4 mg (0.002 mmol) of potassium tetrakis(pentafluorophenyl)borate (KBArF) was added to the mixture to help dissolve the solid through anion exchange. The solution mixture was filtered to obtain a clear solution. 3 ml of the clear solution was transferred to a 1 cm path length Schlenk cuvette. The cuvette was placed inside the cell holder of the cryostat and cooled down to -80 °C. The cuvette was left to equilibrate at -80 °C for 10 minutes after which excess $O_{2(g)}$ was added to give the dark green spectrum corresponding to $[Cu^{II}_2(UN\text{-}O^-)(O_2^{\bullet-})](SbF_6)_2$, Figure 29b. The solution containing

$[Cu^{II}_2(UN\text{-}O^{-})(O_2^{\bullet-})](SbF_6)_2$ was put under vacuum and subsequently purged with argon gas. This process was repeated over five cycles to remove excess $O_{2(g)}$. 0.2 ml of $NO_{(g)}$ (about 20 equiv) was gradually added to the solution using a gastight 3-way syringe and UV-Vis spectral changes over the course of 20 minutes were followed and are depicted as green dotted lines in Figure 29b. Excess $NO_{(g)}$ was removed using vacuum and argon purge cycles. $[Cu^{II}_2(UN\text{-}O^{-})(^{-}OON{=}O)](SbF_6)_2$ (blue spectrum, Figure 29b) was not stable and started to decompose at -80 °C (dotted blue lines, Figure 29b). After 1 hour, the final spectrum containing $[Cu^{II,III}_2(UN\text{-}O^{-})(O^{2-})]^{2+}(SbF_6)_2$ and NO_2 was recorded (magenta line, Figure 29b.).

Formation of $[Cu^{II}_2(UN\text{-}O^{-})(^{-}OON{=}O)](SbF_6)_2$ in MeTHF and reaction with DTBP. The MeTHF solution of $[Cu^{II}_2(UN\text{-}O^{-})(^{-}OON{=}O)](SbF_6)_2$ was generated at -80 °C, *vide supra*. 1 equiv. of DTBP was added to the solution after removing excess $NO_{(g)}$ using vacuum and argon purge cycles. The reaction product was determined to be $[Cu^{II}_2(UN\text{-}O^{-})(OH)](SbF_6)_2$ based on its UV-Vis spectral features. The oxidized substrate was analyzed using GC-MS.

GC-MS characterization of phenol product.

The product mixtures from reaction of $[Cu^{II}_2(UN\text{-}O^{-})(^{-}OON{=}O)](SbF_6)_2$ with 1 equiv. of DTBP in DCM was put on a rotary evaporator to remove the solvent. The solid materials obtained were dissolved using 10 ml of pentane. The solution was filtered through a medium glass-fritted funnel and concentrated to ~ 1 ml for GC-MS tests. The GC-MS conditions for the product analysis were as follows: Injector Port Temperature: 220 ºC; Detector Temperature 280 ºC; Column Temperature: Initial Temperature 120 ºC;

Initial Time, 2 min; Final Temperature 250 °C, Final Time, 25 min, Gradient Rate 10 °C/min; Flow Rate: 16 ml/min; Ionization voltage: 1.5 kV.

EPR spectroscopy of related complexes.

The EPR samples were prepared as follows: 4.9 mg (0.004 mmol) of $[Cu^{I,II}_2(UN\text{-}O^-)(DMF)](SbF_6)_2$ as a crystalline solid was dissolved in 2 ml of DCM in the glovebox to give 2 ml of 2 mM stock solution. 0.5 ml of the stock solution was transferred to a 5mm O.D. quartz sample tube using a 0.5 ml syringe. This process was repeated three more times to obtain four sample tubes each containing 0.5 ml of the stock solution. Each of the tube was sealed with a rubber septum before bringing out of the glovebox. EPR sample preparations and spectra for complex $[Cu^{I,II}_2(UN\text{-}O^-)(DMF)](SbF_6)_2$ and complex $[Cu^{II}_2(UN\text{-}O^-)(O_2^{\bullet-})](SbF_6)_2$ were previously published.[80]

EPR spectrum of complex $[Cu^{I,II}_2(UN\text{-}O^-)(\mu\text{-}\bullet NO)](SbF_6)_2$. The EPR sample tubes were placed in a dry ice/acetone bath to maintain the temperature at -80 °C. After waiting ten minutes for the temperature to equilibrate, 0.2 ml of $NO_{(g)}$ (about 20 equiv) was gradually added to the solution in one of the tube using a gastight 3-way syringe. The tube was subsequently kept frozen in liquid nitrogen and EPR spectrum was taken at 20K and shown to be silent.

EPR spectrum of complex $[Cu^{II}_2(UN\text{-}O^-)(^-OON{=}O)](SbF_6)_2$. Complex $[Cu^{II}_2(UN\text{-}O^-)(^-OON{=}O)](SbF_6)_2$ were prepared using both of the methods, *vide supra*. The EPR spectra for complex prepared in both of the methods were taken at 20 K and shown to be silent.

RESULTS AND DISCUSSION

The $NO_{(g)}$ Adduct.

We previously reported that with this unsymmetrical binucleating ligand framework binding to two copper ions, a mixed-valent $Cu^{I}Cu^{II}$ complex (with localized electronic structure) can be synthesized, $[Cu^{I,II}_2(UN\text{-}O^{-})(DMF)]^{2+}$ (DMF = dimethylformamide; and with two SbF_6^{-} non-coordinating anions), with DMF binds to the Cu(II) ion, in the solid state.[80] Complex $[Cu^{I,II}_2(UN\text{-}O^{-})(DMF)]^{2+}$ is found to react with excess $NO_{(g)}$ in dichloromethane (DCM) as solvent, at –80 °C (see Experimental Section) to form a complex that we formulate as a mixed-valent copper nitrosyl complex $[Cu^{I,II}_2(UN\text{-}O^{-})(\mu\text{-}\bullet NO)]^{2+}$ (Figure 16a). The formation of $[Cu^{I,II}_2(UN\text{-}O^{-})(\mu\text{-}\bullet NO)]^{2+}$ is accompanied by a change in UV-vis spectra, disappearance of the λ_{max} = 350 nm absorption in $[Cu^{I,II}_2(UN\text{-}O^{-})(DMF)]^{2+}$, and appearance of a more complex spectrum possessing features at λ_{max} = 383 nm and 546 nm (Figure 17b).[81]

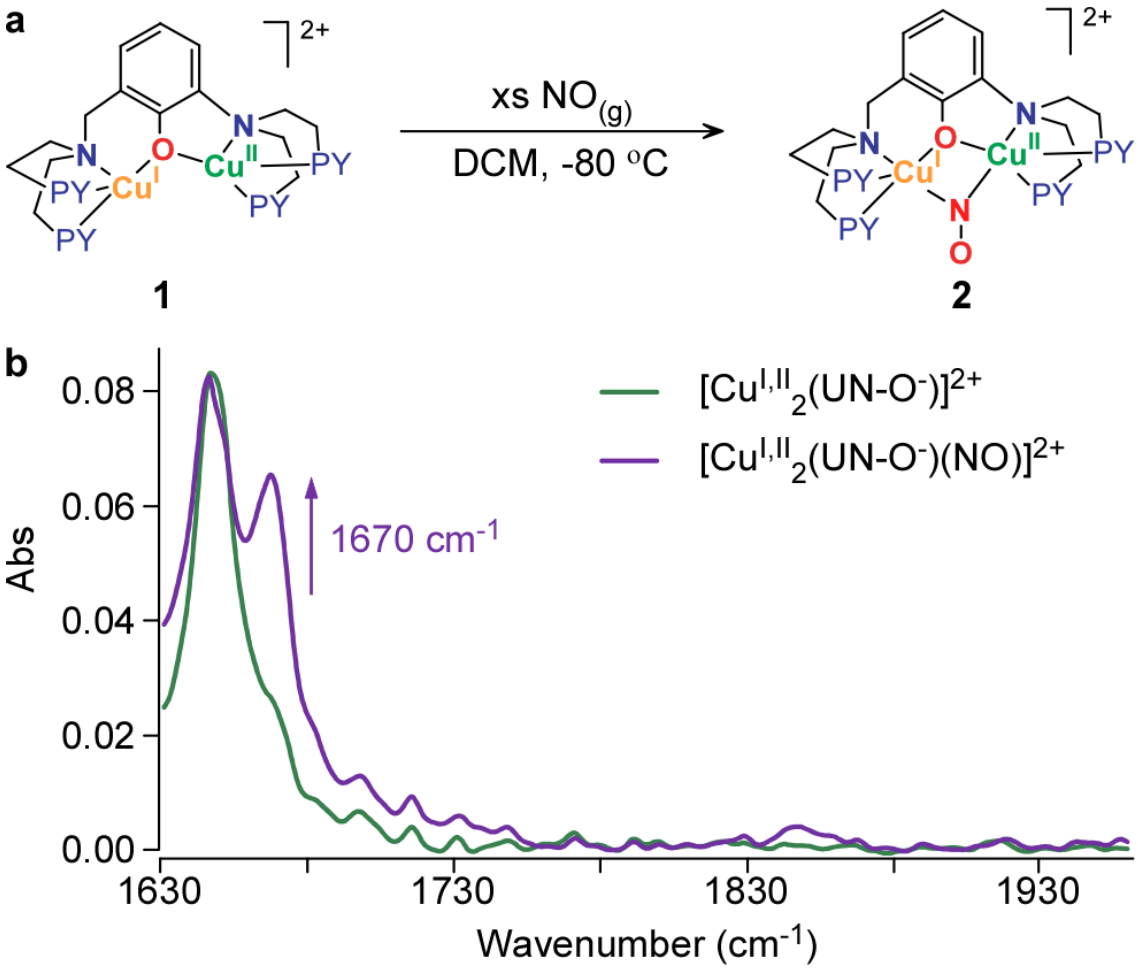

Figure 16. LT-IR of the nitrosyl complex.

(a) $[Cu^{I}Cu^{II}(UN\text{-}O^{-})]^{2+}$ reacts with excess $NO_{(g)}$ to form $[Cu^{I,II}(UN\text{-}O^{-})(NO)]^{2+}$ complex at -80 °C in dichloromethane (DCM) solvent. (b) Low-temperature (-80 °C) infrared spectroscopy of the complex $[Cu^{I}Cu^{II}(UN\text{-}O^{-})]^{2+}$ (green line spectrum) reacting with $NO_{(g)}$ to form complex $[Cu^{I,II}(UN\text{-}O^{-})(NO)]^{2+}$ in purple. The 1670 cm^{-1} full spectrum (in purple) formed within one minute after addition of $NO_{(g)}$.

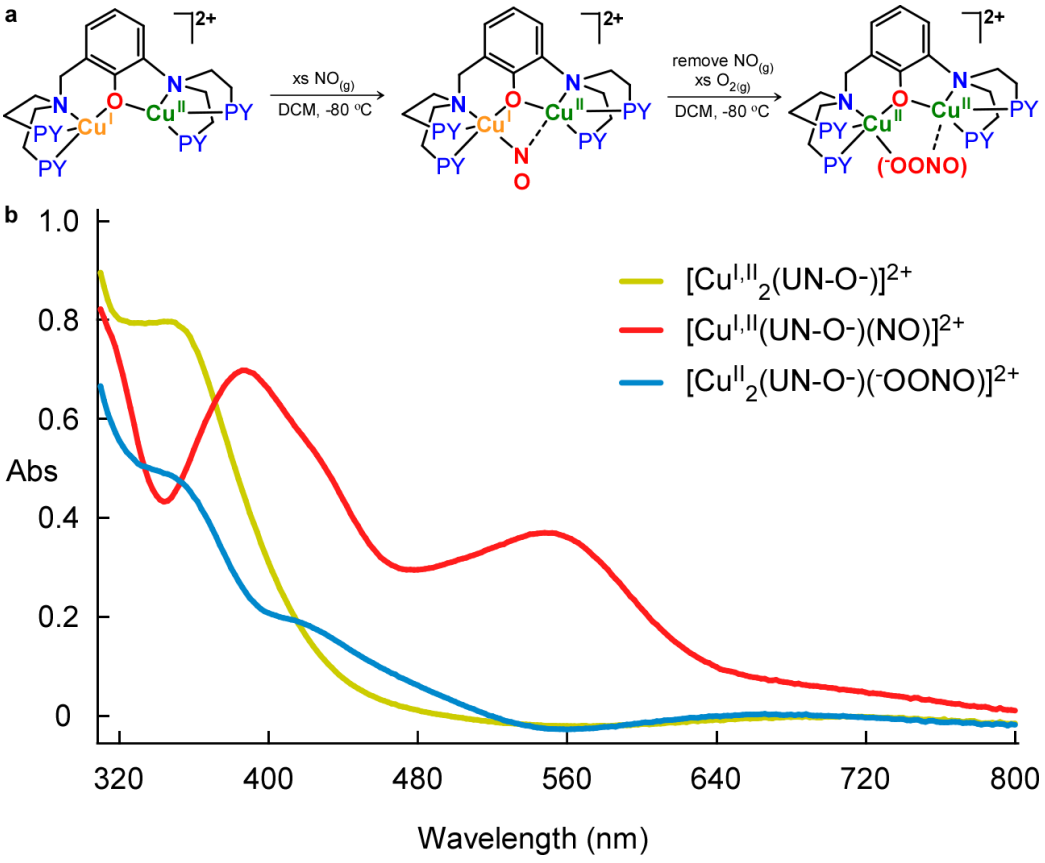

Figure 17. UV-Vis spectra of the nitrosyl and peroxynitrite complexes.

(a) $[Cu^{I,II}_2(UN\text{-}O^-)(DMF)]^{2+}$ reacts with excess $NO_{(g)}$ to form nitrosyl complex $[Cu^{I,II}_2(UN\text{-}O^-)(\mu\text{-}\bullet NO)]^{2+}$ at -80 °C in dichloromethane (DCM) solvent with λ_{max} = 383 nm (3500 $M^{-1}cm^{-1}$) and 546 nm (1900 $M^{-1}cm^{-1}$). After removing excess $NO_{(g)}$ and adding excess $O_{2(g)}$, peroxynitrite complex $[Cu^{II}_2(UN\text{-}O^-)(^-OONO)]^{2+}$ was formed over the course of 10 minutes at -80 °C. (b) UV-Vis spectrum change starting from $[Cu^{I,II}_2(UN\text{-}O^-)(DMF)]^{2+}$, yellow spectrum, upon addition of $NO_{(g)}$ to form the nitrosyl complex $[Cu^{I,II}(UN\text{-}O^-)(NO)]^{2+}$, red spectrum. After removing excess $NO_{(g)}$ and adding excess $O_{2(g)}$, peroxynitrite complex $[Cu^{II}_2(UN\text{-}O^-)(^-OONO)]^{2+}$ is shown in blue spectrum with λ_{max} = 355 (sh, 2500 $M^{-1}cm^{-1}$), 420 (sh, 1000 $M^{-1}cm^{-1}$) and 680 nm (450 $M^{-1}cm^{-1}$).

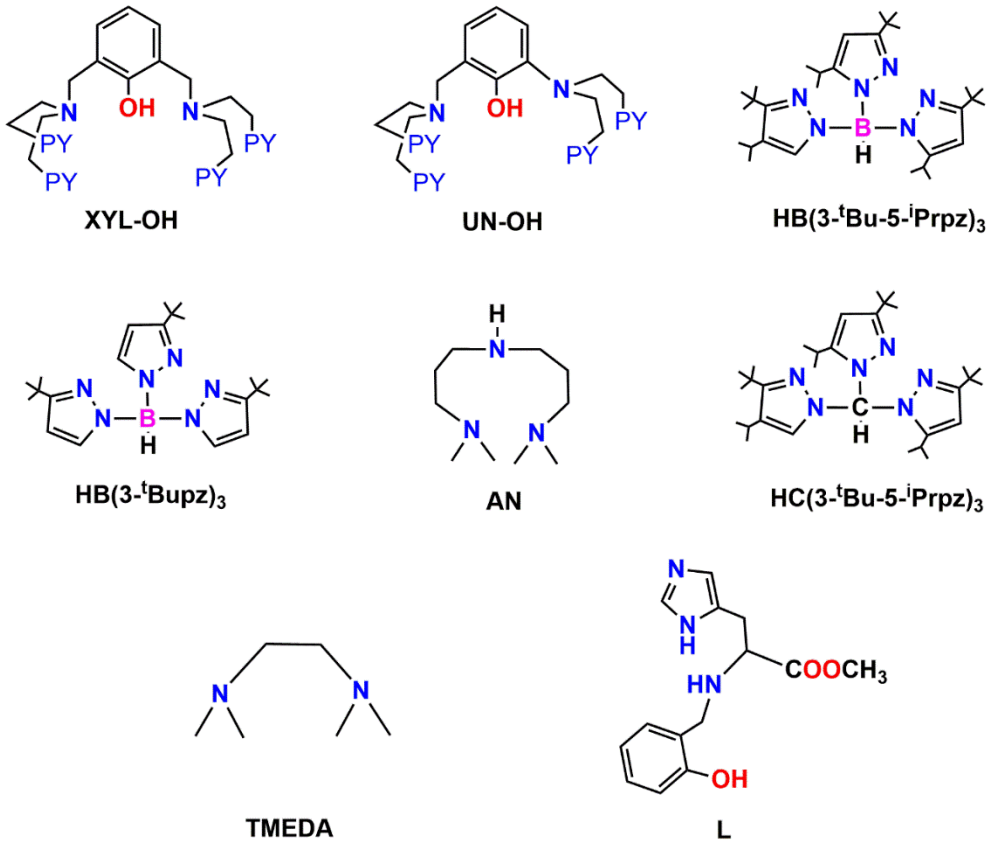

Figure 18. Drawings of the ligands and IUPAC names in Tables 22-23.

XYL-OH = 2,6-bis((bis(2-(pyridin-2-yl)ethyl)amino)methyl)phenol; UN-OH = 2-(bis(2-(pyridin-2-yl)ethyl)ami no)-6-((bis(2-(pyridin-2-yl)ethyl)amino)methyl)phenol; HB(3-^{t}Bu-5-^{i}Prpz)$_3$ = hydrotris(3-*tert*-buty l-5-isopropyl-1-pyrazolyl)borate; HB(^{t}Bupz)$_3$ = hydrotris(3-*tert*-butyl-1-pyrazolyl)borate; AN= N1-(3-(dimethylamino)propyl)-N3,N3-dimethylpropane-1,3-diamine; HC(3-^{t}Bu-5-^{i}Prpz)$_3$ = tris(3-tert-butyl-5-isopropyl-1-pyrazolyl)methane; TMEDA = N,N,N',N'-tetramethylethylenediamine; L = met hyl(2-hydroxybenzyl)histidinate.

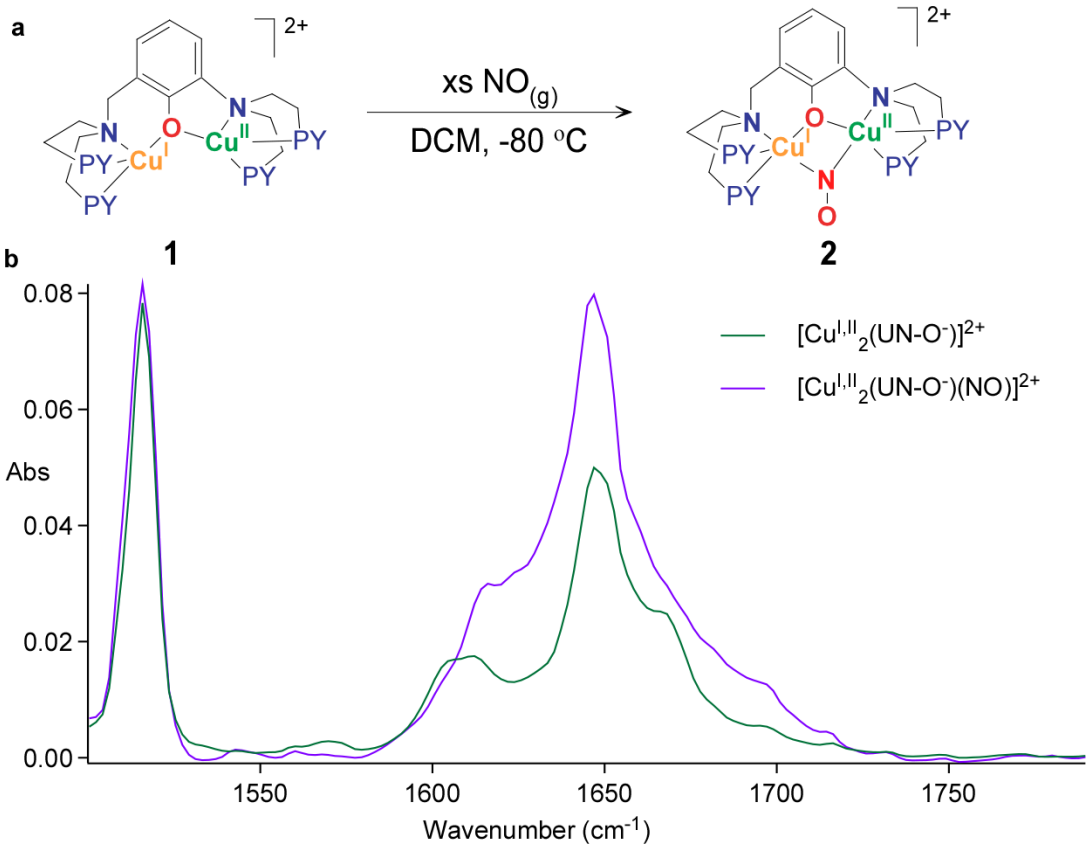

Figure 19. LT-IR of the nitrosyl complex with ^{15}NO labeled.

(a) $[Cu^{I}Cu^{II}(UN\text{-}O^{-})]^{2+}$ reacts with excess labeled $^{15}NO_{(g)}$ to form $[Cu^{I,II}(UN\text{-}O^{-})(NO)]^{2+}$ complex at -80 °C in dichloromethane (DCM) solvent. (b) Low-temperature (-80 °C) infrared spectroscopy of the complex $[Cu^{I}Cu^{II}(UN\text{-}O^{-})]^{2+}$ (green colored spectrum) reacts with $^{15}NO_{(g)}$ to form complex $[Cu^{I,II}(UN\text{-}O^{-})(NO)]^{2+}$ (purple colored spectrum), $\nu(^{15}N\text{-}O)$ = 1645 cm^{-1}, which is down-shifted from the ν(N-O) at 1670 cm^{-1} (Figure 16). Note the band from complex $[Cu^{I,II}(UN\text{-}O^{-})(NO)]^{2+}$, $\nu(^{15}N\text{-}O)$ at 1645 cm^{-1} overlaps with the band in the starting mixed-valent complex $[Cu^{I}Cu^{II}(UN\text{-}O^{-})]^{2+}$ which has the absorption band at 1650 cm^{-1}.

Table 22. List of N-O Stretching Frequency in LCu-NO Complexes

LCu-NO	ν(N-O) (^{15}N-O) cm^{-1}	Ref
$[Cu^{II}_2(XYL\text{-}O^-)(NO^-)]^{2+}$	1536	82
$[Cu^{I,II}(UN\text{-}O^-)(NO)]^{2+}$	1670 (1645)	this work
$[Cu^{I}HB(3\text{-}^{t}Bu\text{-}5\text{-}^{i}Prpz)_3(NO)]^{+}$	1698 (1627[a])	83
$[Cu^{I}HB(^{t}Bupz)_3(NO)]^{+}$	1712 (1679)	84
$[Cu^{I}(AN)(NO)]^{+}$	1736 (1714)	66b
$[Cu^{I}HC(3\text{-}^{t}Bu\text{-}5\text{-}^{i}Prpz)_3(NO)]^{2+}$	1742 (1666[a])	83
$[Cu^{II}L(NO)]$	1846 (1815)	85
$[Cu^{II}_2(UN\text{-}O^-)(O_2^-)(NO)]^{2+}$	1853 (1820)	this work
$[Cu^{II}(CH_3NO_2)_5(NO)]^{2+}$	1933 (1893)	86

[a]Values for $\nu(^{15}N\text{-}^{18}O)$. See Figure 18 for full drawings of the ligands and their IUPAC names.

We justify the description of the NO adduct as $[Cu^{I,II}_2(UN\text{-}O^-)(\mu\text{-}\bullet NO)]^{2+}$ on the basis of the following observations and analysis/arguments: (i) The ν(N-O) value is more consistent with literature values for Cu^{I}-NO species (Table 22). (ii) In $[Cu^{II}_2(XYL\text{-}O^-)(NO^-)]^{2+}$, the very low ν(N-O) value and structural aspects[82] of the complex indicate that a formal negative charge is located on the nitrosyl ligand, i.e., it is a nitroxyl containing compound with a NO^- moiety.[82] The considerably higher ν(N-O) value in $[Cu^{I,II}_2(UN\text{-}O^-$

)(μ-•NO)]$^{2+}$ is thus more consistent with what is expected for a Cu^{I}-$NO_{(g)}$ adduct (Figure 16a),

(iii) Cu^{I}-$NO_{(g)}$ adducts in mononuclear cases are in general best described as Cu^{I}-(•NO) species in terms of their electronic structures,[87] and EPR spectra of such species do in fact exhibit $g \sim 2$ organic radical signals and not spectra associated with Cu(II), such as would be expected for a Cu^{II}-(NO^{-}) formulation and associated electronic structure. The lack of an observable EPR signal in [$Cu^{I,II}_2$(UN-O^{-})(μ-•NO)]$^{2+}$ comes because there is an additional Cu(II) ion present, as the complex is binuclear; so overall this is an even spin system (i.e., one unpaired electron on the •NO ligand and another on the Cu(II) ion).

(iv) Further, the lower value of ν(N-O) in complex [$Cu^{I,II}_2$(UN-O^{-})(μ-•NO)]$^{2+}$ compared to most other Cu^{I}-$NO_{(g)}$ adducts which have ν(N-O) > 1700 cm^{-1} (Table 22), leads us to thoughts that the NO moiety bridges through its N-atom, binding both the Cu^{I} and Cu^{II} ions in [$Cu^{I,II}_2$(UN-O^{-})(μ-•NO)]$^{2+}$ (Figure 16a),

(v) Another argument in favor of this supposition is that if the nitrosyl ligand does not bind to the Cu^{II} ion, the latter would only be tetracoordinate, however, Cu^{II} ion strongly prefers pentacoordination; so addition of this bridging nitrosyl 5th ligand to Cu^{II} seems reasonable,

In summary, complex [$Cu^{I,II}_2$(UN-O^{-})(μ-•NO)]$^{2+}$, the product of addition of $NO_{(g)}$ to mixed-valent complex [$Cu^{I,II}_2$(UN-O^{-})]$^{2+}$, is best described as a mixed-valent copper nitrosyl complex [$Cu^{I,II}_2$(UN-O^{-})(μ-•NO)]$^{2+}$ (Figure 16a).

Formation of a nitrosyl and superoxide intermediate.

After removing excess $NO_{(g)}$ from the solution of $[Cu^{I,II}_2(UN\text{-}O^{-})(\mu\text{-}\bullet NO)]^{2+}$ by the application of vacuum/purge cycles (Figure 20b, spectrum in purple), bubbling the solution of $[Cu^{I,II}_2(UN\text{-}O^{-})(\mu\text{-}\bullet NO)]^{2+}$ with $O_{2(g)}$ resulted in the disappearance of the N-O stretch of 1670 cm^{-1} while a new band at 1853 cm^{-1} grew in (Figure 20b, spectrum in red), all this monitored utilizing *in-situ* LT-IR spectroscopy. We assign this IR band at 1853 cm^{-1} ($\Delta^{15}NO$ = –33 cm^{-1}, Figure 21) to the nitrosyl ligand within a new complex, but now in an altered chemical environment, as discussed below. The presence of the pre-formed 1853 cm^{-1} band in the purple spectrum (Figure 20b) prior to O_2 bubbling is due to a slight air leak while applying vacuum/Ar purging. This band does not belong to $[Cu^{I,II}_2(UN\text{-}O^{-})(\mu\text{-}\bullet NO)]^{2+}$ as presented in Figure 16.

A literature survey of Cu-nitrosyl complexes and even metal-$NO_{(g)}$ adducts in general, suggests that this value falls into the region where the nitrosyl ligand may be best described as having a NO^{+} (nitrosonium) electronic structure. A series of ligand (L) copper(II) nitrosyl complexes LCu^{II}-(NO) studied by Mondal and coworkers[85] reveals that ν(N-O) can vary between 1640 cm^{-1} and 1846 cm^{-1} depending on the ligand (L) environment (and thus the $LCu^{II/I}$ reduction potential). Also, Theopold and coworkers[88] studied a tris(3-*tert*-butyl-5-methylpyrazolyl)borate ($Tp^{t\text{-}Bu,Me}$) ligand derived Cobalt (III) superoxide complex $Tp^{t\text{-}Bu,Me}Co^{III}(O_2^{\bullet-})$ and upon adding excess $NO_{(g)}$ at -78 °C, a new band at 1849 cm^{-1} grew in and was assigned as absorption of the unstable nitrosyl intermediate. A very interesting example from Hayton and coworkers[86] is a penta-nitromethane coordinated Cu^{II}-NO compound where ν(N-O) = 1933 cm^{-1}. This is

suggestive of a nitrosonium characterization of the nitrosyl ligand, and the compound is reported to have a $[Cu^{II}(CH_3NO_2)_5(\bullet NO)]^{2+}$ formulation, while the NO moiety is bound to the Cu^{II} ion in a bent fashion ($\angle$Cu-N-O = 121°). Thus, addition of •NO(g) to Cu(II) gives adducts described either as LCu^{II}-(•NO) or LCu^{I}-NO^+ species. Therefore, $[Cu^{II}_2(UN\text{-}O^-)(\bullet NO)(O_2^{\bullet-})]^{2+}$, the product of addition of O_2 to the nitrosyl complex $[Cu^{I,II}_2(UN\text{-}O^-)(\mu\text{-}\bullet NO)]^{2+}$, can be described to have either the LCu^{II}-(•NO) or LCu^{I}-NO^+ electronic structure.

What about the fate of the $O_{2(g)}$ which was added? As dioxygen typically binds to transition metals when in their reduced state, reaction of $[Cu^{I,II}_2(UN\text{-}O^-)(\mu\text{-}\bullet NO)]^{2+}$ with O_2 likely involves electron-transfer from the cuprous ion in $[Cu^{I,II}_2(UN\text{-}O^-)(\mu\text{-}\bullet NO)]^{2+}$ leading to a cupric-superoxide ($O_2^{\bullet-}$) species. To account for the changes occurring when one $NO_{(g)}$ molecule is added to the mixed-valent complex to give $[Cu^{I,II}_2(UN\text{-}O^-)(\mu\text{-}\bullet NO)]^{2+}$ with a single nitrosyl ligand (excess $NO_{(g)}$ removed by vacuum/purge cycles), followed by $O_{2(g)}$ addition to $[Cu^{I,II}_2(UN\text{-}O^-)(\mu\text{-}\bullet NO)]^{2+}$ (with excess $O_{2(g)}$ removed) to giving an intermediate complex, we must formulate the latter as a superoxide and nitrosyl complex $[Cu^{II}_2(UN\text{-}O^-)(\bullet NO)(O_2^{\bullet-})]^{2+}$ (Figure 20a). The conclusion that this compound contains a single $NO_{(g)}$ plus a single $O_{2(g)}$ derived ligand, as per this formulation, is further supported by its subsequent transformation to a peroxynitrite complex $[Cu^{II}_2(UN\text{-}O^-)(^-OON{=}O)]^{2+}$, which 'logically' forms by the intramolecular coupling of the superoxide ligand with the electrophilic N-atom of the adjacent •NO (or NO^+) molecule.

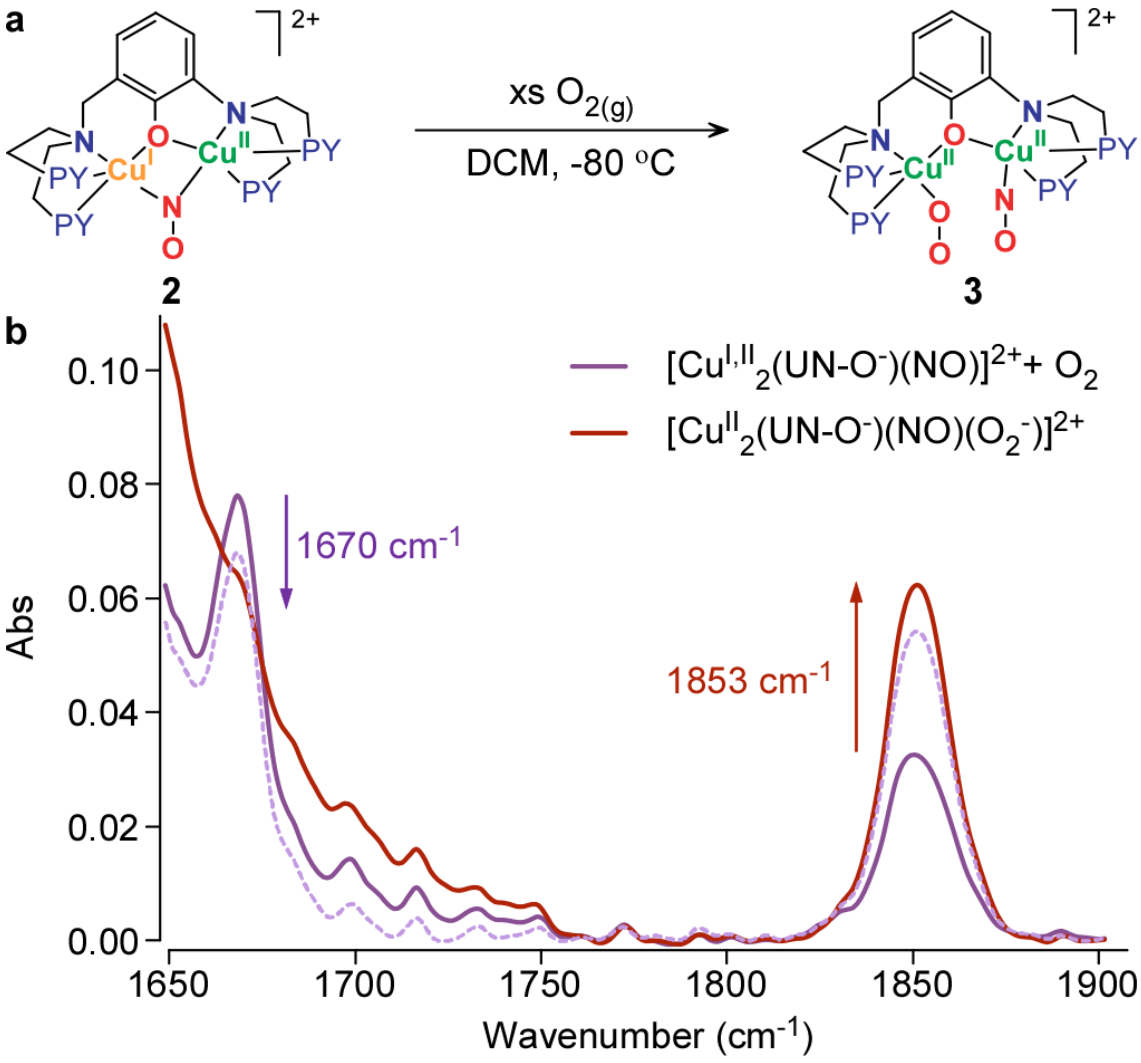

Figure 20. LT-IR of the nitrosyl and superoxide intermediate.

(a) $[Cu^{I,II}_2(UN\text{-}O^{-})(NO)]^{2+}$ reacts with excess $O_{2(g)}$ to form $[Cu^{II}_2(UN\text{-}O^{-})(NO)(O_2^{-})]^{2+}$ at -80 °C in DCM. (b) Low-temperature infrared spectroscopy of the complex $[Cu^{I,II}_2(UN\text{-}O^{-})(NO)]^{2+}$ (spectrum in purple) reacting with $NO_{(g)}$ to form complex $[Cu^{II}_2(UN\text{-}O^{-})(NO)(O_2^{-})]^{2+}$ (spectrum in red) at -80 °C. The dotted purple

spectrum shows the transition for the reaction mentioned above. The last spectrum in red was taken five minutes after adding $O_{2(g)}$.

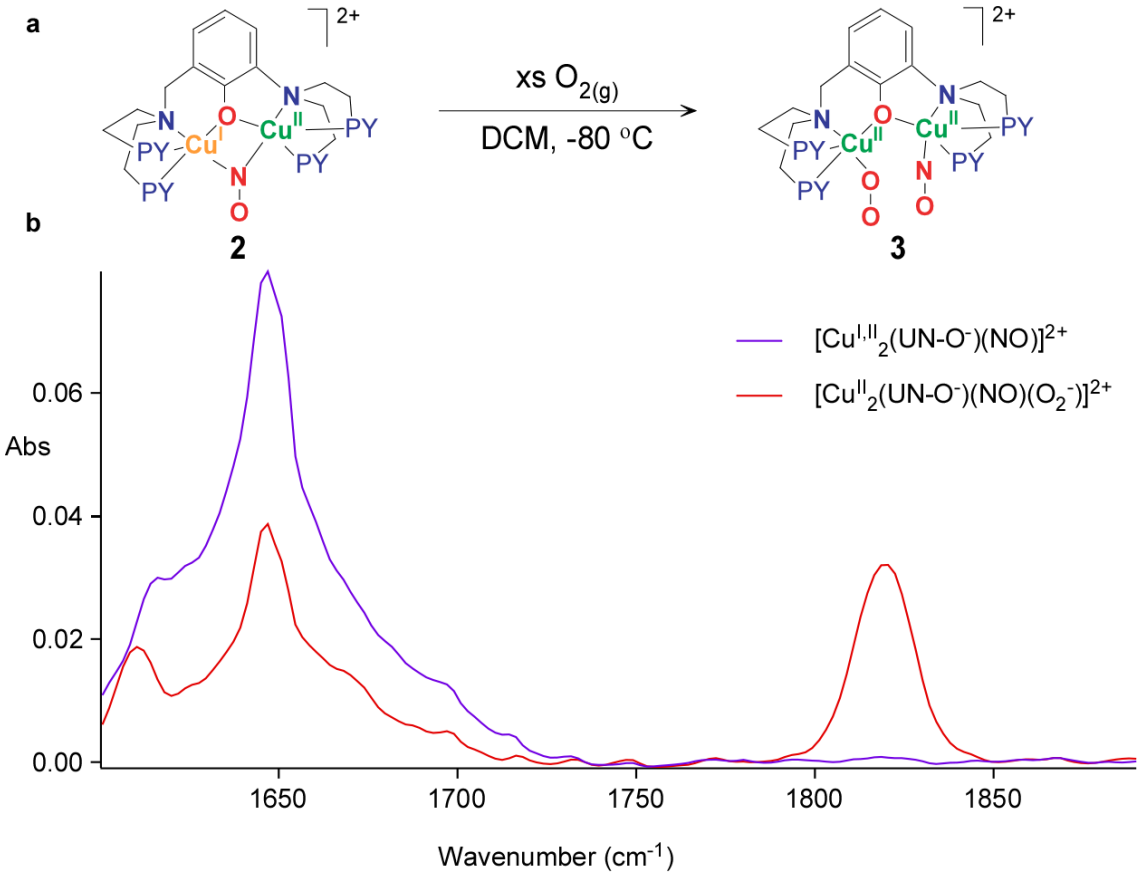

Figure 21. LT-IR of the nitrosyl and superoxide intermediate with ^{15}NO labeled. (method 1)

^{15}NO labeled complex $[Cu^{I,II}_2(UN\text{-}O^{-})(^{15}NO)]^{2+}$ reacts with excess $O_{2(g)}$ to form $[Cu^{II}_2(UN\text{-}O^{-})(^{15}NO)(O_2^{-})]^{2+}$ complex at -80 °C. (b) Low-temperature infrared spectroscopy of the complex $[Cu^{I,II}_2(UN\text{-}O^{-})(^{15}NO)]^{2+}$ (spectrum in purple color) with $\nu(^{15}N\text{-}O)$ at 1645 cm^{-1} (shifted from 1670 cm^{-1}) with $O_{2(g)}$ to form complex

$[Cu^{II}_2(UN\text{-}O^{-})(^{15}NO)(O_2^{-})]^{2+}$ (spectrum in red color) at -80 °C with $\nu(^{15}N\text{-}O)$ at 1820 cm^{-1} (shifted from ν(N-O) at 1853 cm^{-1}).

Formation of the peroxynitrite complex.

Using LT-IR spectroscopy, it is seen that the change from $[Cu^{II}_2(UN\text{-}O^{-})(^{15}NO)(O_2^{-})]^{2+}$ to $[Cu^{II}_2(UN\text{-}O^{-})(^{-}OON{=}O)]^{2+}$ occurs over the course of 20 mins (–80 °C), and the ν(N-O) = 1853 cm^{-1} band disappears. The formation of peroxynitrite dicopper(II) complexes $[Cu^{II}_2(UN\text{-}O^{-})(^{-}OON{=}O)]^{2+}$ is suggested by the appearance of new IR bands at 1520 cm^{-1} ($\Delta^{15}NO$ = –22 cm^{-1})[81] and 1640 cm^{-1} ($\Delta^{15}NO$ = –26 cm^{-1}),[81] assignable to the N=O double bond of the PN ligand (Figure 22b, Figure 25b).

We assign these bands to be two different species (conformers), *cis*- and *trans*-peroxynitrite complexes, respectively (Figure 22a), as also discussed further, below. When the nitrogen atom on the NO moiety forms a bond with the distal (to Cu) oxygen atom of the dioxygen derived moiety (i.e., the $O_2^{\bullet-}$ ligand), a *trans*-peroxynitrite complex is likely formed. However, if or when the proximal superoxide O-atom attacks the electrophilic nitrosyl nitrogen-atom (*vide supra*), the *cis*-peroxynitrite complex can be generated, Figure 22a.

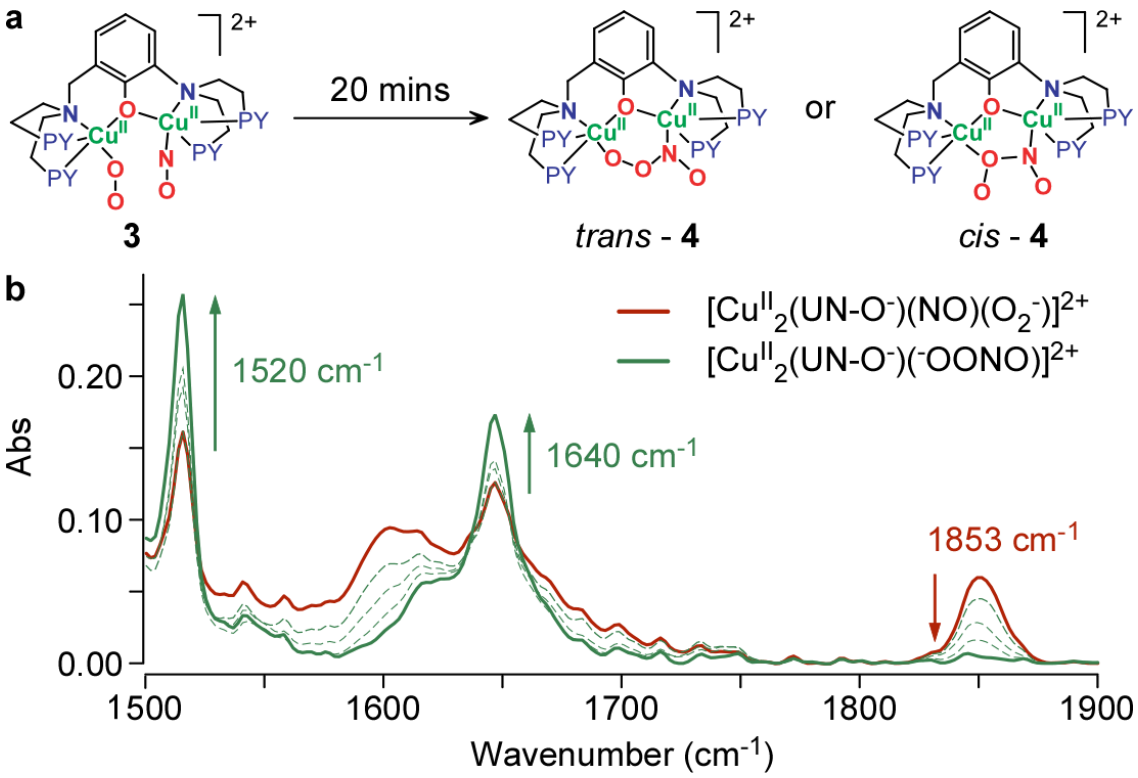

Figure 22. LT-IR of the peroxynitrite complex.

(a) $[Cu^{II}_2(UN\text{-}O^{-})(NO)(O_2^{-})]^{2+}$ gradually transforms to form $[Cu^{II}_2(UN\text{-}O^{-})(^{-}OONO)]^{2+}$ complex at -80 °C. (b) Low-temperature infrared spectroscopy of the complex $[Cu^{II}_2(UN\text{-}O^{-})(NO)(O_2^{-})]^{2+}$ (red) which changes to form complexes $[Cu^{II}_2(UN\text{-}O^{-})(^{-}OON{=}O)]^{2+}$ in (solid green line spectrum) over the course of 20 mins. IR bands at 1520 cm^{-1} ($\Delta^{15}NO = -22\ cm^{-1}$) and 1640 cm^{-1} ($\Delta^{15}NO = -26\ cm^{-1}$).

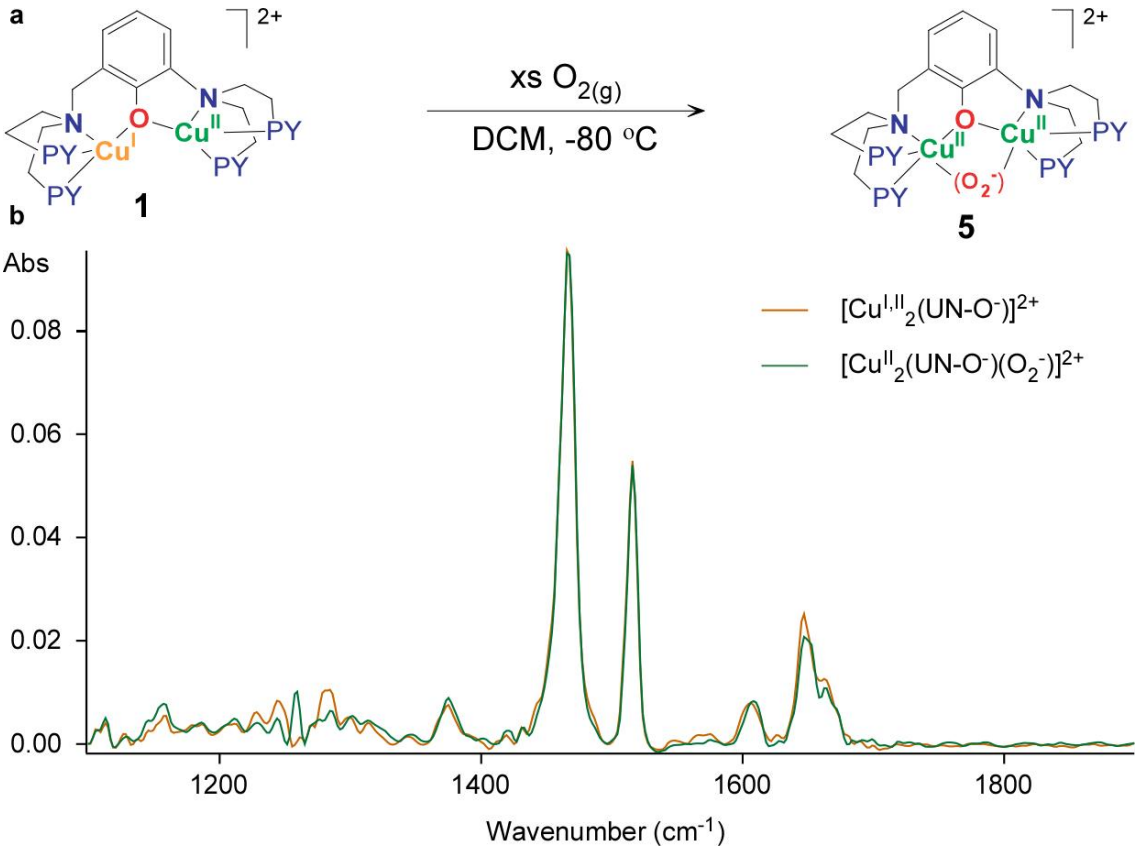

Figure 23. LT-IR of the superoxide complex.

(a) $[Cu^{I}Cu^{II}(UN\text{-}O^{-})]^{2+}$ reacts with excess $O_{2(g)}$ to form superoxide dicopper(II) complex $[Cu^{II}_2(UN\text{-}O^{-})(O_2^{\bullet-})]^{2+}$ at -80 °C in dichloromethane (DCM) solvent. (b) Low-temperature (-80 °C) infrared spectroscopy of the complex $[Cu^{I}Cu^{II}(UN\text{-}O^{-})]^{2+}$ in orange color spectrum reacts with $O_{2(g)}$ to form complex $[Cu^{II}_2(UN\text{-}O^{-})(O_2^{\bullet-})]^{2+}$ in green color spectrum.

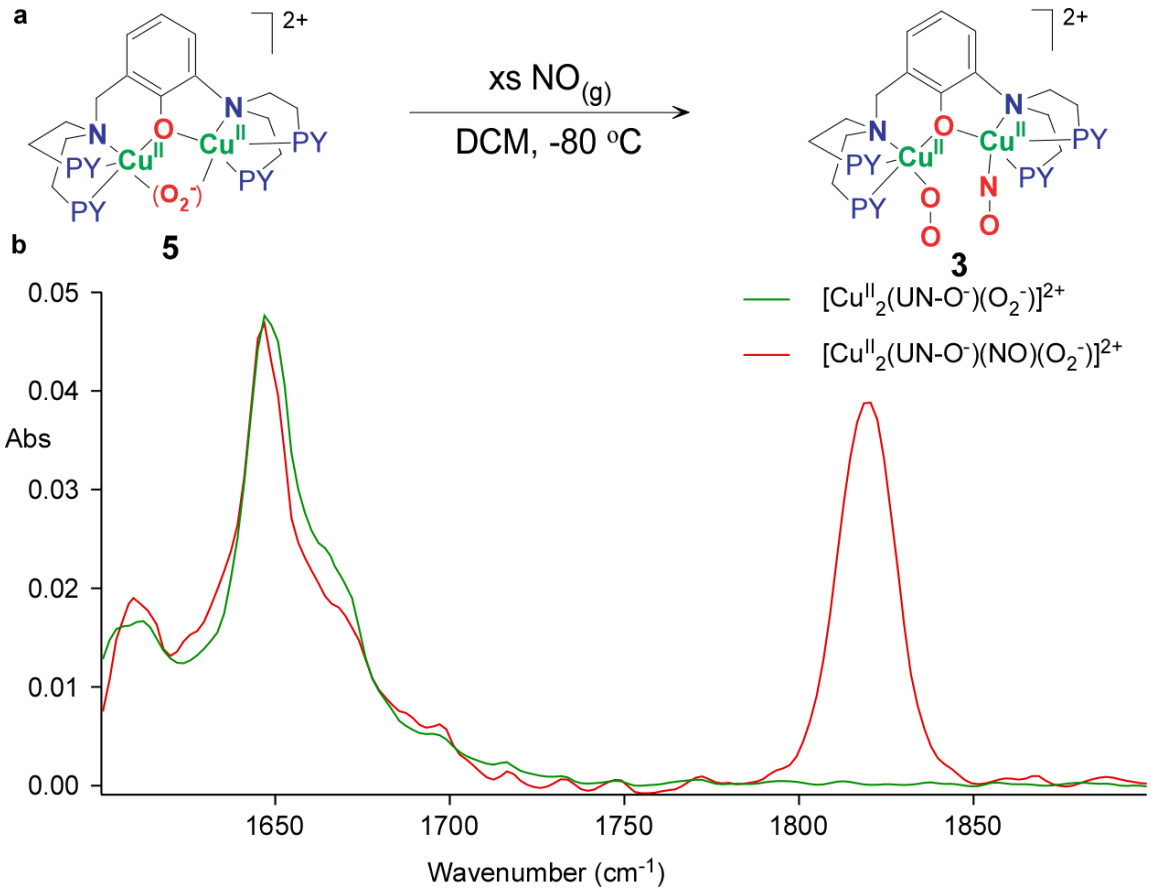

Figure 24. LT-IR of the nitrosyl and superoxide intermediate with ^{15}NO labeled. (method 2)

(a) $[Cu^{II}_2(UN\text{-}O^{-})(O_2^{\bullet-})]^{2+}$ reacts with $^{15}NO_{(g)}$ to form $[Cu^{II}_2(UN\text{-}O^{-})(NO)(O_2^{-})]^{2+}$ complex at -80 °C in DCM. $^{15}NO_{(g)}$ was directly added into the solution of the superoxide complex $[Cu^{II}_2(UN\text{-}O^{-})(O_2^{\bullet-})]^{2+}$ using a gas-tight syringe. (b) Low-temperature (-80 °C) infrared spectroscopy for the formation of the superoxide and nitrosyl complex $[Cu^{II}_2(UN\text{-}O^{-})(\bullet^{15}NO)(O_2^{\bullet-})]^{2+}$ with $\nu(^{15}N\text{-}O)$ at 1820 cm^{-1} (red colored spectrum) from the reaction of ^{15}NO and $[Cu^{II}_2(UN\text{-}O^{-})(O_2^{\bullet-})]^{2+}$ (green colored spectrum).

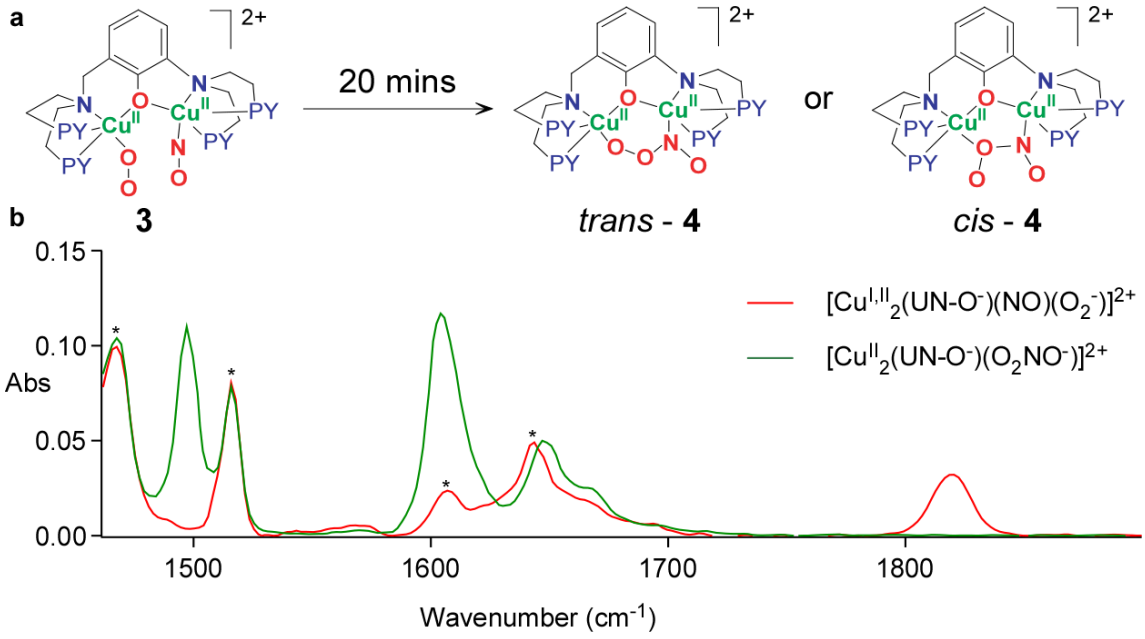

Figure 25. LT-IR of the peroxynitrite complex with ^{15}NO labeled.

(a) The solution of $[Cu^{II}_2(UN\text{-}O^-)(NO)(O_2^-)]^{2+}$ gradually transforms to produce *trans*- and *cis*- isomers of $[Cu^{II}_2(UN\text{-}O^-)(^-OON{=}O)]^{2+}$ at -80 °C. (b) Low-temperature infrared spectroscopy of the complex $[Cu^{II}_2(UN\text{-}O^-)(NO)(O_2^-)]^{2+}$ in red color spectrum gradually changes to complex $[Cu^{II}_2(UN\text{-}O^-)(^-OON{=}O)]^{2+}$ in green color spectrum over the course of 20 mins at -80 °C by the appearance of new IR bands for *cis*-$[Cu^{II}_2(UN\text{-}O^-)(^-OON{=}O)]^{2+}$ with $\nu(^{15}N\text{-}O)$ = 1500 cm^{-1} and *trans*-$[Cu^{II}_2(UN\text{-}O^-)(^-OON{=}O)]^{2+}$ with $\nu(^{15}N\text{-}O)$ = 1614 cm^{-1}. These bands are shifted from 1520 cm^{-1} and 1640 cm^{-1} in the samples prepared with unlabeled NO (see Figure 22). The bands marked in asterisks do not change over time.

Table 23. List of N-O Stretching Frequency in $L_nM_x(^{-}OON=O)$ Complexes

LCu-NO	ν (N=O) cm^{-1}	Ref
cis-NaOONO	1422	[89]
cis-KOONO	1444	[89]
$[Cu^{II}_2(UN\text{-}O^{-})(cis\text{-}^{-}OON=O)]^{2+}$	1520	this work
trans-KOONO	1528	[89]
trans-NaOONO	1580	[89]
[Fe(TMEDA)(NO)($^{-}$OON=O)]	1589	[90]
$(NH_3)Co(TTP)(^{-}OON=O)$	1596	[68]
$[N(CH_2CH_3)_4]_3[Co(CN)_5(^{-}OON=O)]$	1621	[67]
$[Cu^{II}_2(UN\text{-}O^{-})(trans\text{-}^{-}OON=O)]^{2+}$	1640	this work

See Figure 18 for drawings of the ligands and IUPAC names.

In a different route leading for the formation of peroxynitrite complex $[Cu^{II}_2(UN\text{-}O^{-})(^{-}OON=O)]^{2+}$ (Scheme 2), we performed a series of LT-IR experiments starting from the mixed-valent complex $[Cu^{I,II}_2(UN\text{-}O^{-})(DMF)]^{2+}$. Addition of excess $O_{2(g)}$ via syringe, does not incur any significant IR spectral change (Figure 23b), even though we know that the superoxo-dicopper(II) complex $[Cu^{II}_2(UN\text{-}O^{-})(O_2^{\bullet-})]^{2+}$ forms, as previously described.[80] After removing any excess $O_{2(g)}$ through vacuum/purge cycles, an ~7 fold excess of $NO_{(g)}$ was added directly into the solution of $[Cu^{II}_2(UN\text{-}O^{-})(O_2^{\bullet-})]^{2+}$ using a gas-tight syringe. We then observed the formation of the same superoxide and nitrosyl complex $[Cu^{II}_2(UN\text{-}O^{-})(\bullet NO)(O_2^{\bullet-})]^{2+}$, with 1820 cm^{-1} IR absorption (Figure 24b,

method 2), which, as before, leads to the formation of peroxynitrite complex $[Cu^{II}_2(UN\text{-}O^{-})(^{-}OON{=}O)]^{2+}$ over the course of 20 mins (Figure 25b).

Although IR studies on peroxynitrite bound to copper ions are not available in the literature, the *cis*- and *trans*-peroxynitrite N-O stretching frequencies for alkali metals are determined to be in the region of ~1440 cm^{-1} and ~1580 cm^{-1}, respectively (Table 23). So, the difference in ν (N-O) between the cis- and trans- peroxynitrite conformers can be quite large, i.e., > 100 cm^{-1},[89] as is observed here for our *cis*- and *trans*- conformers of the peroxynitrite complex $[Cu^{II}_2(UN\text{-}O^{-})(^{-}OON{=}O)]^{2+}$, and where we can thus assign the 1520 and 1640 IR bands to the *cis*- and *trans*- conformers, respectively (Table 23).

A literature survey on IR data for a few transition metal peroxynitrite complexes supports our assignments for $[Cu^{II}_2(UN\text{-}O^{-})(^{-}OON{=}O)]^{2+}$. With a porphyrinate[68] or cyano[67] groups as co-ligands in Co(III) complexes, the $^{-}$O-O-N=O N=O (double-bond) IR stretching frequencies are in the 1600 to ~1620 cm^{-1} range (Table 23). Thus, Kurtikyan and coworkers[68] observed a ν(N=O) value for the PN ligand in $(NH_3)^{III}Co(TTP)(^{-}OON{=}O)$ (TTP = *meso*-tetra-*p*-tolylporphyrinato dianion) at 1596 cm^{-1}, assigned to be in a *trans*- conformation and ligated axially via the peroxynitrite anionic O-atom. Their DFT calculations supported this assignment, also giving a calculated value of ν(N-O) = 1678 cm^{-1}.

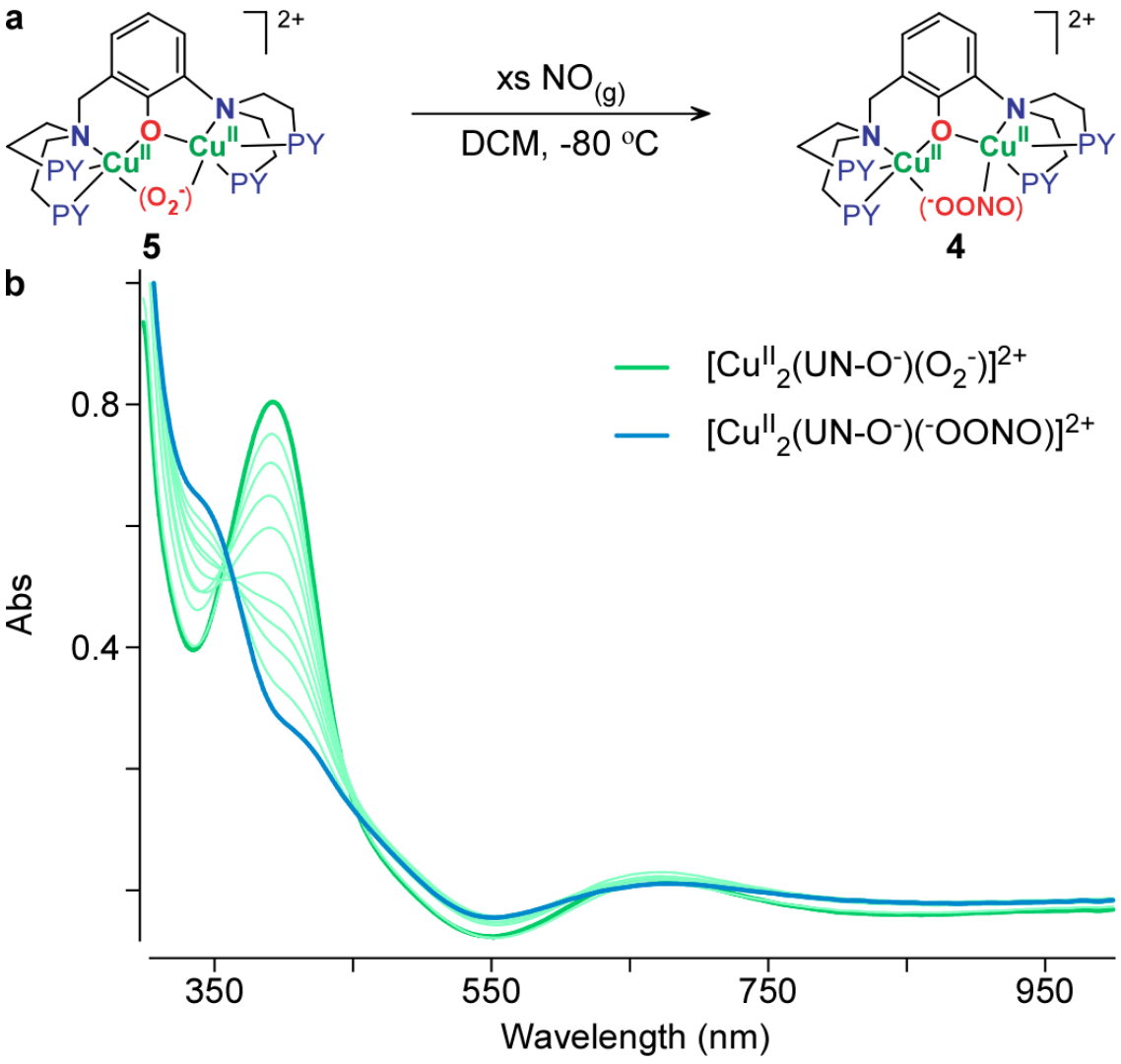

Figure 26. UV-Vis of the peroxynitrite generated from the superoxide complex.

(a) $[Cu^{II}_2(UN\text{-}O^{-})(O_2^{-})]^{2+}$ reacts with excess nitric oxide gas at -80 °C to form the complex $[Cu^{II}_2(UN\text{-}O^{-})(O_2NO^{-})]^{2+}$. (b) UV-Vis spectroscopy of the transformation from the superoxide $[Cu^{II}_2(UN\text{-}O^{-})(O_2^{-})]^{2+}$ to $[Cu^{II}_2(UN\text{-}O^{-})(^{-}OON{=}O)]^{2+}$ by adding excess nitric oxide gas at -80 °C.

In another example, Kim and coworkers[90] reported that with a bidentate tetramethylethelenediamine ligand bound in an iron-dinitrosyl complex, oxygenation results in the generation of new band ν(N–O) at ~1590 cm^{-1}, assigned by those researchers to be a *trans*-peroxynitrite complex (Table 23). As noted, we assign our dicopper complex with cis-peroxynitrite ligand, $[Cu^{II}_2(UN\text{-}O^{-})(cis\text{-}^{-}OON{=}O)]^{2+}$, as having ν(N–O) = 1520 cm^{-1}, a much lower value than for these other coordination complexes.

Formation of peroxynitrite on UV-Vis spectrophotometer.

As described above, the LT-IR studies reveal that the peroxynitrite complex $[Cu^{II}_2(UN\text{-}O^{-})(^{-}OON{=}O)]^{2+}$, the mixture of conformers, can be formed either by addition of O_2 to the nitrosyl complex $[Cu^{I,II}_2(UN\text{-}O^{-})(\mu\text{-}\bullet NO)]^{2+}$, or by adding $NO_{(g)}$ to the superoxide complex $[Cu^{II}_2(UN\text{-}O^{-})(O_2^{\bullet-})]^{2+}$.[80]

In fact, this finding is also supported by UV-vis spectroscopic monitoring. Following the generation of $[Cu^{II}_2(UN\text{-}O^{-})(O_2^{\bullet-})]^{2+}$ by addition of $O_{2(g)}$ to the mixed-valent complex, one obtains the spectrum with λ_{max} = 404 nm (dark green solid line spectrum, Figure 26b). After removal of excess $O_{2(g)}$, addition of excess $NO_{(g)}$ (~20 equiv) into the solution of $[Cu^{II}_2(UN\text{-}O^{-})(O_2^{\bullet-})]^{2+}$ using a gas-tight syringe, an isosbestic conversion occurring over ~ 10 mins is observed for the transformation to form the peroxynitrite complex $[Cu^{II}_2(UN\text{-}O^{-})(^{-}OON{=}O)]^{2+}$ with λ_{max} = 355 (sh), 420 (sh) and 680 nm (blue spectrum, Figure 26b).

The reaction of $[Cu^{I,II}_2(UN\text{-}O^-)(NO)]^{2+}$ with O_2 to give $[Cu^{II}_2(UN\text{-}O^-)(NO)(O_2^-)]^{2+}$ (Figure 20a) and finally leading to $[Cu^{II}_2(UN\text{-}O^-)(^-OON{=}O)]^{2+}$ (Figure 22a), monitored by LT-IR spectroscopy and all described above, was also monitored by UV-vis spectroscopy. These are carried out at low concentrations, ~ 100 times more dilute than for the LT-IR studies. The result is that at the UV-vis scale, the nitrosyl and superoxo complex $[Cu^{II}_2(UN\text{-}O^-)(\bullet NO)(O_2^{\bullet-})]^{2+}$ is meta-stable; UV-vis spectral transformations on going from $[Cu^{II}_2(UN\text{-}O^-)(\bullet NO)(O_2^{\bullet-})]^{2+}$ to $[Cu^{II}_2(UN\text{-}O^-)(^-OON{=}O)]^{2+}$ were monitored (Figure 26b), but stable UV-vis feature for $[Cu^{II}_2(UN\text{-}O^-)(NO)(O_2^-)]^{2+}$ could not be obtained.[81]

Low Temperature ESI-MS of the peroxynitrite complex.

Electrospray ionization mass spectrometry (ESI-MS) was employed to further confirm the formulation for $[Cu^{II}_2(UN\text{-}O^-)(^-OON{=}O)]^{2+}$. By injecting a cold solution (–80 °C) of the complex $[Cu^{II}_2(UN\text{-}O^-)(^-OON{=}O)]^{2+}$, that prepared in a solvent mixture of 80% DCM and 20% acetonitrile (ACN), the peak for complex $[Cu^{II}_2(UN\text{-}O^-)(^-OON{=}O)]^{2+}$ as adduct with one SbF_6^- counter anion is observed as the mono-cation complex $[Cu^{II}_2(UN\text{-}O^-)(^-OON{=}O)]^{2+}(SbF_6^-)$ exhibiting a peak at m/z = 981.92 for complex $[Cu^{II}_2(UN\text{-}O^-)(^-OON{=}O)]^{2+}$ prepared with $^{16}O_{2(g)}$; when superoxide complex $[Cu^{II}_2(UN\text{-}O^-)(O_2^{\bullet-})]^{2+}$ was prepared using $^{18}O_{2(g)}$, the m/z value changed to 986.02 (Figure 27). These values are in very good agreement with the theoretically predicted values of 982.04 for complex $[Cu^{II}_2(UN\text{-}O^-)(^-OON{=}O)]^{2+}$ with $^{16}O_{2(g)}$ and 986.05 for complex $[Cu^{II}_2(UN\text{-}O^-)(^-OON{=}O)]^{2+}$ with $^{18}O_{2(g)}$, respectively.

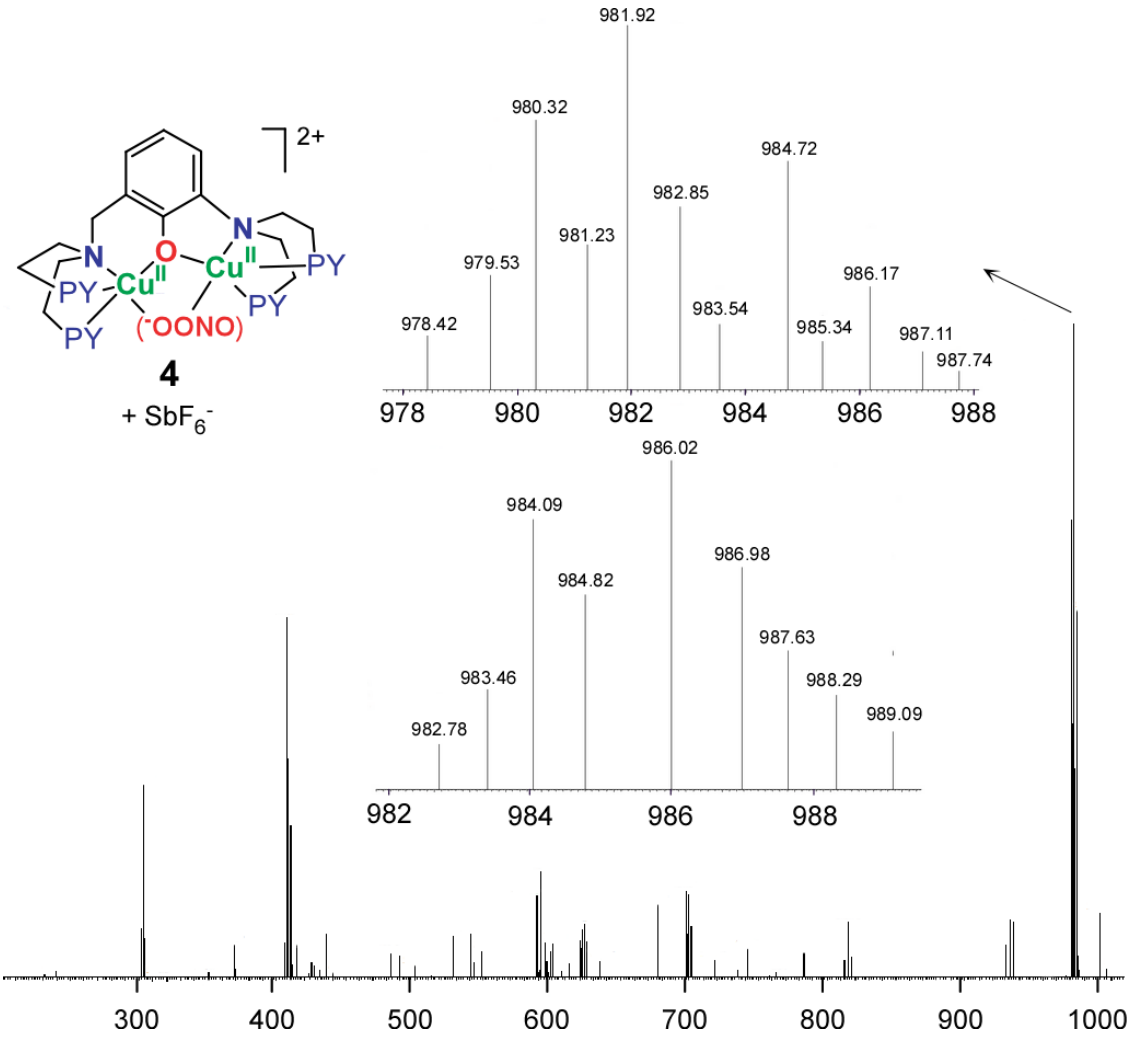

Figure 27. ESI-MS spectrum of the peroxynitrite complex.

Low-temp ESI-MS spectrum of the peroxynitrite complex $[Cu^{II}_2(UN\text{-}O^{-})(^{-}OON{=}O)]^{2+}$, as adduct with one SbF_6^- anion, to give an overall detected mono-cation. Expanded spectra are shown above the full spectrum corresponding to the m/z (greatest intensity peak) = 981.92 and that where $^{18}O_2$ was employed in the synthesis, m/z = 986.02. Good agreement is also observed for comparison of the distribution of peaks due to the presence of different isotopes (mainly due to ^{63}Cu and ^{65}Cu), experiment vs theory, Figure 27-1.[81]

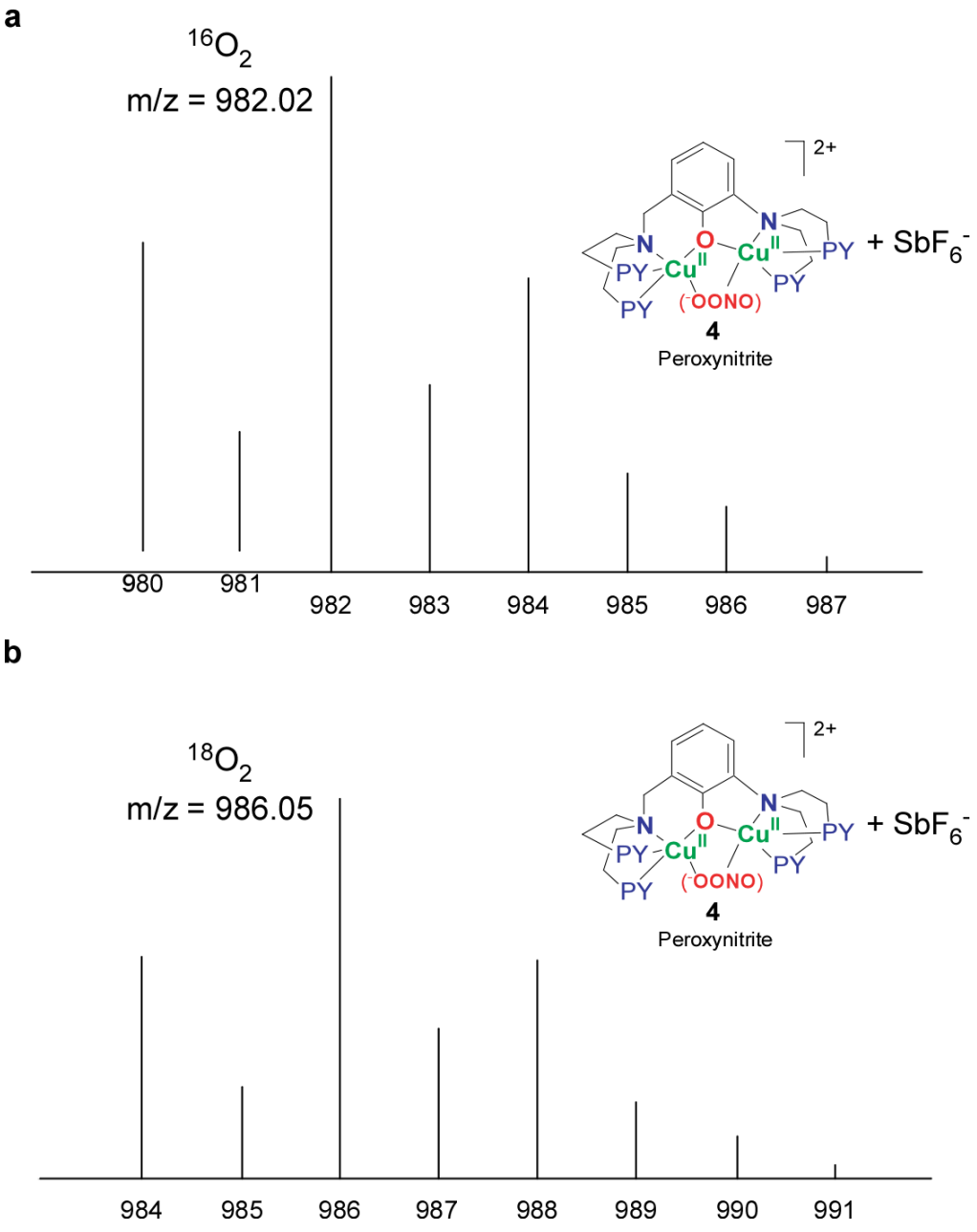

Figure 27-1. Theoretically predicted isotope patterns for the peroxynitrite complex.

(a) Chemdraw predicted isotope distributions for $[Cu^{II}_2(UN\text{-}O^-)(^-OON{=}O)]^{2+}$ with one SbF_6^- anion. (b) Chemdraw predicted isotope distributions for $[Cu^{II}_2(UN\text{-}O^-)(^-{}^{18}O{}^{18}ON{=}O)]^{2+}$ with one SbF_6^- anion.

Phenol Nitration by the peroxynitrite complex.

As described in the Introduction, peroxynitrite, or even metal-mediated peroxynitrite reactions is most likely responsible for biological tyrosine phenol side-chain or in vitro phenol substrate nitration, often biologically damaging. Beckman[56b,56c,56g] and Koppenol[56c] have discussed this in particular in interaction of peroxynitrite with the enzyme CuZn-superoxide dismutase or Fe^{III}-EDTA (or other) coordination complexes, and postulate that metal ions favor the heterolytic cleavage of the PN O-O bond, to give nitronium ion (NO_2^+), which is a powerful nitrating agent. More recently, Girault[66f] has shown that copper ion complexes may mediate peroxynitrite formation and then phenol nitration. Metal bound PN complexes have now been shown by other groups to react with substituted phenols, in particular, 2,4-di-*tert*-butylphenol (DTBP) as an analytically useful substrate.

Thus, it was of considerable interest to examine the behavior of $[Cu^{II}_2(UN\text{-}O^-)(^-OON{=}O)]^{2+}$ with DTBP. Upon addition of one equiv of this substrate to the superoxide-dicopper(II) complex $[Cu^{II}_2(UN\text{-}O^-)(O_2^{\bullet-})]^{2+}$ formed in DCM at –80 °C (green spectrum in Figure 28b), there is no apparent change. The PN complex $[Cu^{II}_2(UN\text{-}O^-)(^-OON{=}O)]^{2+}$ was then generated in situ, by first removing excess dioxygen and then adding $NO_{(g)}$ (blue spectrum) followed by removing any excess in vacuo. This results in an immediate reaction (by this benchtop UV-vis monitoring) and the formation of a new species, identified as the previously well-known μ-OH complex $[Cu^{II}_2(UN\text{-}O^-)(OH)]^{2+}$ (λ_{max} = 348 nm, black spectrum, Figure 28b) formed nearly quantitatively based on known absorptivity data. Warming of this solution to RT followed by workup and analysis of the

reaction mixture using GC-MS (see the SI), showed that 2,4-di-*tert*-butyl-6-nitrophenol formed, essentially in 100 % yield.[81] Thus, the reaction which has occurred is the stoichiometric reaction shown in Figure 28a.

In accordance with the above discussions, we suggest that the peroxynitrite complex $[Cu^{II}_2(UN\text{-}O^{-})(^{-}OON{=}O)]^{2+}$ has undergone O-O bond heterolytic cleavage to produce the nitronium (NO_2^+) ion which efficiently nitrates the DTBP substrate, this being standard electrophilic aromatic substitution chemistry. The dicopper complex initially formed upon O-O cleavage would be an oxo (oxide, O^{2-}) bridged dicopper(II) complex $[Cu^{II}_2(UN\text{-}O^{-})(O^{2-})]^{+}$, where the dianionic oxide ligand is stabilized by the two Cu(II) ions present. In fact, we previously isolated the oxo-dicopper(II) complex with the close analog XYL-O$^-$ binucleating ligand, the complex $[Cu^{II}_2(XYL\text{-}O^{-})(O^{2-})]^{+}$,[91] thus supporting our proposal. The proton released from DTBP upon its *o*-phenol nitration with NO_2^+, would then add to the highly basic oxo-atom in $[Cu^{II}_2(UN\text{-}O^{-})(O^{2-})]^{+}$, giving the observed μ-hydroxide complex $[Cu^{II}_2(UN\text{-}O^{-})(OH)]^{2+}$ (Figure 28b). Scheme 2 outlines the reaction sequence discussed here, involving O-O heterolytic cleavage in $[Cu^{II}_2(UN\text{-}O^{-})(^{-}OON{=}O)]^{2+}$.

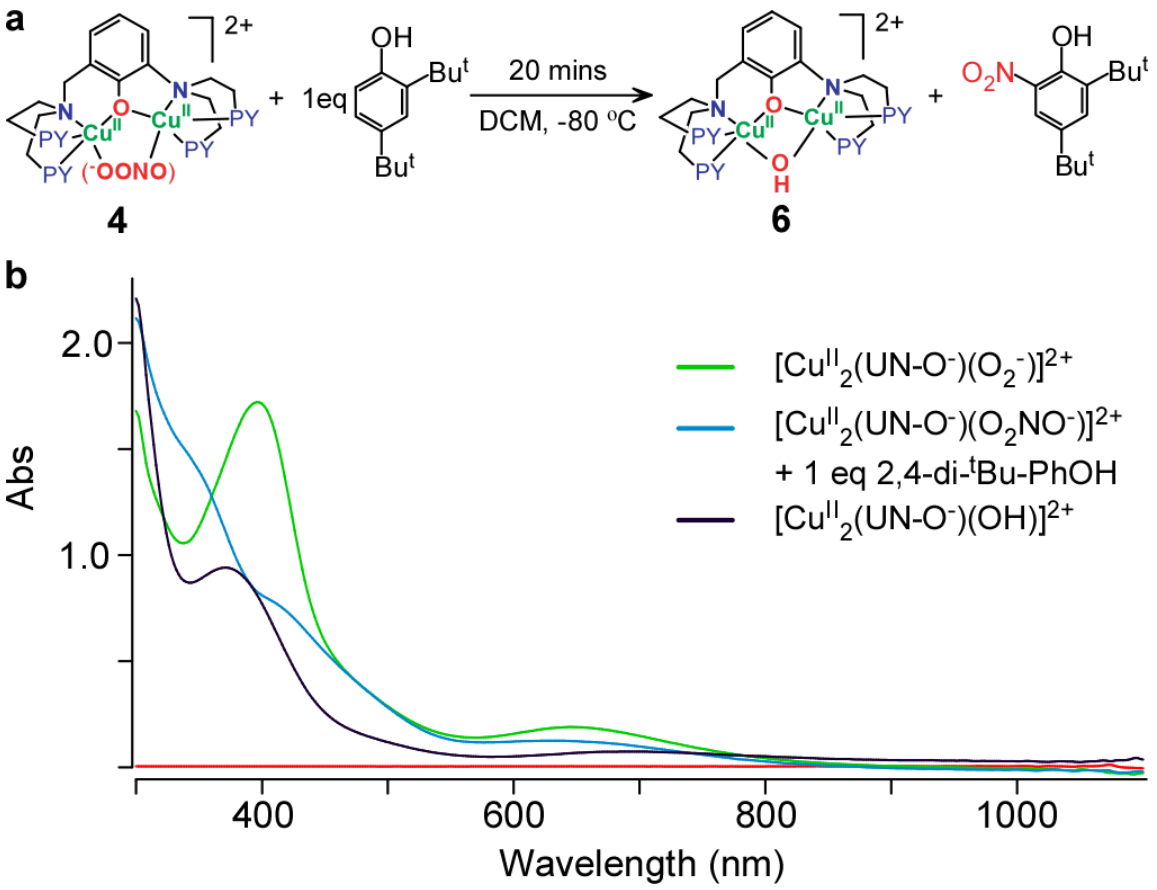

Figure 28. Phenol nitration of the peroxynitrite complex.

(a) Peroxynitrite complex reacts with one equivalent of DTBP at -80 °C in DCM. (b) UV-Vis spectroscopy of the formation of the superoxide $[Cu^{II}_2(UN\text{-}O^-)(O_2^-)]^{2+}$ (green spectrum) and the generation of the peroxynitrite complex $[Cu^{II}_2(UN\text{-}O^-)(^-OONO)]^{2+}$ (blue spectrum) and the final product of $[Cu^{II}_2(UN\text{-}O^-)(OH)]^{2+}$ (black spectrum) by reacting with DTBP at -80 °C in DCM.

The reactivity and products and product yields observed were the same when the experiment was carried out by first fully forming $[Cu^{II}_2(UN\text{-}O^{-})(^{-}OON{=}O)]^{2+}$, having removed excess gases, and then adding one equiv DTBP. Separately, an interesting transformation occurs when $[Cu^{II}_2(UN\text{-}O^{-})(^{-}OON{=}O)]^{2+}$ is warmed to RT in the absence of DTBP. The dicopper complex product formed is that with a *para*-nitrated central aryl-phenol within the UN-O^{-} ligand framework, obtained in ~ 90 % yield (Scheme 2). The product possesses a μ-chloride bridge, instead of hydroxide. The *para* nitro group and μ-Cl^{-} atom were confirmed by X-ray diffraction analysis of this new product; the structure was reported.[80] The high yield of the product with nitrated phenol moiety, again suggests that a peroxynitrite O-O heterolytic cleavage reaction occurred, as that described above, releasing NO_2^{+}, which effects nitration, either at the other end of the same molecule, or it diffuses further to nitrate a nearby dicopper complex. The μ-oxide intermediate likely formed following O–O cleavage molecule would react as a nucleophile with DCM, leading to formation of the chloride-bridged product observed. Further investigations concerning how the chloride product formed from reactions with solvent, were not pursued.

Solvent Effect on the O–O Cleavage mechanism.

In exploring further aspects of the chemistry of peroxynitrite complex $[Cu^{II}_2(UN\text{-}O^{-})(^{-}OON{=}O)]^{2+}$, we happened to also perform UV-Vis studies at -80 °C in 2-methyltetrahydrofuran (MeTHF) as solvent. Formation of the superoxide complex $[Cu^{II}_2(UN\text{-}O^{-})(O_2^{\bullet-})]^{2+}$ in MeTHF, followed by addition of $NO_{(g)}$, did lead to the rapid

formation of $[Cu^{II}_2(UN\text{-}O^{-})(^{-}OON{=}O)]^{2+}$ as judged by the UV-vis changes observed (Figure 29b).

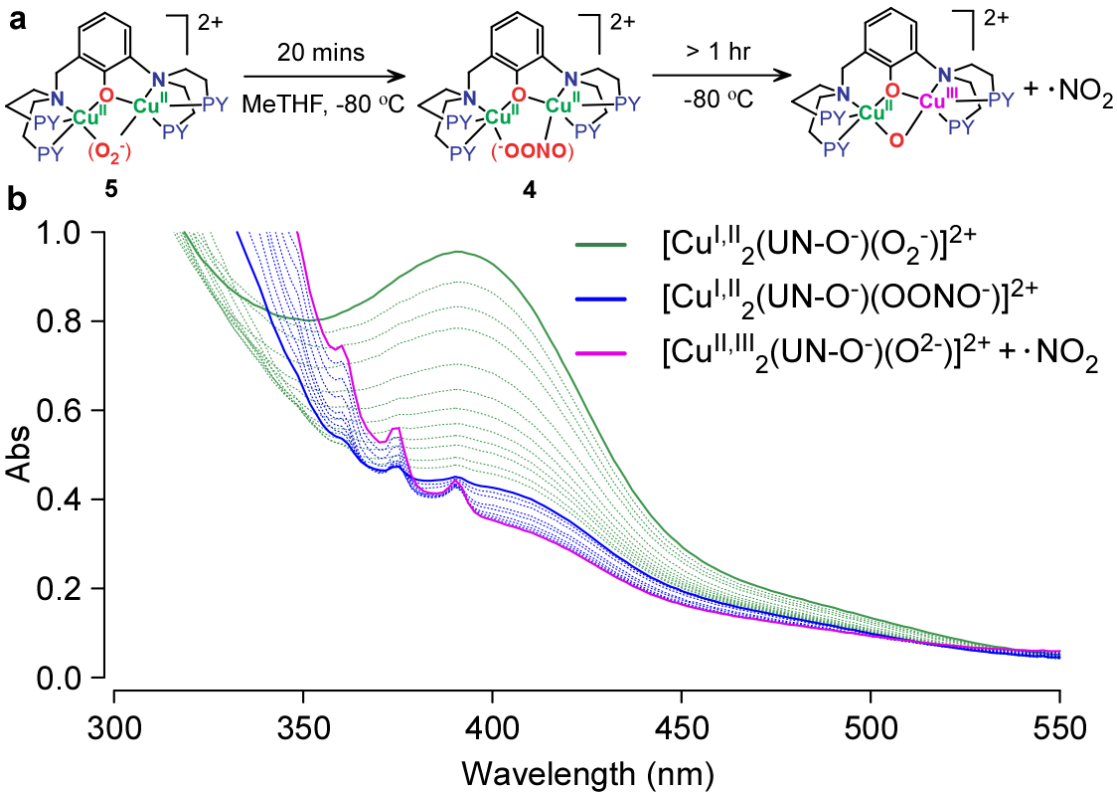

Figure 29. UV-Vis of peroxynitrite formation and decomposition in MeTHF.

(a) Superoxide dicopper(II) complex $[Cu^{II}_2(UN\text{-}O^{-})(O_2^{\bullet-})]^{2+}$ reacts with excess $NO_{(g)}$ at -80 °C in MeTHF solvent. (b) UV-Vis spectroscopy of the formation and decomposition of the peroxynitrite complex $[Cu^{II}_2(UN\text{-}O^{-})(^{-}OONO)]^{2+}$ in MeTHF to give $\bullet NO_2$ dissolved nitrogen dioxide.

However, unlike in DCM as solvent, $[Cu^{II}_2(UN\text{-}O^-)(^-OON{=}O)]^{2+}$ is not stable in MeTHF. In ~ 15 minutes (still at –80 °C) the absorptivity in the 300-400 nm region starts to diminish and eventually (after ~ 1 hour) sharp peaks (spikes) grow in (Figure 29b). These new absorptions are characteristic of the presence of dissolved nitrite (or actually nitrous acid HONO);[92] we can conclude that HONO derives from release of nitrogen dioxide ($\bullet NO_{2(g)}$) when $[Cu^{II}_2(UN\text{-}O^-)(^-OON{=}O)]^{2+}$ decomposes via homolytic O-O cleavage (vide infra). Nitrogen dioxide is known to attack ethers (i.e., MeTHF), effecting H-atom abstraction with the resulting formation of HONO.[93] (Note: in independent experiments we carried out, addition of $NO_{2(g)}$ to a cold MeTHF solution slowly leads to the characteristic sharp 350-400 nm absorption features).

The reaction was repeated, however where one equiv DTBP was added to the –80 °C solution immediately following formation of peroxynitrite complex $[Cu^{II}_2(UN\text{-}O^-)(^-OON{=}O)]^{2+}$. After warming and workup of the decomposed solution, GC-MS analysis revealed that a mixture of ~20% bis-phenol dimer (i.e., ~40 % phenoxyl radical coupling) and ~60% of the *ortho*-nitrated phenol (Scheme 2) was obtained (Scheme 2).

These results/observations lead us to propose that in MeTHF solvent, in contrast to that in DCM, peroxynitrite complex $[Cu^{II}_2(UN\text{-}O^-)(^-OON{=}O)]^{2+}$ undergoes a homolytic O–O bond cleavage reaction. This supposition can explain the formation of a substantial quantity of bis-phenol dimer, known to be the product obtained when the phenoxyl radical derived from DTBP forms. We propose that when O–O homolytic cleavage occurs in MeTHF, $\bullet NO_2$ is formed (as observed) and the dicopper product obtained would then be formally a mixed-valent complex $[Cu^{II,III}_2(UN\text{-}O^-)(O^{2-})]^{2+}$. This

presumed transient species would be an effective hydrogen-atom abstractor, converting DTBP to its phenoxyl radical derivative which would then couple with the $\bullet NO_2$ produced to give nitrated phenol. This is equivalent to what is proposed for many systems, including hemes, where the M^{n+}-PN species cleaves homolytically to give a M^{n+1}=O complex + $\bullet NO_2$; an ArO-H substrate H-atom abstraction by M^{n+1}=O and coupling to $\bullet NO_2$ leads to nitrated phenol product. However, since a phenoxyl radical ArO• is formed during the process, some of it will self-couple giving the bis-phenol dimer observed. Such a product cannot be explained by formation of nitronium ion obtained from heterolytic O–O peroxynitrite cleavage. Note that H-atom abstraction by a putative $[Cu^{II,III}_2(UN\text{-}O^{-})(O^{2-})]^{2+}$ species would directly produce the very stable μ-hydroxide complex $[Cu^{II}_2(UN\text{-}O^{-})(OH)]^{2+}$,[80,94] that being the product identified in this reaction in THF solvent.

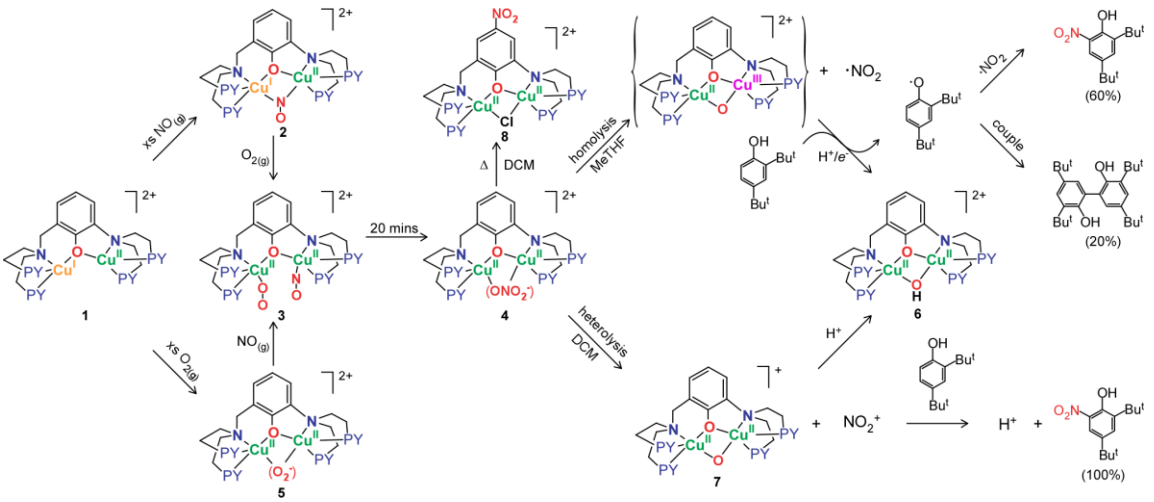

Scheme 2. PN complex $[Cu^{II}_2(UN\text{-}O^{-})(^{-}OON{=}O)]^{2+}$ chemistry performed at -80 °C in solvent dichloromethane (DCM) and 2-methyltetrahydrofuran (MeTHF).

See Scheme 2 for a summary of these reactions involving peroxynitrite-dicopper(II) complex heterolytic vs homolytic O-O cleavage. The solvent effect, may simply be derived from the difference in dielectric constant (ε) of the solvents, DCM vs MeTHF, the latter being much less polar and with a smaller ε value. The heterolytic cleavage, producing a nitronium cation and oxide anion (although dicopper coordinated) might expected to be a more favorable O-O cleavage pathway in a higher dielectric solvent, and this is what is found, as described above.

CONCLUSIONS

Scheme 2 summarizes all of the chemistry observed of the UN-O^{-} ligand dicopper complexes with O_2 and $NO_{(g)}$ chemistry. We have described the generation of a peroxynitrite complex $[Cu^{II}_2(UN\text{-}O^{-})(^{-}OON{=}O)]^{2+}$ that can be formed in two pathways: (i) The mixed-valent complex$[Cu^{I,II}_2(UN\text{-}O^{-})(DMF)]^{2+}$, when reacted with nitric oxide, forms a nitrosyl complex best described as a mixed-valent μ-•NO species $[Cu^{I,II}(UN\text{-}O^{-})(NO)]^{2+}$; this is found to form a new superoxide and nitrosyl complex $[Cu^{II}_2(UN\text{-}O^{-})(NO)(O_2^{-})]^{2+}$ when exposed to dioxygen. However, $[Cu^{II}_2(UN\text{-}O^{-})(NO)(O_2^{-})]^{2+}$ undergoes a relatively fast intramolecular coupling reaction of superoxide and nitrosyl ligands to form the peroxynitrite dicopper(II) product, $[Cu^{II}_2(UN\text{-}O^{-})(^{-}OON{=}O)]^{2+}$. (ii) The superoxide adduct $[Cu^{II}_2(UN\text{-}O^{-})(O_2^{\bullet-})]^{2+}$, reported previously to form by oxygenation of the mixed-valent complex, undergoes further reaction with nitric oxide gas, producing the same new intermediate species $[Cu^{II}_2(UN\text{-}O^{-})(NO)(O_2^{-})]^{2+}$, which again transforms into peroxynitrite complex $[Cu^{II}_2(UN\text{-}O^{-})(^{-}OON{=}O)]^{2+}$. The peroxynitrite complex $[Cu^{II}_2(UN\text{-}O^{-})(^{-}OON{=}O)]^{2+}$, as deduced by IR spectroscopy, is a mixture of *cis*-PN and *trans*-PN forms. In any case, $[Cu^{II}_2(UN\text{-}O^{-})(^{-}OON{=}O)]^{2+}$ as formed by either pathway very efficiently (even at –80 °C), effects phenol *o*-nitration of DTBP, even with only one equiv of this substrate added. Our studies reveal the decomposition, or rather transformation of the peroxynitrite complex $[Cu^{II}_2(UN\text{-}O^{-})(^{-}OON{=}O)]^{2+}$, can proceed by either a heterolytic PN O–O cleavage which putatively

produces the nitronium ion (NO_2^+), or in a different solvent (i.e., MeTHF) strong evidence for substantial homolytic cleavage chemistry occurs.

Thus, the major advances from this present work can be summarized as follows:

1. We report in a system first time in literature where both of pathways (M^{n+}+ $NO_{(g)}$ + $O_{2(g)}$ or M^{n+} + $O_{2(g)}$ + $NO_{(g)}$) within a single complex lead to the formation of the same PN complex $M^{(n+1)+}(^{-}OON{=}O)$.

2. In this synthetically challenging and biologically relevant binuclear ligand copper framework, detailed LT-IR characterizations of the key complexes are presented and a new nitrosyl-superoxide intermediate complex $M^{(n+1)+}(NO)(O_2^{\bullet-})$ is proposed to form. The intermediate transforms to the PN complex $M^{(n+1)+}(^{-}OON{=}O)$ that consists of both *cis*- and *trans*- conformers based on low-temperature IR spectroscopy.

3. In further support of the formation of PN complex $[Cu^{II}_2(UN\text{-}O^{-})(^{-}OON{=}O^{-})]^{2+}$, it is observed to efficiently effect phenol substrate nitration.

4. Unique insights concerning the rich chemistry which a metal bound peroxynitrite moiety can undergo, come from the observation that either O-O homolytic vs heterolytic cleavage may occur. In DCM, the O-O cleavage is heterolytic, and quantitative *o*-phenol (DTBP) nitration can be attributed to the generation of nitronium ion (NO_2^+) in solution. This supposition is also supported by the observation of the efficient nitration of the ligand in the dicopper complex when in the absence of substrate DTBP. However, in the much less polar solvent 2-methyltetrahydrofuran, the O-O bond undergoes homolysis to generate $\bullet NO_2$ (detected spectrophotometrically, indirectly) and a putative higher-valent complex $Cu^{II,III}_2(UN\text{-}O^{-})(O^{2-})]^{2+}$ that abstracts a H-atom from

DTBP to give $Cu^{II}_2(UN\text{-}O^{-})(OH)]^{2+}$ (as observed) and a phenoxyl radical; the latter may dimerize to form the bis-phenol observed experimentally, or couple with the $\bullet NO_2$ present leading to the observed *o*-nitrophenol.

As previously postulated,[66a,66b,66f] and as supported by the rich chemistry observed here, it seems likely that copper ion chemistry with O_2 and/or NO may be important biologically, contributing significantly to (i) the known formation of nitrated protein residues (e.g., tyrosine),[56d,56f,56h-l] or (ii) other oxidative or nitrative damage, or (iii) possibly even in signaling. In fact, peroxynitrite chemistry at heme centers, produced via metal/$NO_{(g)}$/$O_{2(g)}$ chemistry, can lead to protein residue nitration. Most recently,[95] such biochemistry has been applied in the practical organic synthesis of nitrated substrates, in heme or non-heme iron enzymes.[96] The extensive chemistry observed here calls for the further investigations of the scope and mechanisms involved in metal ion mediated peroxynitrite formation and reactivity; such will, at least in part, be included in research goals in our own laboratories.

CHAPTER THREE

Nitric Oxide Reduction in a dicopper(I) center----Formation and Characterization of a Hyponitrite Complex

INTRODUCTION

Most animals and microorganisms breathe dioxygen (O_2) and carry out enzyme catalyzed O_2 reduction processes coupled with energy production. In cytochrome *c* oxidase, the terminal respiratory oxidase found in eukaryotic mitochondria and some bacteria, a heme-copper active site mediates four-electron-four-proton reduction of O_2 to water to generate a proton motive force for downstream ATP synthesis.[1] Likewise, anaerobic respiration is found in bacteria under dioxygen deprived conditions such as frozen soil or in the ocean. Denitrification belongs to one of the anaerobic respiration mechanisms that utilize nitrate ion as the initial electron acceptor.[97] Compared to four-electron-four-proton reductions of dioxygen, denitrification processes are even more complicated and require a number of different enzymes to catalyze four reduction steps.[97]

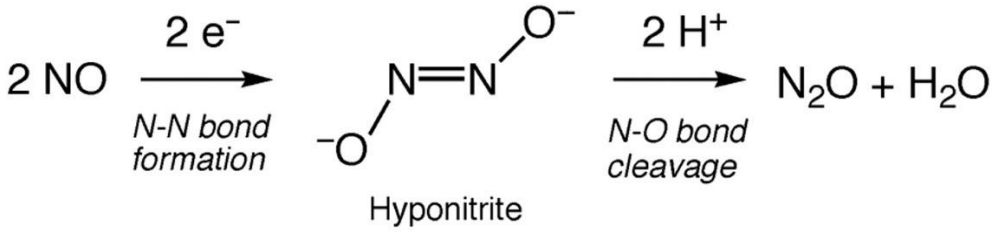

Chart 3. Nitric oxide reduction, adapted from ref.[98]

We are focusing here on the nitric oxide reduction[99] to form nitrous oxide, Chart 3, adapted from ref. 98. This is a two electron two proton reduction that is enzyme catalyzed. This is Nitric Oxide Reductase (NOR) and the active site consists of a heme non-heme di-iron heterobinuclear center, which binds the two NO molecules required and effects their reductive coupling; mechanistic details are still lacking. The genetically

related enzymes cytochrome *c* oxidases also can catalyze the NOR reaction, although not as efficiently as in the all-iron NOR's.

The first step is N-N bond formation where upon adding two electrons to the nitric oxide moieties, a hyponitrite dianion ($N_2O_2^{2-}$) was proposed as the reaction intermediate. Upon adding two protons, the N-O bond is cleaved to give the nitrous oxide and water. However, many aspects of the chemical mechanism involving bond formation and bond cleavage reactions require more insights. In a recent example, this chemistry has been very well characterized with certain ruthenium metal complexes and X-ray structures were determined.[100]

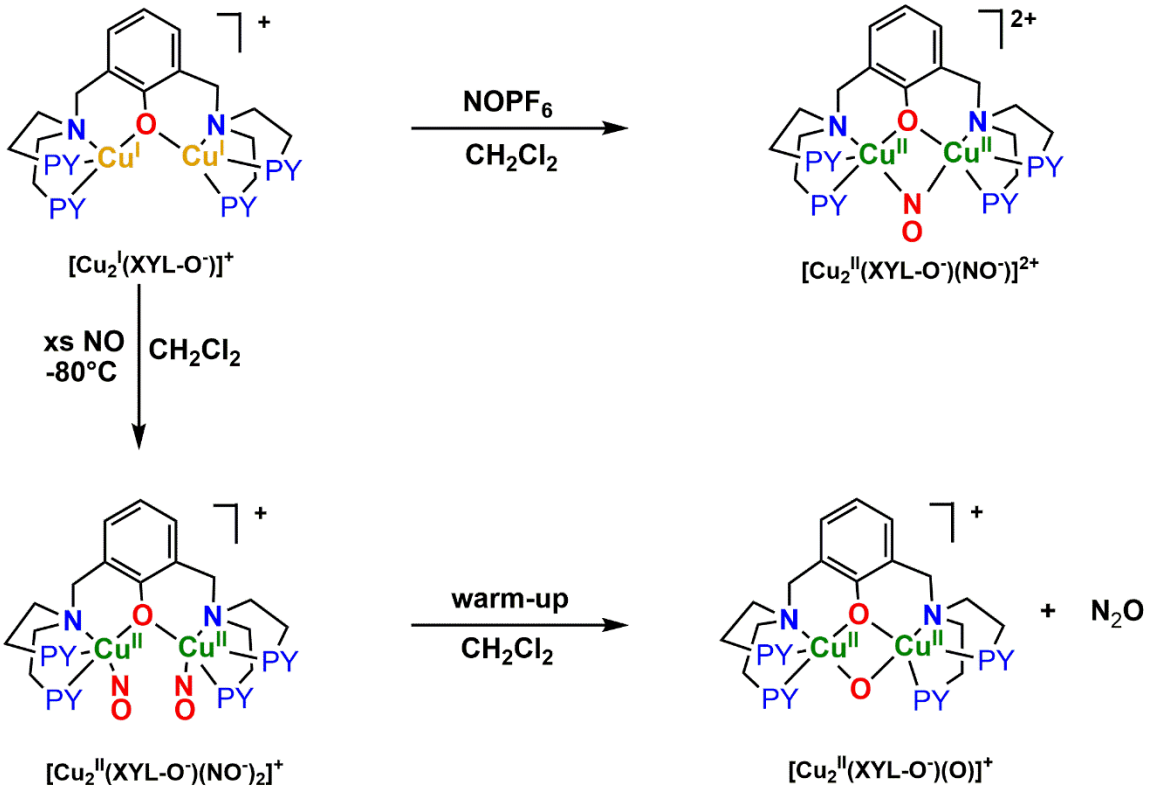

Scheme 3. $[Cu^{I}_2(XYL\text{-}O^{-})]^{+}$ derived reactions with $NO_{(g)}$ and $NOPF_6$.

Similar chemistry was conducted by Karlin and coworkers studied $[Cu^{I}_2(XYL\text{-}O^{-})]^{+}$ complex and found out that by reacting this $[Cu^{I}_2(XYL\text{-}O^{-})]^{+}$ with one equiv of nitrosonium hexafluorophosphate under a nitrogen atmosphere at room temperature, a new nitroxyl complex $[Cu^{I}_2(XYL\text{-}O^{-})(NO^{-})]^{2+}$ could be formed and X-ray crystal structure was determined.[82] Based on Nujol Mull IR studies this complex revealed a very low ν(NO) of 1536 cm^{-1}, consistent with an assignment as being a nitroxyl (NO^{-}) bridged complex. $[Cu^{II}_2(XYL\text{-}O^{-})(NO^{-})]^{2+}$ was found to have UV-Vis absorption features at 382 nm (5300 M^{-1} cm^{-1}) and 545 (2200 M^{-1} cm^{-1}) and 730 nm (500 M^{-1} cm^{-1}) and it was shown to be EPR silent.

$[Cu^{I}_2(XYL\text{-}O^{-})]^{+}$ also reacts with excess nitric oxide at -80 °C in dichloromethane to give a putative unstable dinitroxyl species $[Cu^{II}_2(XYL\text{-}O^{-})(NO^{-})_2]^{+}$ and upon warming this transforms to an oxide complex $[Cu^{I}_2(XYL\text{-}O^{-})(O^{2-})]^{+}$ and gave off nitrous oxide that was detected using reaction flask headspace GC (Scheme 3). This reaction described was a net two electron reduction of two nitric oxide molecules to form a nitrous oxide molecule. The copper ions involved here provide two electrons by oxidation of the intial dicopper(I) ions to copper(II) and this dicopper(II) center can also act as a Lewis acid and stabilize the oxide ligand.

In this study, we employed a phenol-containing binucleating ligand ($UN\text{-}O^{-}$) giving rise to a series of phenolate-bridged dicopper complexes of various types. In particular, the dicopper(I) complex $[Cu^{I}_2(UN\text{-}O^{-})]^{+}$ was found to reduce nitric oxide to nitrous oxide at various temperatures. With low temperature spectroscopic techniques, we can now observe a new hyponitrite intermediate species at much lower temperature (-

120 °C). This hyponitrite complex can be alternatively synthesized using a dicopper(II) oxide complex $[Cu^{II}_2(UN\text{-}O^{-})(O^{2-})]^{+}$ with hyponitrous acid. The detailed characterization/reactivity are discussed as follows.

EXPERIMENTAL SECTION

Materials and Instrumentations.

All chemicals were purchased from Sigma-Aldrich Co. in the highest available quality unless otherwise specified. Preparation and handling of air sensitive compounds were achieved using either standard Schlenk line techniques under an argon atmosphere or in an MBraun Labmaster 130 nitrogen atmosphere glovebox with $O_{2(g)}$ and $H_2O_{(g)}$ levels < 1 ppm. HPLC grade dichloromethane (DCM), acetonitrile (ACN) and diethyl ether (Et_2O) were passed through a 60 cm long column of activated alumina under an argon atmosphere before use (Innovative Technologies, Inc.). 2-methyltetrahydrofuran (MeTHF) was distilled over sodium benzophenone under an argon atmosphere prior to use. Solvent deoxygenation was achieved by bubbling argon through the solvent for 30 mins in an addition funnel connected to a receiving Schlenk flask. Deoxygenated solvents were stored in the glovebox inside amber glass bottles and further dried over activated 3 or 4 Å molecular sieves. Dioxygen was dried by passing the gas through a short column of Drierite prior to usage. Nitric oxide was purchased from Matheson Gases and purified according to a literature method.[69a] UV-Vis absorption spectra were recorded on a Cary-50 Bio spectrophotometer using 10 mm path length Schlenk quartz cuvettes. The reaction temperature maintained by a UnispeKs CoolSpeK cryostat controller and a cell holder kit

by Unisoku Scientific Instruments. EPR samples were prepared in 5mm O.D. quartz sample tubes (Wilmad-LabGlass) and spectra recorded on an X-band Bruker EMX-plus spectrophotometer equipped with a dual mode cavity (ER 4116DM) Bruker EMX CW EPR controller with a Bruker ER 041 XG microwave bridge operating at the X band (~9 GHz). Electrospray ionization mass spectrometry (ESI-MS) experiments were performed on a Thermo Finnigan LCQ Deca XP Plus spectrometer. GC-MS analysis was carried out on a Shimadzu GC-17A/GCMS0QP5050 gas chromatograph/mass spectrometer. GC-MS analysis was carried out on a Shimadzu GC-17A/GCMS0QP5050 gas chromatograph/mass spectrometer. Synthesis and characterization of the dicopper(I) complex was described in chapter 1 and M_w = 961.6.

UV-Vis characterizations of each complex

UV-Vis experiments of the $[Cu^{I}_2(UN\text{-}O^{-})(NO)]^{+}$.

$[Cu^{I}_2(UNO^{-})](SbF_6)(CH_3CN)$ (5.5 mg, 0.006 mmol) was used to prepare a 25 ml stock solution using a 25 ml volumetric flask using DCM as solvent. From here, 3 ml of the stock solution were transferred to a Schlenk cuvette and charged with a magnetic stir-bar in the inert-atmosphere box. The cuvette was placed inside the cell holder of the cryostat and cooled down to -80 °C. The cuvette was left to equilibrate at -80 °C for 10 minutes. 0.2 ml of $NO_{(g)}$ (about 20 equiv) was gradually added to the solution using a 3-way gastight syringe and UV-Vis spectrum were recorded.

UV-Vis experiments of the $[Cu^{II}_2(UN\text{-}O^{-})(O^{2-})]^{+}$.

After UV-Vis spectrum were recorded for the nitrosyl complex $[Cu^{I}_2(UN\text{-}O^{-})(NO)]^{+}$, the solution was put under vacuum and purged with argon gas five times to remove excess $NO_{(g)}$. The solution was then let to warm up to room temperature and the spectrum of $[Cu^{II}_2(UN\text{-}O^{-})(O^{2-})]^{+}$ was recorded.

UV-Vis experiments of $[Cu^{I}_2(UN\text{-}O^{-})(NO)_2]^{+}$.

$[Cu^{I}_2(UNO^{-})](SbF_6)(CH_3CN)$ (5.5 mg, 0.006 mmol) was used to prepare a 25 ml stock solution using a 25 ml volumetric flask using 50:50 DCM/MeTHF mixture as solvent. From here, 3 ml of the stock solution were transferred to a Schlenk cuvette and charged with a magnetic stir-bar in the inert-atmosphere box. The cuvette was placed inside the cell holder of the cryostat and cooled down to -120 °C. The cuvette was left to equilibrate at -120 °C for 10 minutes. 0.2 ml of $NO_{(g)}$ (about 20 equiv) was gradually added to the solution using a 3-way gastight syringe and UV-Vis spectra were recorded every one minute.

UV-Vis experiments of $[Cu^{II}_2(UN\text{-}O^{-})(N_2O_2^{2-})]^{+}$. (N bound)

The solution was put under vacuum and purged with argon gas five times to remove excess $NO_{(g)}$. The solution containing $[Cu^{I}_2(UN\text{-}O^{-})(NO)_2]^{+}$ was kept at -120 °C and UV-Vis kinetics studied were performed. The spectra were recorded automatically

every one minute in the course of six hours and all the spectra overlay were recorded to give the putative $[Cu^{II}_2(UN\text{-}O^{-})(N_2O_2)]^{+}$ (N bound).

UV-Vis experiments of $[Cu^{II}_2(UN\text{-}O^{-})(N_2O_2)]^{+}$. (O bound)

The solution containing $[Cu^{II}_2(UN\text{-}O^{-})(N_2O_2^{2-})]^{+}$ (N bound) was warmed up to room temperature and allowing the temperature to equilibrate for a few hours while the solution was still kept in an inert atmosphere and away from the light. The spectrum was recorded to give rise to the putative $[Cu^{II}_2(UN\text{-}O^{-})(N_2O_2^{2-})]^{+}$ (O bound).

Electrospray ionization mass spectrometry (ESI-MS) of each complex

ESI-MS of $[Cu^{II}_2(UN\text{-}O^{-})(O^{2-})]^{+}$.

The solution containing $[Cu^{II}_2(UN\text{-}O^{-})(O^{2-})]^{+}$ was concentrated to about 1 ml by applying active vacuum. Then 0.25 ml of acetonitrile solvent was added to the solution of $[Cu^{II}_2(UN\text{-}O^{-})(O^{2-})]^{+}$. The solution was then injected to the ESI-MS instrument with a gastight syringe and the mass spectrum was recorded.

ESI-MS of $[Cu^{II}_2(UN\text{-}O^{-})(N_2O_2^{2-})]^{+}$. (O bound)

The solution containing $[Cu^{II}_2(UN\text{-}O^{-})(N_2O_2^{2-})]^{+}$ (O bound) was added with 0.6 ml of acetonitrile solvent. The solution was then injected to the ESI-MS instrument with a gastight syringe and the mass spectrum was recorded.

ESI-MS of $[Cu^{II}_2(UN\text{-}O^{-})(O^{2-})]^{+}$. (regenerated from hyponitrite)

In a separate experiment, the solution containing $[Cu^{II}_2(UN\text{-}O^{-})(N_2O_2^{2-})]^{+}$ was prepared, *vide supra*. The solution was put under active vacuum to remove all the solvent together with nitrous oxide (N_2O). The remaining solid was dissolved using 1.5 ml of 80 percent dichloromethane and 20 percent acetonitrile solvent mixture. The solution was then injected to the ESI-MS instrument with a gastight syringe and the mass spectrum was recorded. The spectrum match with the $[Cu^{II}_2(UN\text{-}O^{-})(O^{2-})]^{+}$ that was previously made.

ESI-MS of $[Cu^{II}_2(UN\text{-}O^{-})(N_2O_2^{2-})]^{+}$ (regenerated with hyponitrous acid)

The hyponitrous acid ($H_2N_2O_2$) was prepared using a modified literature method. [101] 10.6 mg (0.1 mmol) of $Na_2N_2O_2$ was dissolved in 1 ml of water. 33.9 mg (0.2 mmol) of $AgNO_3$ was dissolved in 1 ml of water. Gradually add the $AgNO_3$ solution to the $Na_2N_2O_2$ resulting 21.5 mg (0.08 mmol, 78% yield) bright yellow precipitate of $Ag_2N_2O_2$. The yellow colored solid was washed with water and dried under vacuum over 24 hours. 3 ml of ether was added to the $Ag_2N_2O_2$ solid under argon atmosphere, then 0.08 ml (0.16 mmol) of HCl in ether solution (2.0 M bottle) was added to the reaction mixture using a gas-tight syringe. The reaction mixture was left to stir for over one hour and then filtered to remove the AgCl precipitate. About one equiv of freshly made hyponitrous acid ($H_2N_2O_2$) (0.02 ml) was added to the solution containing $[Cu^{II}_2(UN\text{-}O^{-})(O^{2-})]^{+}$ and

allowed to stir for half hour. The solution was then injected into the ESI-MS instrument with a gastight syringe and the mass spectrum was recorded. The spectrum match with the $[Cu^{II}_2(UN\text{-}O^{-})(N_2O_2^{2-})]^{+}$ that was previously made.

ESI-MS of $[Cu^{II}_2(UN\text{-}O^{-})(OH)]^{2+}$

In a separate experiment, the solution containing $[Cu^{II}_2(UN\text{-}O^{-})(O^{2-})]^{+}$ (0.006mmol) was added with one equiv of fluoroantimonic acid and the solution was then injected into the ESI-MS instrument with a gastight syringe and the mass spectrum was recorded. The spectrum match with the $[Cu^{II}_2(UN\text{-}O^{-})(OH)]^{2+}$ that was previously made.

Nujol Mull Infrared Spectroscopy of related complexes

Nujol Mull infrared of $[Cu^{II}_2(UN\text{-}O^{-})(O^{2-})]^{+}$.

The solution containing $[Cu^{II}_2(UN\text{-}O^{-})(O^{2-})]^{+}$ prepared, *vide supra* was put under vacuum for over 2 hours to remove all the solvent. Then the solid was scraped out and mix with Nujol to make samples on a KBr plate. The plate was placed in a FT-IR spectrometer and the spectrum was recorded.

Nujol Mull infrared of $[Cu^{II}_2(UN\text{-}O^{-})(OH)]^{2+}$

The solution containing $[Cu^{II}_2(UN\text{-}O^{-})(O^{2-})]^{+}$ prepared, *vide supra* and one equiv of fluoroantimonic acid was added to the solution. The solution was put under vacuum for over 2 hours to remove all the solvent.

EPR spectroscopy of related complexes.

EPR spectrum of complex $[Cu^{I}_2(UN\text{-}O^{-})(NO)]^{+}$.

$[Cu^{I}_2(UNO^{-})](SbF_6)(CH_3CN)$ (3.8 mg, 0.004 mmol) was dissolved in 2 ml of 50:50 DCM/MeTHF solvent mixture in the glovebox to give 2 ml of 2 mM stock solution. 0.5 ml of the stock solution was transferred to a 5mm O.D. quartz sample tube using a 0.5 ml syringe. This process was repeated three more times to obtain four sample tubes each containing 0.5 ml of the stock solution. Each of the tube was sealed with a rubber septum before bringing out of the glovebox. The EPR sample tubes were placed in a dry ice/acetone bath to maintain the temperature at -80 °C. After waiting ten minutes for the temperature to equilibrate, 0.2 ml of $NO_{(g)}$ (about 20 equiv) was gradually added to the solution in one of the tube using a gastight 3-way syringe. The tube was subsequently kept frozen in liquid nitrogen and EPR spectrum was taken at 20K and exhibited a g ~ 2.0 signal.

EPR spectrum of complex $[Cu^{I}_2(UN\text{-}O^{-})(NO)_2]^{+}$.

The EPR sample tubes were placed in a pentane/liquid nitrogen bath to maintain the temperature at -125 °C. After waiting ten minutes for the temperature to equilibrate, 0.2 ml of $NO_{(g)}$ (about 20 equiv) was gradually added to the solution in one of the tube using a gastight 3-way syringe. The tube was subsequently kept frozen in liquid nitrogen and EPR spectrum was taken at 20K and exhibited a silengt signal.

RESULTS AND DISCUSSION

Nitric oxide reduction at the dicopper (I) center.

$[Cu^{I}_{2}(UN\text{-}O^{-})]^{+}$ was previously synthesized and crystallized (see Figure 30) with SbF_6^- as counter anion. Upon addition of excess nitric oxide to the solution of $[Cu^{I}_{2}(UN\text{-}O^{-})]^{+}$ at room temperature a significant color change from yellow to green accompanied by the formation of $[Cu^{II}_{2}(UN\text{-}O^{-})(O^{2-})]^{+}$ occurred, as illustrated in Figure 31. This oxide complex was characterized using UV-Vis and electrospray ionization mass spectrometry. As mentioned in the introduction, a similar reaction on a closely related XYL-O^- ligand dicopper(I) complex was also observed. This reaction described here is a net two electron reduction of two molar equiv of nitric oxide gas to form one molar equiv of nitrous oxide and one molar equiv of dicopper(II) oxide. The dicopper moiety here is acting as both electron source by giving off two electrons thus accompanied by oxidation of the starting dicopper(I)complex to the dicopper(II) complex in the product. As mentioned before, the two copper(II) provide a source of strong Lewis acidity to stabilize the negative charge of the oxide ligand.

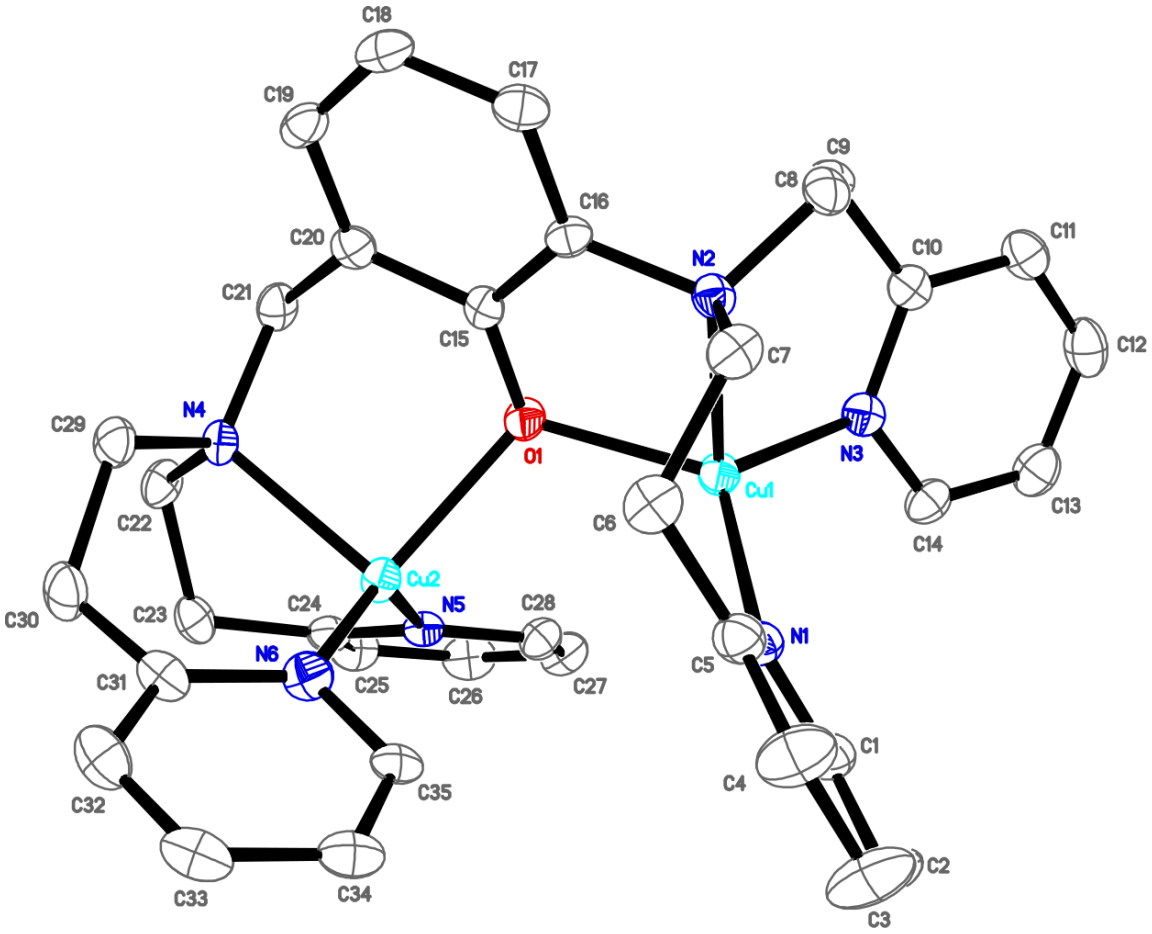

Figure 30. X-ray structure of dicopper(I) complex.

Displacement ellipsoid plot of $[Cu^{I}_{2}(UN\text{-}O^{-})]SbF_6$. The counter anion and hydrogen atoms were omitted.

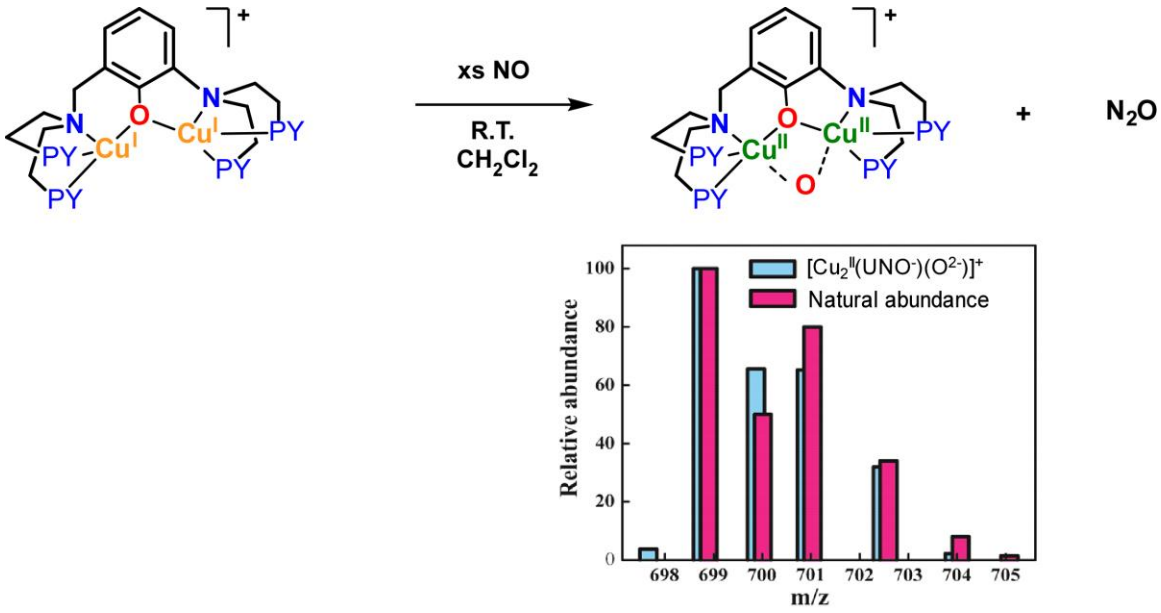

Figure 31. Nitric oxide reduction by dicopper(I) complex at room temperature.

$[Cu^{I}_2(UN\text{-}O^{-})]^{+}$, when reacted with an excess of purified NO(g), undergoes a significant color change from yellow to green, and this is accompanied by the formation of the complex $[Cu^{II}_2(UN\text{-}O^{-})(O^{2-})]^{+}$, that is characterized using UV-Vis spectroscopy and electrospray ionization mass spectrometry (ESI-MS), m/z = 699.16 (Figure 31). The N_2O was detected and quantified using reaction flask headspace GC.

Protonation of the oxide complex.

The oxide complex $[Cu^{II}_2(UN\text{-}O^{-})(O^{2-})]^{+}$ was in part identified and characterized by analysis of the protonated product $[Cu^{II}_2(UN\text{-}O^{-})(OH)]^{2+}$. In a separate experiment, the oxide complex $[Cu^{II}_2(UN\text{-}O^{-})(O^{2-})]^{+}$ was synthesized through addition of excess nitric oxide gas (~ 20 equiv) using gas-tight syringe to the dicopper(I) complex $[Cu^{I}_2(UN\text{-}O^{-})]^{+}$ in dichloromethane solvent at room temperature.

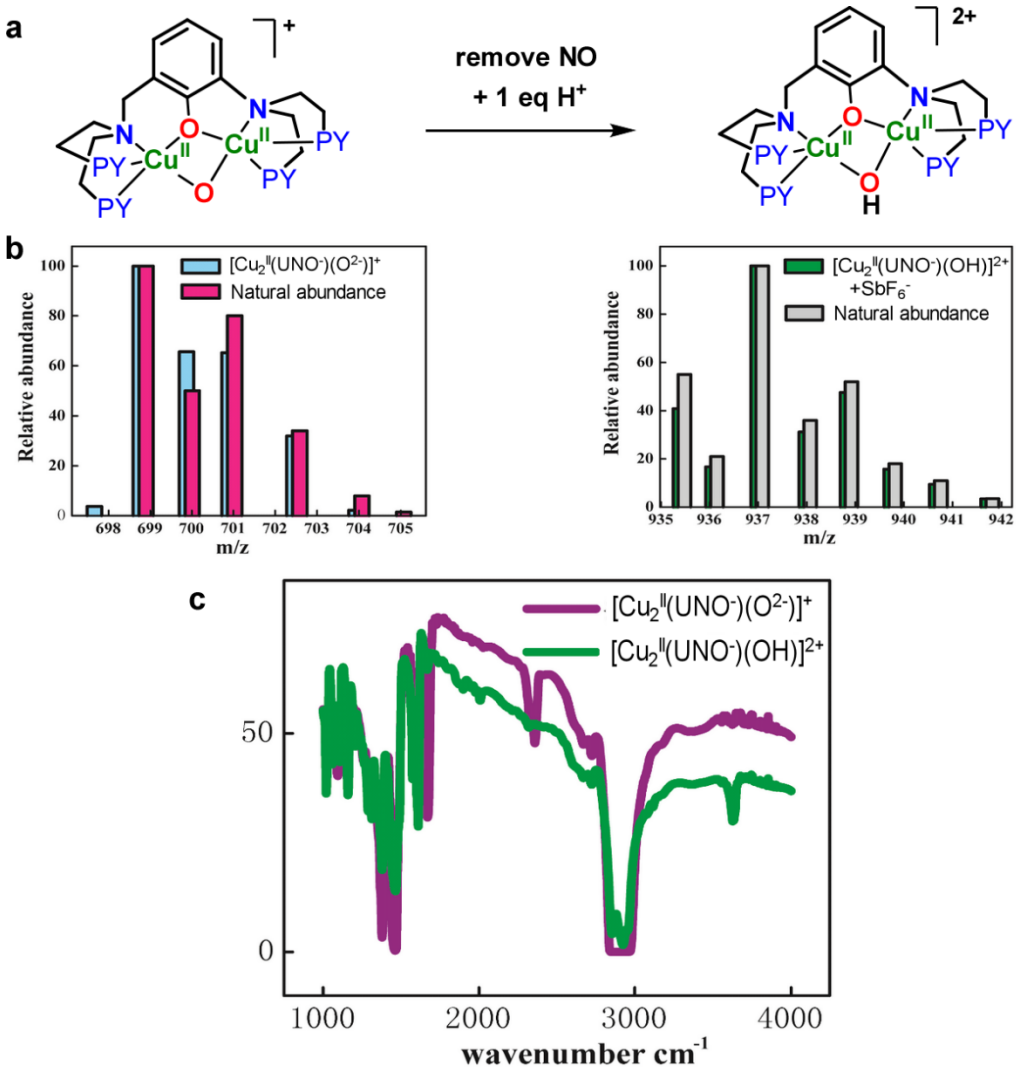

Figure 32. Protonation of the oxide complex to form a hydroxide complex.

(a) $[Cu^{II}_2(UN\text{-}O^{-})(O^{2-})]^{+}$ complex that is characterized using UV-Vis and electrospray ionization spectroscopy (ESI-MS) is removed of excess $NO_{(g)}$ and added 1 equiv of H^{+} and formed the $[Cu^{II}_2(UN\text{-}O^{-})(OH)]^{2+}$ complex that is characterized using UV-Vis and electrospray ionization spectroscopy (ESI-MS). (b) ESI-MS spectra of the $[Cu^{II}_2(UN\text{-}O^{-})(O^{2-})]^{+}$, m/z = 699.16 and $[Cu^{II}_2(UN\text{-}O^{-})(OH)]^{2+}$ complex, m/z = 937.06. (c) Nujol Mull IR spectra of $[Cu^{II}_2(UN\text{-}O^{-})(O^{2-})]^{+}$ and $[Cu^{II}_2(UN\text{-}O^{-})(OH)]^{2+}$.

The excess nitric oxide gas was removed by application of a vacuum followed by Ar gas purging for several cycles. The remaining solution was characterized using electrospray ionization mass spectrometry (ESI-MS) (Figure 32b). The isotope patterns of the $[Cu^{II}_2(UN\text{-}O^{-})(O^{2-})]^{+}$ agree well with theoretically predicted values. The remaining $[Cu^{II}_2(UN\text{-}O^{-})(O^{2-})]^{+}$ was further dried under vacuum and the resulting solid was scraped out using a spatula and mixed with Nujol on a KBr plate. An infrared spectrum of $[Cu^{II}_2(UN\text{-}O^{-})(O^{2-})]^{+}$ was recorded (i.e., the purple colored spectrum, Figure 32c); the band at 2250 cm^{-1} corresponds to the acetonitrile residue solvent. The synthesis of $[Cu^{II}_2(UN\text{-}O^{-})(O^{2-})]^{+}$ was then repeated, and to the solution containing $[Cu^{II}_2(UN\text{-}O^{-})(O^{2-})]^{+}$ was added with one equiv. of fluoroantimonic acid. The resulting solution was presumed to contain $[Cu^{II}_2(UN\text{-}O^{-})(OH)]^{2+}$ and this could be confirmed using ESI-MS and IR spectroscopy. Injection of the product solution into the ESI-MS instrument leads to the mass spectrum shown in Figure 32b (right side). The isotope patterns of $[Cu^{II}_2(UN\text{-}O^{-})(OH)]^{2+}$ agree well with theoretically predicted values. The remaining solution of $[Cu^{II}_2(UN\text{-}O^{-})(OH)]^{2+}$ was dried under vacuum and the solid was scraped out and mixed with Nujol on a KBr plate. The infrared spectrum of compound $[Cu^{II}_2(UN\text{-}O^{-})(OH)]^{2+}$ was then recorded and in shown in Figure 32c, the green colored spectrum in fact containing a characteristic ν(OH) stretching vibration at ~3600 cm^{-1}.

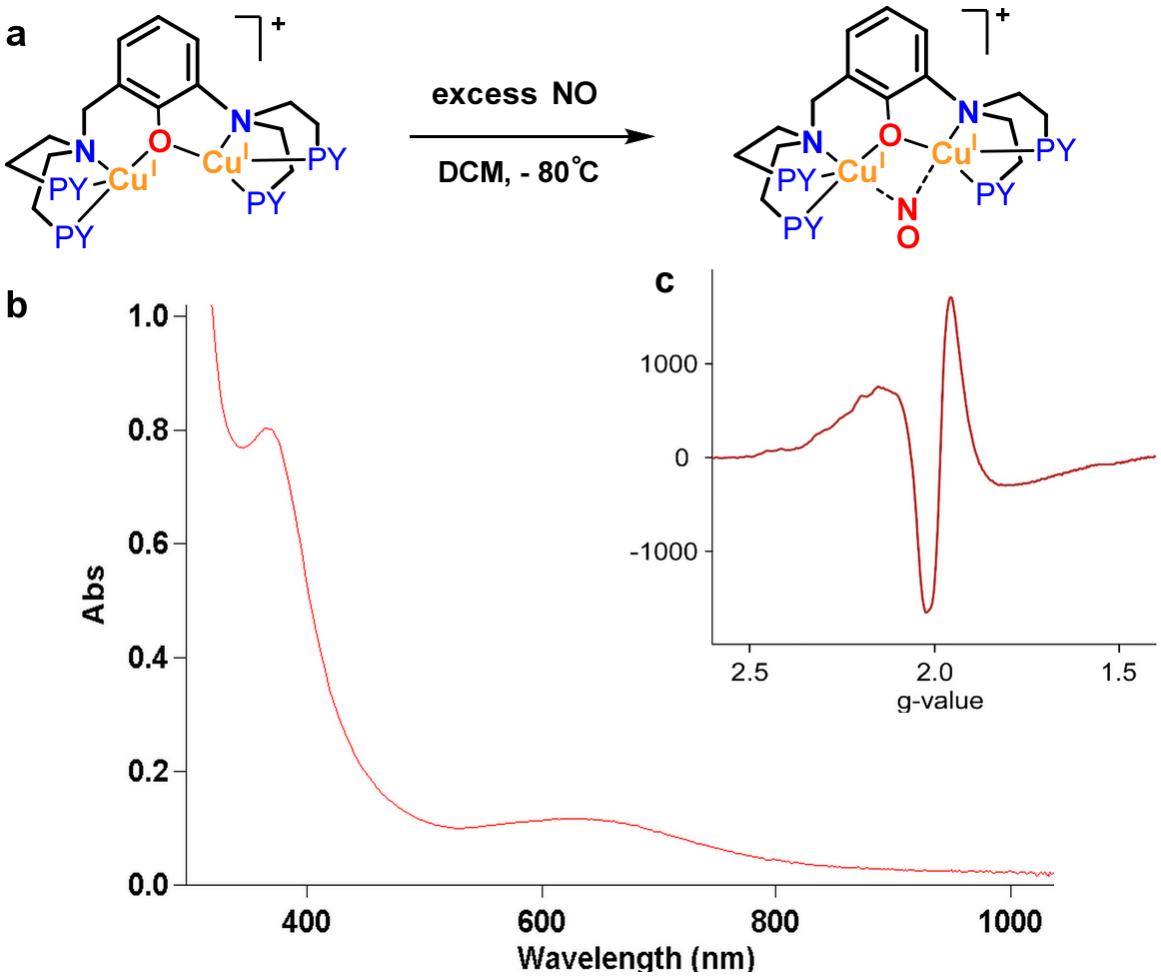

Figure 33. Formation of the nitrosyl complex at -80 °C.

(a) Addition of excess nitric oxide gas to the solution of $[Cu^{I}_{2}(UN\text{-}O^{-})]^{+}$ resulting in the formation of $[Cu^{I}_{2}(UN\text{-}O^{-})(NO)]^{+}$ at -80 °C in DCM. (b) UV-Vis spectrum of $[Cu^{I}_{2}(UN\text{-}O^{-})(NO)]^{+}$ at -80 °C in DCM. (c) EPR spectrum of frozen DCM/MeTHF solution $[Cu^{I}_{2}(UN\text{-}O^{-})(NO)]^{+}$ showing a g ~ 2.0 signal.

Reacting dicopper(I) with excess $NO_{(g)}$ at low temperature

The dicopper(I) complex $[Cu^{I}_{2}(UN\text{-}O^{-})]^{+}$ was found to react with nitric oxide gas at low temperature, Figure 33a. A solution of $[Cu^{I}_{2}(UN\text{-}O^{-})]^{+}$ in DCM solvent was prepared and kept at -80 °C. Addition of excess nitric oxide gas using a gas-tight syringe resulted in a change in the UV-Vis spectrum, Figure 33b. An EPR spectrum of the frozen DCM solution showing a g ~ 2.0 signal, Figure 33c, which is indicative that the product at -80 °C is a mononitrosyl complex $[Cu^{I}_{2}(UN\text{-}O^{-})(NO)]^{+}$. In a separate experiment, the dicopper(I) complex $[Cu^{I}_{2}(UN\text{-}O^{-})]^{+}$ was dissolved in DCM/MeTHF 50:50 solvent mixture and cooled down to -120 °C, Figure 34a. Addition of excess nitric oxide gas using a gas-tight syringe resulting a change in the UV-Vis spectrum change, as shown by the dark green colored line, Figure 34b. Over the course of 20 minutes, the spectral changes (light green colored spectra) and finally transformed to a species having the purple colored spectrum, Figure 34b, which was assigned as $[Cu^{I}_{2}(UN\text{-}O^{-})(NO)_{2}]^{+}$ based on the finding that this species formed is EPR silent.

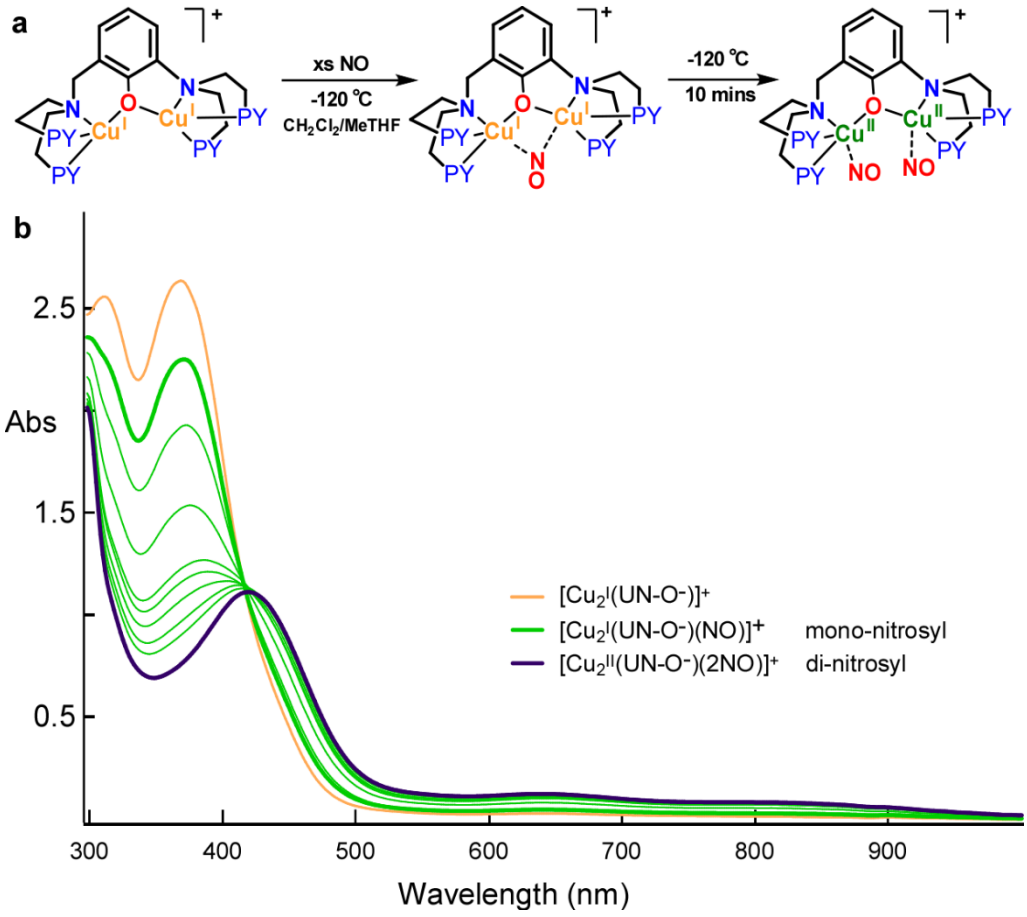

Figure 34. Formation of the nitrosyl complexes at -120 °C.

(a) Addition of excess nitric oxide gas to the solution of $[Cu^{I}_{2}(UN\text{-}O^{-})]^{+}$ at -120 °C in a 50:50 DCM/MeTHF solvent mixture to initially form the mononitrosyl complex $[Cu^{I}_{2}(UN\text{-}O^{-})(NO)]^{+}$. Over the course of ten minutes, $[Cu^{I}_{2}(UN\text{-}O^{-})(NO)]^{+}$ transformed into the dinitrosyl complex $[Cu^{I}_{2}(UN\text{-}O^{-})(NO)_{2}]^{+}$. (b) The starting complex $[Cu^{I}_{2}(UN\text{-}O^{-})]^{+}$ possesses the orange colored spectrum. Upon addition of excess nitric oxide gas, the spectrum was recorded as the dark thick green colored line. Over the course of the next 20 minutes, the spectral change occurring are shown in the in light green colored spectra with decreasing intensity in the ~350 nm region until there is a

transformation to a species with purple colored spectrum, assigned as $[Cu^{I}_2(UN\text{-}O^{-})(NO)_2]^{+}$ based on its EPR silence.

The UV-Vis spectra of $[Cu^{I}_2(UN\text{-}O^{-})(NO)_2]^{+}$, λ_{max}: 420 nm (4550), 640nm (450), 810nm (330), were followed at -120 °C in the course of 6 hours, Figure 35b. The resulting spectrum was assigned as a N bound hyponitrite complex based on 1) Its distinctively shifted UV-Vis absorption features λ_{max}: 380nm (sh), 570nm (sh) from the dinitrosyl complex $[Cu^{I}_2(UN\text{-}O^{-})(NO)_2]^{+}$. 2) It is reasonable to assume that the nitrogen atom in the nitrosyl moiety bound to the copper from the start and switching from nitrogen atom bound to copper to oxygen atom bound to copper would incur significant reorganization energy (Figure 36a) therefore, the N-bound hyponitrite product is the kinetically favored product and the corresponding warmup complex, would be a thermodynamically favored O-bound hyponitrite complex, Figure 36b, λ_{max}: 365nm (9600), 671nm (170).

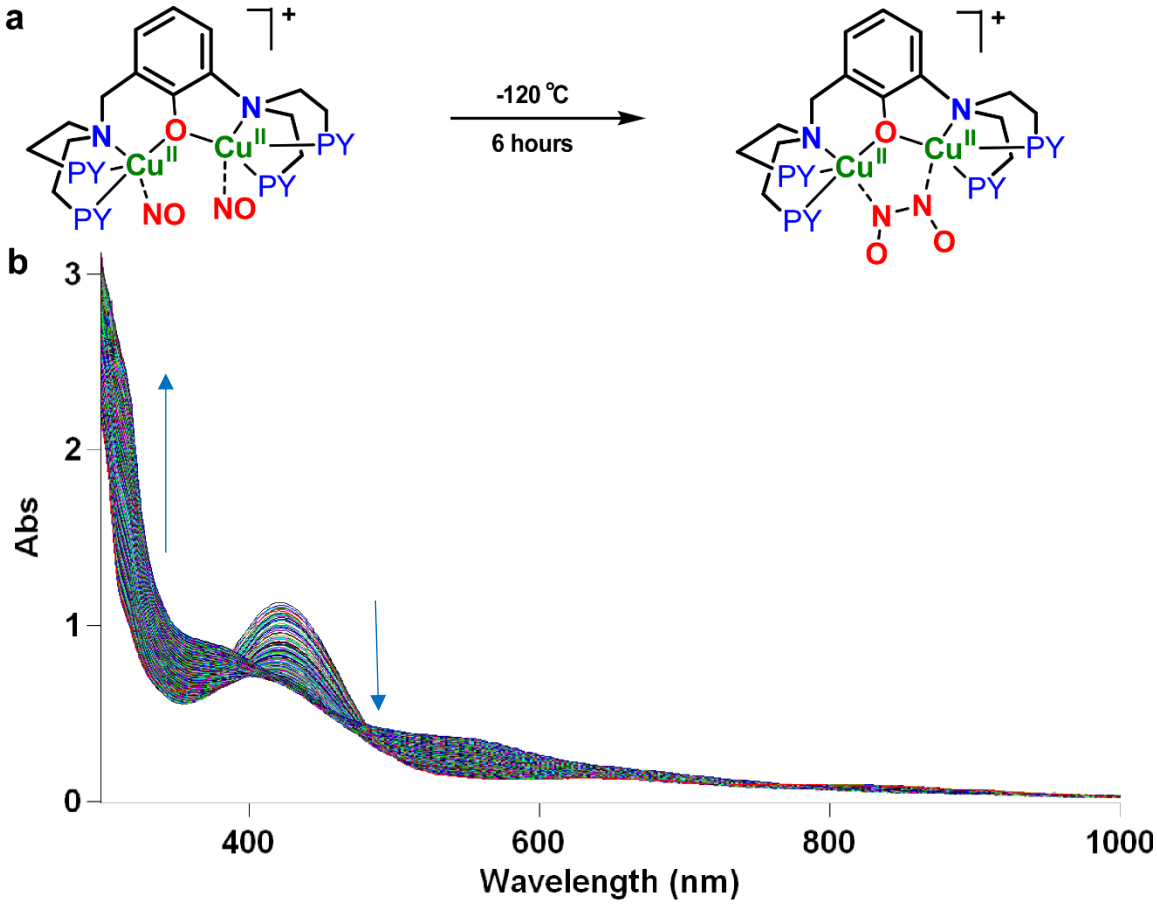

Figure 35. Formation of N-bound hyponitrite complex at -120 °C.

(a) The dinitrosyl complex $[Cu^{I}_2(UN\text{-}O^{-})(NO)_2]^{+}$ (λ_{max}: 420nm (4550), 640nm (450), 810nm (330)) converts to a N-bound hyponitrite complex at -120 °C in the course of 6 hours. (b) UV-Vis spectra change from the dinitrosyl complex $[Cu^{I}_2(UN\text{-}O^{-})(NO)_2]^{+}$ to the hyponitrite complex $[Cu^{II}_2(UN\text{-}O^{-})(N_2O_2^{2-})]^{+}$.

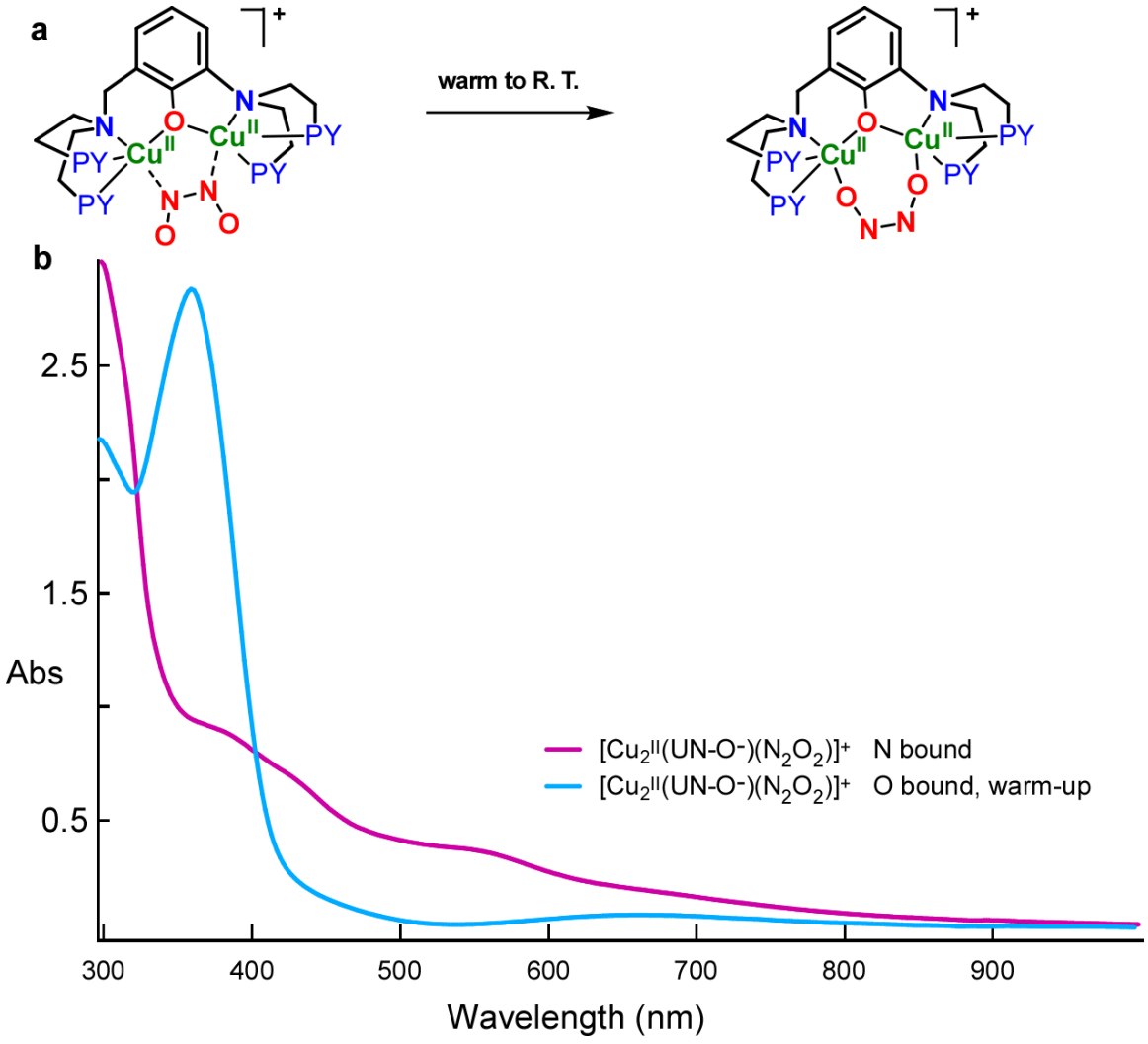

Figure 36. Warm up of the hyponitrite complex and switch from N bound to O bound.

(a) The N-bound hyponitrite complex $[Cu^{II}_2(UN\text{-}O^{-})(N_2O_2^{2-})]^{+}$ when warmed up turned to the O-bound hyponitrite complex. (b) UV-Vis spectrum of the putative N-bound hyponitrite complex $[Cu^{II}_2(UN\text{-}O^{-})(N_2O_2^{2-})]^{+}$ in magenta colored spectrum at -120 °C. Upon warming, spectral changes occur, turning the blue-colored line which corresponds to the O-bound hyponitrite complex $[Cu^{II}_2(UN\text{-}O^{-})(N_2O_2^{2-})]^{+}$.

Characterization of the hyponitrite complex

The hyponitrite complex $[Cu^{II}_2(UN\text{-}O^{-})(N_2O_2^{2-})]^{+}$ was prepared by reacting one equiv of hyponitrous acid ($H_2N_2O_2$) with the dicopper(II) oxide complex $[Cu^{II}_2(UN\text{-}O^{-})(O^{2-})]^{+}$ in DCM solvent, Figure 37a. This solution was subsequently injected into the ESI-MS spectrometer leading to the mass-spectrum shown in Figure 37b (right part). The isotope patterns agree well with theoretically predicted value with m/z = 745.16. Application of a vacuum to the hyponitrite solution $[Cu^{II}_2(UN\text{-}O^{-})(N_2O_2^{2-})]^{+}$ over a warm water bath resulted in regeneration of the oxide complex $[Cu^{II}_2(UN\text{-}O^{-})(O^{2-})]^{+}$ and this was confirmed using ESI-MS. The spectrum in Figure 37b, left part corresponds to the complex $[Cu^{II}_2(UN\text{-}O^{-})(O^{2-})]^{+}$ with isotope patterns matching the theoretical prediction, m/z = 699.16.

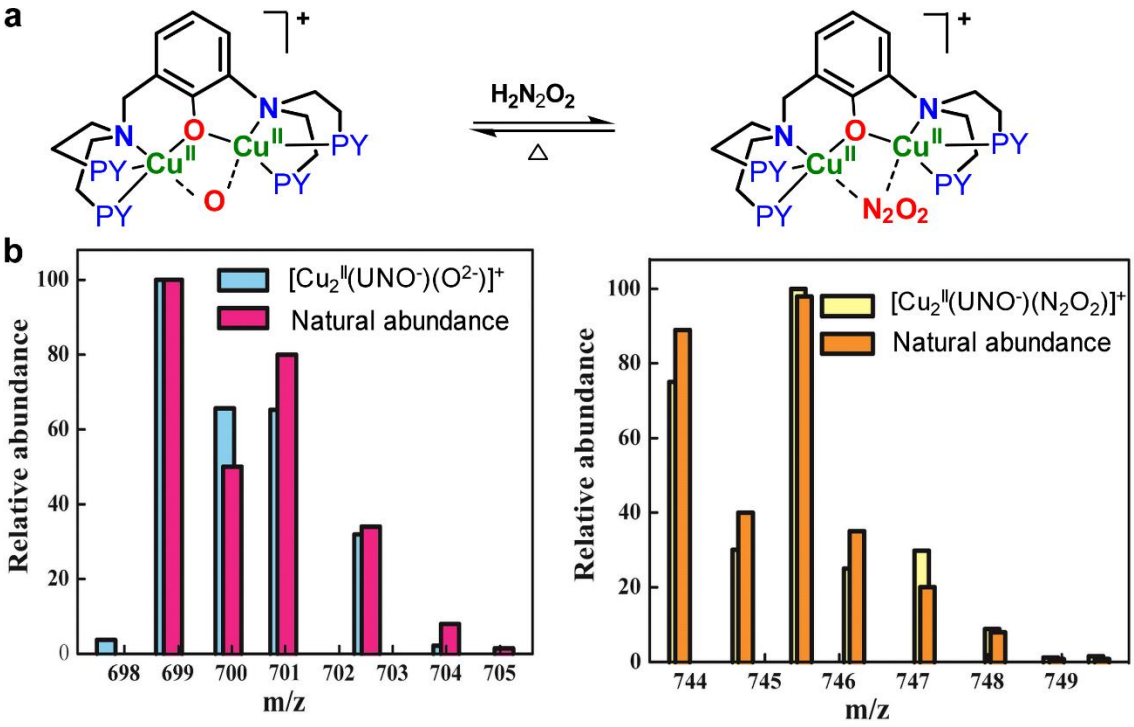

Figure 37. Formation of the hyponitrite complex using hyponitrous acid.

(a) Addition of one equiv of $H_2N_2O_2$ to the $[Cu^{II}_2(UN\text{-}O^-)(O^{2-})]^+$ in DCM form the hyponitrite complex $[Cu^{II}_2(UN\text{-}O^-)(N_2O_2^{2-})]^+$. The oxide complex $[Cu^{II}_2(UN\text{-}O^-)(O^{2-})]^+$ was regenerated over warm water bath under vacuum. (b) ESI-MS of $[Cu^{II}_2(UN\text{-}O^-)(O^{2-})]^+$ m/z = 699.16 (left part) and $[Cu^{II}_2(UN\text{-}O^-)(N_2O_2^{2-})]^+$, m/z = 745.16 (right part).

CONCLUSIONS

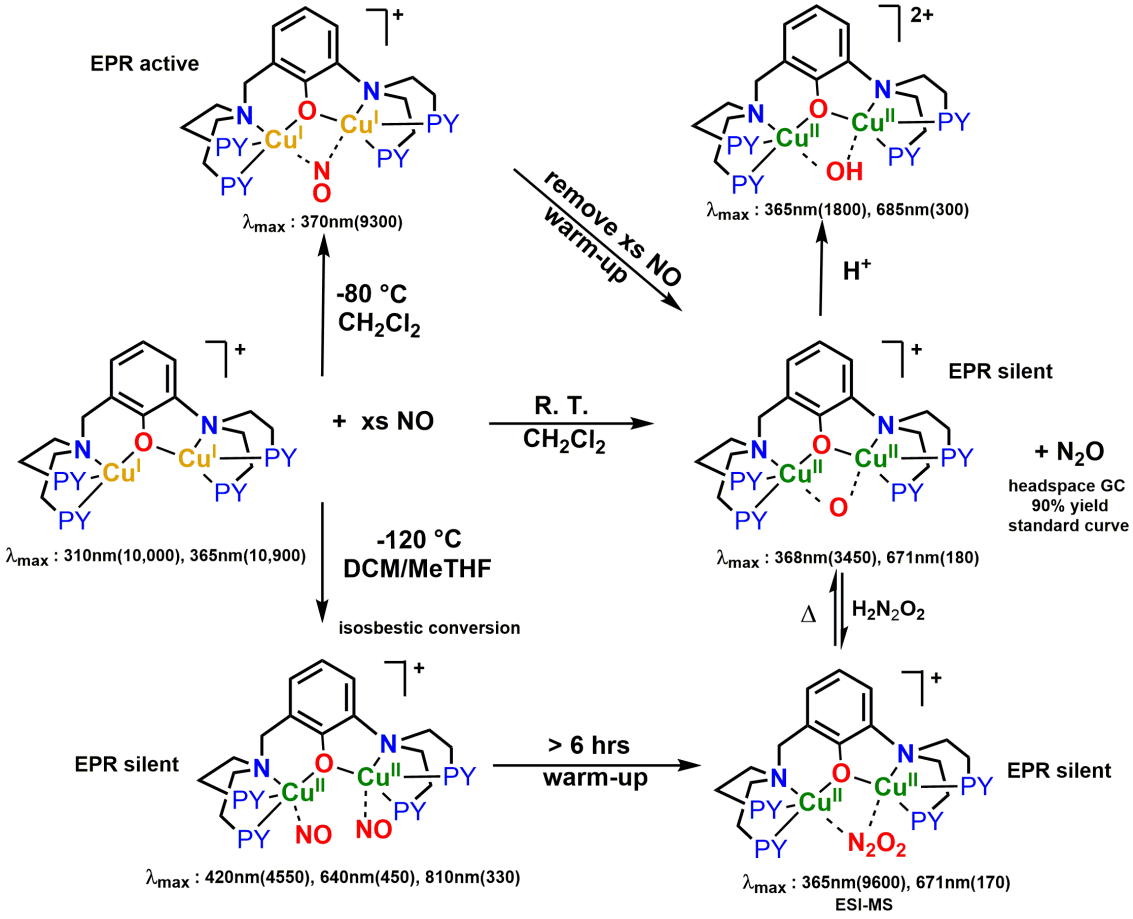

Scheme 4. Summary of the multiple steps involved in the $[Cu^{I}_{2}(UN\text{-}O^{-})]^{+}$ reaction with nitric oxide gas in DCM solvent at room temperature, -80 °C and -120 °C.

The dicopper(I) complex $[Cu^{I}_{2}(UN\text{-}O^{-})]^{+}$, reacts with excess nitric oxide in DCM at room temperature to form the oxide complex $[Cu^{II}_{2}(UN\text{-}O^{-})(O^{2-})]^{+}$, Scheme 4. The oxide complex $[Cu^{II}_{2}(UN\text{-}O^{-})(O^{2-})]^{+}$ was characterized using Nujol IR and ESI-MS. Upon protonation of the oxide complex $[Cu^{II}_{2}(UN\text{-}O^{-})(O^{2-})]^{+}$, a hydroxide bridged dicopper(II) complex $[Cu^{II}_{2}(UN\text{-}O^{-})(OH)]^{2+}$ was generated and characterized using Nujol

IR and ESI-MS. This oxide complex can also be react with one equiv of $H_2N_2O_2$ to form the corresponding hyponitrite complex $[Cu^{II}_2(UN\text{-}O^{-})(N_2O_2^{2-})]^{+}$ that was characterized using ESI-MS and UV-Vis spectroscopy, Scheme 4. The hyponitrite complex $[Cu^{II}_2(UN\text{-}O^{-})(N_2O_2^{2-})]^{+}$ can regenerate the oxide complex $[Cu^{II}_2(UN\text{-}O^{-})(O^{2-})]^{+}$ simply by heating and applying a vacuum, Scheme 4. The reaction of dicopper(I) complex $[Cu^{I}_2(UN\text{-}O^{-})]^{+}$, reacts with excess nitric oxide in DCM was also carried out at -80 °C. The resulting complex is EPR active with g ~2 and formulated to be $[Cu^{I}_2(UN\text{-}O^{-})(NO)]^{+}$, by warming up the complex $[Cu^{I}_2(UN\text{-}O^{-})(NO)]^{+}$ and removing excess nitric oxide gas, the same oxide complex was $[Cu^{II}_2(UN\text{-}O^{-})(O^{2-})]^{+}$ produced, Scheme 4. The dicopper(I) complex $[Cu^{I}_2(UN\text{-}O^{-})]^{+}$ also reacts with excess nitric oxide at -120 °C to first form the mononitrosyl complex $[Cu^{I}_2(UN\text{-}O^{-})(NO)]^{+}$ and this mononitrosyl complex transformed into dinitrosyl complex $[Cu^{I}_2(UN\text{-}O^{-})(NO)_2]^{+}$ which is EPR silent, Scheme 4. This dinitrosyl complex $[Cu^{I}_2(UN\text{-}O^{-})(NO)_2]^{+}$ undergoes slow transformation at -120 °C to form a N-bound hyponitrite complex, the N-bound hyponitrite complex upon warming up become an O-bound hyponitrite complex, Scheme 4.

REFERENCES

(1) (a) Babcock, G. T.; Wikstrom, M. *Nature* **1992**, *356*, 301; (b) Yoshikawa, S.; Shimada, A. *Chem. Rev.* **2015**, *115*, 1936.
(2) Field, C. B.; Behrenfeld, M. J.; Randerson, J. T.; Falkowski, P. *Science* **1998**, *281*, 237.
(3) Zhang, M.; de Respinis, M.; Frei, H. *Nat. Chem.* **2014**, *6*, 362.
(4) Koppenol, W. H.; Stanbury, D. M.; Bounds, P. L. *Free. Radic. Biol. Med.* **2010**, *49*, 317.
(5) (a) Meunier, B.; de Visser, S. P.; Shaik, S. *Chem. Rev.* **2004**, *104*, 3947; (b) Shaik, S.; Cohen, S.; Wang, Y.; Chen, H.; Kumar, D.; Thiel, W. *Chem. Rev.* **2010**, *110*, 949.
(6) (a) Mirica, L. M.; Ottenwaelder, X.; Stack, T. D. P. *Chem. Rev.* **2004**, *104*, 1013; (b) Itoh, S. *Curr. Opin. Chem. Biol.* **2006**, *10*, 115; (c) Hatcher, L. Q.; Karlin, K. D. *J. Biol. Inorg. Chem.* **2004**, *9*, 669; (d) Gagnon, N.; Tolman, W. B. *Acc. Chem. Res.* **2015**, *48*, 2126.
(7) Lee, J. Y.; Karlin, K. D. *Curr. Opin. Chem. Biol.* **2015**, *25*, 184.
(8) Mahroof-Tahir, M.; Karlin, K. D. *J. Am. Chem. Soc.* **1992**, *114*, 7599.
(9) Mahroof-Tahir, M.; Murthy, N. N.; Karlin, K. D.; Blackburn, N. J.; Shaikh, S. N.; Zubieta, J. *Inorg Chem* **1992**, *31*, 3001.
(10) Thorp, H. H. *Inorg Chem* **1992**, *31*, 1585.
(11) Addison, A. W.; Rao, T. N.; Reedijk, J.; van Rijn, J.; Verschoor, G. C. *J. Chem. Soc., Dalton. Trans.* **1984**, 1349.
(12) Robin, M. B.; Day, P. *Adv. Inorg. Chem. Radiochem.* **1968**, *10*, 247
(13) Cruse, R. W.; Kaderli, S.; Karlin, K. D.; Zuberbühler, A. D. *J. Am. Chem. Soc.* **1988**, *110*, 6882.
(14) Fry, H. C.; Scaltrito, D. V.; Karlin, K. D.; Meyer, G. J. *J. Am Chem. Soc.* **2003**, *125*, 11866.
(15) Saracini, C.; Liakos, D. G.; Zapata Rivera, J. E.; Neese, F.; Meyer, G. J.; Karlin, K. D. *J. Am. Chem. Soc.* **2014**, *136*, 1260.
(16) Weitzer, M.; Schindler, S.; Brehm, G.; Schneider, S.; Hoermann, E.; Jung, B.; Kaderli, S.; Zuberbuehler, A. D. *Inorg Chem* **2003**, *42*, 1800.
(17) Kobayashi, Y.; Ohkubo, K.; Nomura, T.; Kubo, M.; Fujieda, N.; Sugimoto, H.; Fukuzumi, S.; Goto, K.; Ogura, T.; Itoh, S. *Eur J Inorg Chem* **2012**, *2012*, 4574.
(18) Kunishita, A.; Ertem, M. Z.; Okubo, Y.; Tano, T.; Sugimoto, H.; Ohkubo, K.; Fujieda, N.; Fukuzumi, S.; Cramer, C. J.; Itoh, S. *Inorg Chem* **2012**, *51*, 9465.
(19) Aboelella, N. W.; Kryatov, S. V.; Gherman, B. F.; Brennessel, W. W.; Young, V. G.; Sarangi, R.; Rybak-Akimova, E. V.; Hodgson, K. O.; Hedman, B.; Solomon, E. I.; Cramer, C. J.; Tolman, W. B. *J. Am. Chem. Soc.* **2004**, *126*, 16896.
(20) Maiti, D.; Fry, H. C.; Woertink, J. S.; Vance, M. A.; Solomon, E. I.; Karlin, K. D. *J. Am. Chem. Soc.* **2007**, *129*, 264.

(21) Noviandri, I.; Brown, K. N.; Fleming, D. S.; Gulyas, P. T.; Lay, P. A.; Masters, A. F.; Phillips, L. *J. Phys. Chem. B* **1999**, *103*, 6713.
(22) (a) Vad, M. S.; Nielsen, A.; Lennartson, A.; Bond, A. D.; McGrady, J. E.; McKenzie, C. J. *Dalton. Trans.* **2011**, *40*, 10698; (b) Vad, M. S.; Johansson, F. B.; Seidler-Egdal, R. K.; McGrady, J. E.; Novikov, S. M.; Bozhevolnyi, S. I.; Bond, A. D.; McKenzie, C. J. *Dalton. Trans.* **2013**, *42*, 9921.
(23) (a) Barriere, F.; Camire, N.; Geiger, W. E.; Mueller-Westerhoff, U. T.; Sanders, R. *J. Am. Chem. Soc.* **2002**, *124*, 7262; (b) Barriere, F.; Geiger, W. E. *J. Am. Chem. Soc.* **2006**, *128*, 3980; (c) Srivastava, K.; Srivastava, A. K.; Porwal, D.; Prasad, J. *J. Indian Chem. Soc.* **2007**, *84*, 1195; (d) Sasaki, K.; Kashimura, T.; Ohura, M.; Ohsaki, Y.; Ohta, N. *J. Electrochem. Soc.* **1990**, *137*, 2437; (e) Guirado, G.; Fleming, C. N.; Lingenfelter, T. G.; Williams, M. L.; Zuilhof, H.; Dinnocenzo, J. P. *J. Am. Chem. Soc.* **2004**, *126*, 14086; (f) Svith, H.; Jensen, H.; Almstedt, J.; Andersson, P.; Lundback, T.; Daasbjerg, K.; Jonsson, M. *J. Phys. Chem. A* **2004**, *108*, 4805; (g) Konezny, S. J.; Doherty, M. D.; Luca, O. R.; Crabtree, R. H.; Soloveichik, G. L.; Batista, V. S. *J. Phys. Chem. C* **2012**, *116*, 6349; (h) Araujo, C. M.; Doherty, M. D.; Konezny, S. J.; Luca, O. R.; Usyatinsky, A.; Grade, H.; Lobkovsky, E.; Soloveichik, G. L.; Crabtree, R. H.; Batista, V. S. *Dalton. Trans.* **2012**, *41*, 3562.
(24) (a) Mclendon, G.; Mooney, W. F. *Inorg Chem* **1980**, *19*, 12; (b) Richens, D. T.; Sykes, A. G. *Dalton. Trans.* **1982**, 1621.
(25) Henthorn, J. T.; Agapie, T. *Angew. Chem. Int. Ed.* **2014**, *53*, 12893.
(26) O'Reilly, N. J.; Magner, E. *Langmuir* **2005**, *21*, 1009.
(27) Warren, J. J.; Mayer, J. M. *J. Am. Chem. Soc.* **2008**, *130*, 7546.
(28) Mase, K.; Ohkubo, K.; Xue, Z. L.; Yamada, H.; Fukuzumi, S. *Chem. Sci.* **2015**, *6*, 6496.
(29) Peterson, R. L.; Ginsbach, J. W.; Cowley, R. E.; Qayyum, M. F.; Himes, R. A.; Siegler, M. A.; Moore, C. D.; Hedman, B.; Hodgson, K. O.; Fukuzumi, S.; Solomon, E. I.; Karlin, K. D. *J. Am. Chem. Soc.* **2013**, *135*, 16454.
(30) Lopez, N.; Graham, D. J.; McGuire, R., Jr.; Alliger, G. E.; Shao-Horn, Y.; Cummins, C. C.; Nocera, D. G. *Science* **2012**, *335*, 450.
(31) Chikushi, N.; Nishikami, Y.; Nishide, H. *Chem. Lett.* **2014**, *43*, 760.
(32) Koppenol, W. H. *J. Am. Chem. Soc.* **2007**, *129*, 9686.
(33) Root, D. E.; Mahroof-Tahir, M.; Karlin, K. D.; Solomon, E. I. *Inorg Chem* **1998**, *37*, 4838.
(34) (a) Marcus, R. A. *Annl. Rev. Phys. Chem.* **1964**, *15*, 155; (b) Marcus, R. A. *Angew. Chem., Int. Ed.* **1993**, *32*, 1111.
(35) Nielson, R. M.; Mcmanis, G. E.; Safford, L. K.; Weaver, M. J. *J Phys Chem-Us* **1989**, *93*, 2152.
(36) Marcus, R. A.; Sutin, N. *Biochim. Biophys. Acta* **1985**, *811*, 265.
(37) Endicott, J. F.; Kumar, K. *ACS Symp. Ser.* **1982**, *198*, 425.
(38) (a) Ghosh, S. P.; Ghosh, M. C.; Gould, E. S. *Int. J. Chem. Kinet.* **1994**, *26*, 665; (b) Ghosh, S. P.; Gelerinter, E.; Pyrka, G.; Gould, E. S. *Inorg Chem* **1993**, *32*, 4780.
(39) Anderson, B. L.; Maher, A. G.; Nava, M.; Lopez, N.; Cummins, C. C.; Nocera, D. G. *J. Phys. Chem. B* **2015**, *119*, 7422.

(40) Tahsini, L.; Kotani, H.; Lee, Y.-M.; Cho, J.; Nam, W.; Karlin, K. D.; Fukuzumi, S. *Chem. Eur. J.* **2012**, *18*, 1084.
(41) (a) Karlin, K. D.; Haka, M. S.; Cruse, R. W.; Meyer, G. J.; Farooq, A.; Gultneh, Y.; Hayes, J. C.; Zubieta, J. *J. Am. Chem. Soc.* **1988**, *110*, 1196; (b) Thyagarajan, S.; Murthy, N. N.; Narducci Sarjeant, A. A.; Karlin, K. D.; Rokita, S. E. *J. Am. Chem. Soc.* **2006**, *128*, 7003.
(42) (a) Karlin, K. D.; Gultneh, Y.; Hayes, J. C.; Cruse, R. W.; McKown, J. W.; Hutchinson, J. P.; Zubieta, J. *J. Am. Chem. Soc.* **1984**, *106*, 2121; (b) Karlin, K. D.; Tyeklár, Z.; Farooq, A.; Haka, M. S.; Ghosh, P.; Cruse, R. W.; Gultneh, Y.; Hayes, J. C.; Toscano, P. J.; Zubieta, J. *Inorg Chem* **1992**, *31*, 1436.
(43) (a) Fukuzumi, S.; Kotani, H.; Lucas, H. R.; Doi, K.; Suenobu, T.; Peterson, R. L.; Karlin, K. D. *J. Am. Chem. Soc.* **2010**, *132*, 6874; (b) Fukuzumi, S.; Karlin, K. D. *Coord. Chem. Rev.* **2013**, *257*, 187.
(44) (a) Lee, Y.-M.; Kotani, H.; Suenobu, T.; Nam, W.; Fukuzumi, S. *J. Am. Chem. Soc.* **2008**, *130*, 434; (b) Fukuzumi, S. *Coord. Chem. Rev.* **2013**, *257*, 1564.
(45) Skov, L. K.; Pascher, T.; Winkler, J. R.; Gray, H. B. *J. Am. Chem. Soc.* **1998**, *120*, 1102.
(46) Fukuzumi, S.; Kotani, H.; Prokop, K. A.; Goldberg, D. P. *J. Am. Chem. Soc.* **2011**, *133*, 1859.
(47) Lind, J.; Shen, X.; Merenyi, G.; Jonsson, B. O. *J. Am. Chem. Soc.* **1989**, *111*, 7654.
(48) Roth, J. P.; Klinman, J. P. *Proc. Natl. Acad. Sci.* **2003**, *100*, 62.
(49) (a) Heller, A. *Acc. Chem. Res.* **1990**, *23*, 128; (b) Gray, H. B.; Winkler, J. R. *Annu. Rev. Biochem.* **1996**, *65*, 537; (c) Warshel, A.; Sharma, P. K.; Kato, M.; Xiang, Y.; Liu, H.; Olsson, M. H. *Chem. Rev.* **2006**, *106*, 3210.
(50) Solomon, E. I.; Szilagyi, R. K.; George, S. D.; Basumallick, L. *Chem. Rev.* **2004**, *104*, 419.
(51) Solomon, E. I.; Heppner, D. E.; Johnston, E. M.; Ginsbach, J. W.; Cirera, J.; Qayyum, M.; Kieber-Emmons, M. T.; Kjaergaard, C. H.; Hadt, R. G.; Tian, L. *Chem. Rev.* **2014**, *114*, 3659.
(52) Citek, C.; Lin, B. L.; Phelps, T. E.; Wasinger, E. C.; Stack, T. D. *J. Am. Chem. Soc.* **2014**, *136*, 14405.
(53) Vendelboe, T. V.; Harris, P.; Zhao, Y.; Walter, T. S.; Harlos, K.; El Omari, K.; Christensen, H. E. *Sci. Adv.* **2016**, *2*, e1500980.
(54) Ray, K.; Pfaff, F. F.; Wang, B.; Nam, W. *J. Am. Chem. Soc.* **2014**, *136*, 13942.
(55) (a) Campbell, A.; Smith, M. A.; Sayre, L. M.; Bondy, S. C.; Perry, G. *Brain Res Bull* **2001**, *55*, 125; (b) Perry, G.; Sayre Lawrence, M.; Atwood Craig, S.; Castellani Rudolph, J.; Cash Adam, D.; Rottkamp Catherine, A.; Smith Mark, A. *CNS Drugs.* **2002**, *16*, 339; (c) Gaggelli, E.; Kozlowski, H.; Valensin, D.; Valensin, G. *Chem. Rev.* **2006**, *106*, 1995.
(56) (a) Beckman, J. S.; Beckman, T. W.; Chen, J.; Marshall, P. A.; Freeman, B. A. *Proc. Natl. Acad. Sci.* **1990**, *87*, 1620; (b) Beckman, J. S. *Chem. Res. Toxicol.* **1996**, *9*, 836; (c) Beckman, J. S.; Koppenol, W. H. *Amer. J. Physiol.* **1996**, *271*, C1424; (d) MacMillan-Crow, L. A.; Crow, J. P.; Thompson, J. A. *Biochemistry* **1998**, *37*, 1613; (e) Radi, R. *Proc. Natl. Acad. Sci.* **2004**, *101*, 4003; (f) Quint, P.; Reutzel, R.; Mikulski, R.; McKenna, R.; Silverman, D. N. *Free. Radic. Biol. Med.* **2006**, *40*, 453; (g) Pacher, P.; Beckman, J. S.;

Liaudet, L. *Physiol. Rev.* **2007**, *87*, 315; (h) Reynolds, M. R.; Berry, R. W.; Binder, L. I. *Biochemistry* **2007**, *46*, 7325; (i) Surmeli, N. B.; Litterman, N. K.; Miller, A. F.; Groves, J. T. *J. Am. Chem. Soc.* **2010**, *132*, 17174; (j) Jones, L. H. *Chem. Biol.* **2012**, *19*, 1086; (k) Radi, R. *Acc. Chem. Res.* **2013**, *46*, 550; (l) Yu, F.; Li, M.; Xu, C.; Wang, Z.; Zhou, H.; Yang, M.; Chen, Y.; Tang, L.; He, J. *Plos One* **2013**, *8*, e81526.
(57) (a) Blough, N. V.; Zafiriou, O. C. *Inorg Chem* **1985**, *24*, 3502; (b) Nauser, T.; Koppenol, W. H. *J. Phys. Chem. A* **2002**, *106*, 4084; (c) Goldstein, S.; Lind, J.; Merenyi, G. *Chem. Rev.* **2005**, *105*, 2457.
(58) (a) Palmer, R. M.; Ferrige, A. G.; Moncada, S. *Nature* **1987**, *327*, 524; (b) Moncada, S.; Palmer, R. M.; Higgs, E. A. *Pharmacol. Rev.* **1991**, *43*, 109; (c) Nathan, C. *FASEB. J.* **1992**, *6*, 3051; (d) Garthwaite, J.; Boulton, C. L. *Annu. Rev. Physiol.* **1995**, *57*, 683; (e) Bogdan, C. *Nat. Immunol.* **2001**, *2*, 907.
(59) (a) Mattson, M. P.; Goodman, Y.; Luo, H.; Fu, W.; Furukawa, K. *J. Neurosci. Res.* **1997**, *49*, 681; (b) Keller, J. N.; Kindy, M. S.; Holtsberg, F. W.; St Clair, D. K.; Yen, H. C.; Germeyer, A.; Steiner, S. M.; Bruce-Keller, A. J.; Hutchins, J. B.; Mattson, M. P. *J. Neurosci.* **1998**, *18*, 687.
(60) (a) Ischiropoulos, H.; Beckman, J. S. *J. Clin. Invest.* **2003**, *111*, 163; (b) Valko, M.; Morris, H.; Cronin, M. T. *Curr. Med. Chem.* **2005**, *12*, 1161; (c) Zhu, X.; Su, B.; Wang, X.; Smith, M. A.; Perry, G. *Cell. Mol. Life. Sci.* **2007**, *64*, 2202; (d) Uttara, B.; Singh, A. V.; Zamboni, P.; Mahajan, R. T. *Curr. Neuropharmacol.* **2009**, *7*, 65; (e) Kozlowski, H.; Janicka-Klos, A.; Brasun, J.; Gaggelli, E.; Valensin, D.; Valensin, G. *Coord. Chem. Rev.* **2009**, *253*, 2665; (f) Savelieff, M. G.; Lee, S.; Liu, Y.; Lim, M. H. *ACS Chem. Biol.* **2013**, *8*, 856.
(61) (a) Scheuner, D.; Eckman, C.; Jensen, M.; Song, X.; Citron, M.; Suzuki, N.; Bird, T. D.; Hardy, J.; Hutton, M.; Kukull, W.; Larson, E.; Levy-Lahad, E.; Viitanen, M.; Peskind, E.; Poorkaj, P.; Schellenberg, G.; Tanzi, R.; Wasco, W.; Lannfelt, L.; Selkoe, D.; Younkin, S. *Nat. Med.* **1996**, *2*, 864; (b) Multhaup, G.; Schlicksupp, A.; Hesse, L.; Beher, D.; Ruppert, T.; Masters, C. L.; Beyreuther, K. *Science* **1996**, *271*, 1406; (c) Atwood, C. S.; Scarpa, R. C.; Huang, X.; Moir, R. D.; Jones, W. D.; Fairlie, D. P.; Tanzi, R. E.; Bush, A. I. *J. Neurochem.* **2000**, *75*, 1219.
(62) (a) Smith, M. A.; Richey Harris, P. L.; Sayre, L. M.; Beckman, J. S.; Perry, G. *J. Neurosci.* **1997**, *17*, 2653; (b) Castegna, A.; Thongboonkerd, V.; Klein, J. B.; Lynn, B.; Markesbery, W. R.; Butterfield, D. A. *J. Neurochem.* **2003**, *85*, 1394; (c) Kummer, M. P.; Hermes, M.; Delekarte, A.; Hammerschmidt, T.; Kumar, S.; Terwel, D.; Walter, J.; Pape, H. C.; Konig, S.; Roeber, S.; Jessen, F.; Klockgether, T.; Korte, M.; Heneka, M. T. *Neuron* **2011**, *71*, 833.
(63) (a) Shearer, J.; Szalai, V. A. *J. Am. Chem. Soc.* **2008**, *130*, 17826; (b) Shin, B. K.; Saxena, S. *Biochemistry* **2008**, *47*, 9117; (c) Faller, P.; Hureau, C. *Chem. Eur. J.* **2012**, *18*, 15910.
(64) In the amyloid beta (Aβ) peptides, the position 10 is a tyrosine residue that is subjected to nitration to form 3-nitrotyrosine.
(65) Giacovazzi, R.; Ciofini, I.; Rao, L.; Amatore, C.; Adamo, C. *Phys Chem Chem Phys* **2014**, *16*, 10169.

(66) (a) Maiti, D.; Lee, D.-H.; Narducci Sarjeant, A. A.; Pau, M. Y. M.; Solomon, E. I.; Gaoutchenova, K.; Sundermeyer, J.; Karlin, K. D. *J. Am. Chem. Soc.* **2008**, *130*, 6700; (b) Park, G. Y.; Deepalatha, S.; Puiu, S. C.; Lee, D.-H.; Mondal, B.; Narducci Sarjeant, A. A.; del Rio, D.; Pau, M. Y. M.; Solomon, E. I.; Karlin, K. D. *J. Biol. Inorg. Chem.* **2009**, *14*, 1301; (c) There are cases in the literature for copper ion, where hydrogen peroxide in some form, reacts with $NO_{(g)}$ to give peroxynitrite chemistry. Mondal and coworkers reported the nitrosyl adduct of a Cu(II) ligand complex reacts with externally added H_2O_2 to form a reduced metal ion Cu^{I}-PN complex; Karlin and coworkers found that a $LCu^{II}(OOH)$ complex reacts with $NO_{(g)}$ to form a LCu^{I}-PN species. ; (d) Kalita, A.; Kumar, P.; Mondal, B. *Chem. Commun.* **2012**, *48*, 4636; (e) Kim, S.; Siegler, M. A.; Karlin, K. D. *Chem. Commun.* **2014**, *50*, 2844; (f) Qiao, L.; Lu, Y.; Liu, B.; Girault, H. H. *J. Am. Chem. Soc.* **2011**, *133*, 19823.
(67) Wick, P. K.; Kissner, R.; Koppenol, W. H. *Helv. Chim. Acta* **2000**, *83*, 748.
(68) Kurtikyan, T. S.; Eksuzyan, S. R.; Hayrapetyan, V. A.; Martirosyan, G. G.; Hovhannisyan, G. S.; Goodwin, J. A. *J. Am. Chem. Soc.* **2012**, *134*, 13861.
(69) (a) Schopfer, M. P.; Mondal, B.; Lee, D.-H.; Sarjeant, A. A. N.; Karlin, K. D. *J. Am. Chem. Soc.* **2009**, *131*, 11304; (b) Kurtikyan, T. S.; Ford, P. C. *Chem. Commun.* **2010**, *46*, 8570; (c) Kurtikyan and Ford showed for a heme complex this isomerization occurs extremely rapidly even is a 100 K matrix. .
(70) Richeson, C. E.; Mulder, P.; Bowry, V. W.; Ingold, K. U. *J. Am. Chem. Soc.* **1998**, *120*, 7211.
(71) (a) Stern, M. K.; Jensen, M. P.; Kramer, K. *J. Am. Chem. Soc.* **1996**, *118*, 8735; (b) Lee, J. B.; Hunt, J. A.; Groves, J. T. *Bioorg. Med. Chem. Lett.* **1997**, *7*, 2913; (c) Haber, A.; Gross, Z. *Chem. Commun.* **2015**, *51*, 5812.
(72) (a) Misko, T. P.; Highkin, M. K.; Veenhuizen, A. W.; Manning, P. T.; Stern, M. K.; Currie, M. G.; Salvemini, D. *J. Biol. Chem.* **1998**, *273*, 15646; (b) Salvemini, D.; Jensen, M. P.; Riley, D. P.; Misko, T. P. *Drug. News. Perspect.* **1998**, *11*, 204; (c) Shimanovich, R.; Hannah, S.; Lynch, V.; Gerasimchuk, N.; Mody, T. D.; Magda, D.; Sessler, J.; Groves, J. T. *J. Am. Chem. Soc.* **2001**, *123*, 3613; (d) Szabo, C.; Ischiropoulos, H.; Radi, R. *Nat. Rev. Drug. Discov.* **2007**, *6*, 662; (e) Haber, A.; Aviram, M.; Gross, Z. *Chem. Sci.* **2011**, *2*, 295.
(73) (a) Ford, P. C.; Lorkovic, I. M. *Chem. Rev.* **2002**, *102*, 993; (b) Roncaroli, F.; Videla, M.; Slep, L. D.; Olabe, J. A. *Coord. Chem. Rev.* **2007**, *251*, 1903; (c) Kumar, P.; Lee, Y. M.; Hu, L.; Chen, J.; Park, Y. J.; Yao, J.; Chen, H.; Karlin, K. D.; Nam, W. *J. Am. Chem. Soc.* **2016**, *138*, 7753.
(74) Clarkson, S. G.; Basolo, F. *Inorg Chem* **1973**, *12*, 1528.
(75) (a) Pfeiffer, S.; Gorren, A. C. F.; Schmidt, K.; Werner, E.; Hansert, B.; Bohle, D. S.; Mayer, B. *J. Biol. Chem.* **1997**, *272*, 3465; (b) Kissner, R.; Koppenol, W. H. *J. Am Chem. Soc.* **2002**, *124*, 234; (c) Lymar, S. V.; Khairutdinov, R. F.; Hurst, J. K. *Inorg Chem* **2003**, *42*, 5259; (d) Koppenol, W. H.; Bounds, P. L.; Nauser, T.; Kissner, R.; Ruegger, H. *Dalton. Trans.* **2012**, *41*, 13779; (e) Molina, C.; Kissner, R.; Koppenol, W. H. *Dalton. Trans.* **2013**, *42*, 9898.

(76) (a) Hughes, M. N.; Nicklin, H. G. *J. Chem. Soc. A* **1970**, 925; (b) Hughes, M. N.; Nicklin, H. G.; Sackrule, W. A. C. *J. Chem. Soc. A* **1971**, 3722; (c) Babich, O. A.; Gould, E. S. *Res. Chem. Intermed* **2002**, *28*, 575.
(77) (a) Yokoyama, A.; Han, J. E.; Cho, J.; Kubo, M.; Ogura, T.; Siegler, M. A.; Karlin, K. D.; Nam, W. *J. Am. Chem. Soc.* **2012**, *134*, 15269; (b) Yokoyama, A.; Cho, K. B.; Karlin, K. D.; Nam, W. *J. Am. Chem. Soc.* **2013**, *135*, 14900.
(78) Yokoyama, A.; Han, J. E.; Karlin, K. D.; Nam, W. *Chem. Commun.* **2014**, *50*, 1742.
(79) Kumar, P.; Lee, Y. M.; Park, Y. J.; Siegler, M. A.; Karlin, K. D.; Nam, W. *J. Am. Chem. Soc.* **2015**, *137*, 4284.
(80) Cao, R.; Saracini, C.; Ginsbach, J. W.; Kieber-Emmons, M. T.; Siegler, M. A.; Solomon, E. I.; Fukuzumi, S.; Karlin, K. D. *J. Am. Chem. Soc.* **2016**, *138*, 7055.
(81) See Supporting Information.
(82) Paul, P. P.; Tyeklár, Z.; Farooq, A.; Karlin, K. D.; Liu, S.; Zubieta, J. *J. Am Chem. Soc.* **1990**, *112*, 2430.
(83) Fujisawa, K.; Tateda, A.; Miyashita, Y.; Okamoto, K.; Paulat, F.; Praneeth, V. K. K.; Merkle, A.; Lehnert, N. *J. Am. Chem. Soc.* **2008**, *130*, 1205.
(84) Ruggiero, C. E.; Carrier, S. M.; Antholine, W. E.; Whittaker, J. W.; Cramer, C. J.; Tolman, W. B. *J. Am. Chem. Soc.* **1993**, *115*, 11285.
(85) Kalita, A.; Deka, R. C.; Mondal, B. *Inorg Chem* **2013**, *52*, 10897.
(86) Wright, A. M.; Wu, G. A.; Hayton, T. W. *J. Am. Chem. Soc.* **2010**, *132*, 14336.
(87) (a) Silaghi-Dumitrescu, R. *J. Inorg. Biochem.* **2006**, *100*, 396; (b) Ghosh, S.; Dey, A.; Usov, O. M.; Sun, Y.; Grigoryants, V. M.; Scholes, C. P.; Solomon, E. I. *J. Am. Chem. Soc.* **2007**, *129*, 10310.
(88) Thyagarajan, S.; Incarvito, C. D.; Rheingold, A. L.; Theopold, K. H. *Inorg. Chim. Acta* **2003**, *345*, 333.
(89) Lo, W. J.; Lee, Y. P.; Tsai, J. H. M.; Tsai, H. H.; Hamilton, T. P.; Harrison, J. G.; Beckman, J. S. *J Chem Phys* **1995**, *103*, 4026.
(90) Tran, N. G.; Kalyvas, H.; Skodje, K. M.; Hayashi, T.; MoeÃànne-Loccoz, P.; Callan, P. E.; Shearer, J.; Kirschenbaum, L. J.; Kim, E. *J. Am. Chem. Soc.* **2011**, *133*, 1184.
(91) Paul, P. P.; Karlin, K. D. *J. Am. Chem. Soc.* **1991**, *113*, 6331.
(92) (a) Johnston, H. S.; Graham, R. *Can. J. Chem.* **1974**, *52*, 1415; (b) Harwood, M. H.; Jones, R. L. *J. Geophys. Res.* **1994**, *99*, 22955; (c) Riordan, E.; Minogue, N.; Healy, D.; O'Driscoll, P.; Sodeau, J. R. *J. Phys. Chem. A* **2005**, *109*, 779.
(93) (a) Laarhoven, L. J. J.; Mulder, P. *J. Phys. Chem. B* **1997**, *101*, 73; (b) Tinberg, C. E.; Lippard, S. J. *Biochemistry* **2010**, *49*, 7902; (c) Shenghur, A.; Weber, K. H.; Nguyen, N. D.; Sontising, W.; Tao, F. M. *J. Phys. Chem. A* **2014**, *118*, 11002.
(94) Nasir, M. S.; Karlin, K. D.; McGowty, D.; Zubieta, J. *J. Am. Chem. Soc.* **1991**, *113*, 698.
(95) (a) Barry, S. M.; Kers, J. A.; Johnson, E. G.; Song, L.; Aston, P. R.; Patel, B.; Krasnoff, S. B.; Crane, B. R.; Gibson, D. M.; Loria, R.; Challis, G. L. *Nat. Chem. Biol.* **2012**, *8*, 814; (b) Matthews, M. L.; Chang, W. C.; Layne, A. P.; Miles, L. A.; Krebs, C.; Bollinger, J. M., Jr. *Nat. Chem. Biol.* **2014**, *10*, 209; (c) Dodani, S. C.; Cahn, J. K.; Heinisch, T.; Brinkmann-Chen, S.; McIntosh, J. A.; Arnold, F. H. *Chembiochem* **2014**, *15*, 2259; (d) Attia, A. A.; Silaghi-Dumitrescu, R. *Int J Quantum Chem* **2014**, *114*, 652; (e)

Dodani, S. C.; Kiss, G.; Cahn, J. K.; Su, Y.; Pande, V. S.; Arnold, F. H. *Nat. Chem.* **2016**, *8*, 419.
(96) The nitrogen oxide source may be nitrite ion (NO_2^-) in some of these cases.
(97) (a) Zumft, W. G. *Microbiol. Mol. Biol. Rev.* **1997**, *61*, 533; (b) Wasser, I. M.; de Vries, S.; Moënne-Loccoz, P.; Schröder, I.; Karlin, K. D. *Chem. Rev.* **2002**, *102*, 1201; (c) Watmough, N. J.; Field, S. J.; Hughes, R. J.; Richardson, D. J. *Biochem. Soc. Trans.* **2009**, *37*, 392.
(98) Hino, T.; Matsumoto, Y.; Nagano, S.; Sugimoto, H.; Fukumori, Y.; Murata, T.; Iwata, S.; Shiro, Y. *Science* **2010**, *330*, 1666.
(99) (a) Wang, J.; Schopfer, M. P.; Sarjeant, A. A. N.; Karlin, K. D. *Journal of the American Chemical Society* **2009**, *131*, 450; (b) Wang, J.; Schopfer, M. P.; Puiu, S. C.; Sarjeant, A. A.; Karlin, K. D. *Inorg Chem* **2010**, *49*, 1404.
(100) (a) Arikawa, Y.; Asayama, T.; Moriguchi, Y.; Agari, S.; Onishi, M. *J. Am. Chem. Soc.* **2007**, *129*, 14160; (b) Suzuki, T.; Tanaka, H.; Shiota, Y.; Sajith, P. K.; Arikawa, Y.; Yoshizawa, K. *Inorg Chem* **2015**, *54*, 7181.
(101) Xu, N.; Campbell, A. L. O.; Powell, D. R.; Khandogin, J.; Richter-Addo, G. B. *J. Am. Chem. Soc.* **2009**, *131*, 2460.

Scholarly Life

I was born in Lanzhou, China in 1986. I developed strong interest in chemistry since high school. I was admitted to a top university, University of Science and Technology of China. My undergraduate major is in Chemical Physics and studied DFT calculations. I coauthored two peer reviewed papers and did the calculations. In the year 2009, I was admitted to The Johns Hopkins University, Department of Chemistry. I have been studying copper coordination chemistry over the past years under direction by Prof. Kenneth D. Karlin and some of my work has been published in the *Journal of American Chemical Society*.

CURRICULUM VITAE

RUI CAO

1(443)847-4324·caorrr@gmail.com

EDUCATION

Doctor of Philosophy in Chemistry
The Johns Hopkins University Fall 2016

Dissertation title: "Binuclear Ligand Copper Dioxygen/Nitric Oxide Adducts: Characterization and Reactivity"
Advisor: Professor Kenneth D. Karlin

Bachelor of Science in Chemical Physics May 2009
University of Science and Technology of China (USTC)

RESEARCH INTERESTS

Investigations of unsymmetrical binuclear copper ligand scaffold and its reactivity with small molecules such as oxygen and nitric oxide.

RESEARCH EXPERIENCE

Graduate Research Assistant
Department of Chemistry, The Johns Hopkins University

- Handling air-sensitive compound in the glove-box and using standard Schlenk technique
- Measurement of UV-Vis and IR spectroscopy at low temperature
- Low temperature EPR and NMR spectroscopy experiment
- Low temperature Stopped-flow kinetics study
- X-ray crystallography

Undergraduate Research
Department of Chemical Physics, USTC

- Participate in installing and linking a Computing Cluster with Linux System
- Research Experience: Adjustment of trochoidal electron monochromator and quadrupole mass filter apparatus
- Course project in Data Structure and Database: design of file compressor on the level of Hoffmann Tree

TEACHING EXPERIENCE

Teaching Assistant, Introduction to Chemistry
Department of Chemistry, The Johns Hopkins University

- Attend TA session and grade exam

Lecturer of graduate and undergraduate seminar
Department of Chemistry, The Johns Hopkins University

- Present research topics

Graduate mentor
Department of Chemistry, The Johns Hopkins University

HONORS AND AWARDS

2008 Best Thesis for Summer Undergraduate Research Project
2006-2008 Scholarship for outstanding student
2005 Scholarship for outstanding new student

PUBLICATIONS

1: Peroxo and Superoxo Moieties Bound to Copper Ion: Electron-Transfer Equilibrium with a Small Reorganization Energy
Cao, R.; Saracini, C.; Ginsbach, J. W.; Kieber-Emmons, M. T.; Siegler, M. A.; Solomon, E. I.; Fukuzumi, S.; Karlin, K. D.
J. Am. Chem. Soc. **2016**, 138, 7055-7066.

3: Photoelectron spectroscopy of homogeneous nucleic acid base dimer anions
Ko,Y. J.; Wang,H.; **Cao, R.**; Radisic, D.; Eustis, S. N.; Stokes, S. T.; Lyapustina, S.; Shan Xi Tian, S.; Bowen, K. H.
Phys. Chem. Chem. Phys. **2010**, 12, 3535-3541.

4: Thermal Stabilities of the Microhydrated Zwitterionic Glycine: A Kinetics and Dynamics Study
Tian, S; Sun, X.; **Cao, R.**; Yang, J.
J. Phys. Chem. A **2009**, *113*, 480–483.

Computer techniques

Programming language:
C++ (familiar), Matlab, SQL

System: Linux, Windows
Software: Gaussian 09W, VASP, Molden, Multiwell, Unimol, VC++, Visual FROTRAN Matlab, ChemOffice 2015, Adobe Photoshop, Adobe Illustrator, Opera, LaTex, Origin.